

**HYDROCARBON REARRANGEMENTS AND
SYNTHESIS USING AN ALTERNATING
CURRENT SILENT GLOW
DISCHARGE REACTOR**

By

DENNIS KEITH MANNING

Bachelor of Science

Pittsburg State University

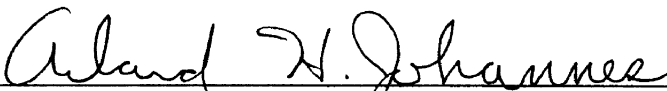
Pittsburg, Kansas

1991


**Submitted to the Faculty of the
Graduate College of the
Oklahoma State University
in partial fulfillment of
the requirements for
the degree of
MASTER OF SCIENCE
December, 1993**

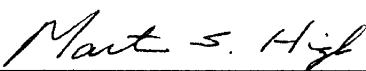
**HYDROCARBON REARRANGEMENTS AND
SYNTHESIS USING AN ALTERNATING
CURRENT SILENT GLOW
DISCHARGE REACTOR**


Thesis Approved:



Thesis Advisor







Dean of the Graduate College

ACKNOWLEDGMENTS

First and with greatest sincerity, I wish to thank my wife, Lorri and our sons Jacob and Lucas, for the sacrifices they have made during this time of study. No monetary value can repay the understanding and patience shown throughout the past two years. I only hope the future will yield the rewards they deserve for past negligence.

To my parents and in-laws a special debt is owed. For the extra time and support given when I was not available, thank you. Knowing you were there when we were faced with adversity, and were willing to assist without complaint or question was a constant source of ease.

I also wish to thank Dr. Arland , A.J., Johannes for his support and guidance through this research. His ability to invoke "thinking about what's really going on", has already greatly added to my awareness as an engineer. The open mind approach taken in material presentation is an asset to all students under his guidance.

To the other members of the Faculty in the Chemical Engineering Department, I also thank you. The knowledge gained from their instruction, experience and personal interest can only be measured in the success of those they have been in contact with. I hope not to deduct the outstanding standard set by my predecessors.

To Charles Baker a special acknowledgment is required. His consistency for "coming up with the unattainable" is truly a gift. His humor, cheerfulness and caring attitude to students, faculty and staff always eased stress at just the right time. His efforts to OSU are not without recognition.

TABLE OF CONTENTS

Chapter	Page
I. INTRODUCTION	1
II. LITERATURE SURVEY	5
Background Information	5
Generalizations For Hydrocarbon Pyrolysis	5
Generalization Summary	7
Propane Pyrolysis	8
Propane Pyrolysis Summary	11
Plasma Origin And Definitions	11
General Plasma Mechanisims	13
Literature Survey Summary	14
III. EXPERIMENTAL DESIGN	15
Safety Considerations	15
Experimental Apparatus Description	16
Procedure	22
Analytical Procedure	23
Gas Phase Analysis	23
Liquid Phase Analysis	23
Solid Phase Analysis	25

Chapter	Page
IV. REACTOR EVALUATIONS UNDER NON-DESTRUCTIVE TEST	26
Procedure	26
Reactor A	27
Reactor B	32
Reactor C	35
Length Effects on Plasma Formation	42
V. MODEL MODIFICATIONS	51
VI. DESTRUCTIVE TEST	58
Initial Observations	58
Initial Rearrangement Test	59
Rearrangement Test Using Reactor E	61
Secondary Voltage Effects	62
Residence Time Effects on Group Distribution	64
Frequency Effects on Group Distribution	65
Conversion Results From Residue Production	67
Summary	67
VII. CONCLUSIONS AND RECOMMENDATIONS	68
LIST OF REFERENCES	72
APPENDICES	76
APPENDIX A - REACTION MECHANISMS	76
APPENDIX B - REGRESSION ANALYSIS FOR FLOW METER CALIBRATION	79
APPENDIX C - ANALYSIS OF PROPANE FEEDSTOCK	84

Chapter	Page
APPENDIX D - EXAMPLE OF RUN DATA SHEET FOR HYDROCARBON REARRANGEMENT TESTING	86
APPENDIX E - EXPERIMENTAL DATA FOR NON-DESTRUCTIVE TEST IN REACTOR A	88
APPENDIX F - EXPERIMENTAL DATA FOR NON-DESTRUCTIVE TEST IN REACTOR B	96
APPENDIX G - EXPERIMENTAL DATA FOR NON-DESTRUCTIVE TEST IN REACTOR C	102
APPENDIX H - SUPPORTING DATA FOR SECONDARY VOLTAGE LOSS RATE IN REACTORS A & B	107
APPENDIX I - EXPERIMENTAL DATA FOR LENGTH EFFECTS IN REACTOR C	110
APPENDIX J - STATISTICAL DATA FROM TABLECURVE™ ANALYSIS	124
APPENDIX K - OPERATION PARAMETERS AND ANALYSIS OF PRELIMINARY RUNS	127
APPENDIX L - OPERATION PARAMETERS AND ANALYSIS OF DESTRUCTIVE TEST	131
APPENDIX M - ANALYTICAL CHROMATOGRAMS	134

LIST OF TABLES

Table	Page
I. Bond Dissociation Energies for A-B Bonds	14
II. Reactor Specifications for Reactors Used	17
III. Equipment List for Experimental Apparatus	20
IV. Gas Chromatograph Specifications for Liquid Phase Analysis.	24
V. Component Retention Times	24
VI. Comparison of Secondary Voltage Rate Loss for Reactor A.	39
VII. Comparison of Secondary Voltages for Reactor A at Various Primary Voltages and Electrode Configurations.	40
VIII. Deviations of Predicted Breakthrough Voltages as Compared to Experimental Values	52
IX. Calculated Capacitance of Reactors Using Equation 11	57
X. Conclusions From Propane Pyrolysis Using a SGDR for Energy Transfer	68
XI. Recommendations for Future Research	69
B1. Data for Regression Analysis	80
C1. Percentages of Components Found in Propane Feed Stock	85
E1. Experimental Data Corresponding to Figure 4	89
E2. Experimental Data Corresponding to Figure 5	90
E3. Experimental Data Corresponding to Figure 6	91

Table	Page
E4. Experimental Data Corresponding to Figure 7	92
E5. Experimental Data Corresponding to Figure 8	93
E6. Experimental Data Corresponding to Figure 9	94
E7. Experimental Data Corresponding to Figure 10	95
F1. Experimental Data Corresponding to Figure 11	97
F2. Experimental Data Corresponding to Figure 12	98
F3. Experimental Data Corresponding to Figure 13	99
F4. Experimental Data Corresponding to Figure 14	100
F5. Experimental Data Corresponding to Figure 15	101
G1. Experimental Data Corresponding to Figure 16	103
G2. Experimental Data Corresponding to Figure 17	104
G3. Experimental Data Corresponding to Figure 18	105
G4. Experimental Data Corresponding to Figure 19	106
H1. Supporting Data for Linear Regression Analysis	108
I1. Experimental Data Corresponding to Figure 21	111
I2. Experimental Data Corresponding to Figure 22	112
I3. Experimental Data Corresponding to Figure 23	113
I4. Experimental Data Corresponding to Figure 24	114
I5. Experimental Data Corresponding to Figure 25	115
I6. Experimental Data Corresponding to Figure 26	116
I7. Experimental Data Corresponding to Figure 27	117
I8. Experimental Data Corresponding to Figure 28	118

Table	Page
I9. Experimental Data Corresponding to Figure 29	119
I10. Experimental Data Corresponding to Figure 30	120
I11. Experimental Data Corresponding to Figure 31	121
I12. Experimental Data Corresponding to Figure 32	122
I13. Experimental Data Corresponding to Figure 33	123
J1. Statistical Data From TableCurve™ Analysis	126
K1. Operation Parameters	128
K2. Analysis of Preliminary Samples 04, 05 and 06	129
K3. Analysis of Preliminary Samples, 015 and 016	130
L1. Operation Parameters of Destructive Test	132
L2. Analysis Summary of Destruction Test	133

LIST OF FIGURES

Figure	Page
1. Location of Experimental Equipment	16
2. Lateral Cross-Section of Reactor Configuration	18
3. Experimental Apparatus for SGDR	21
4. Effects of Frequency on Secondary Voltage at Various Primary Voltages, Ambient Air With a Wrapped Outer Electrode Configuration.	27
5. Effects of Frequency on Secondary Voltage at Various Primary Voltages, Nitrogen With a Wrapped Outer Electrode Configuration.	28
6. Effects of Frequency on Secondary Voltage at Various Primary Voltages, Propane With a Wrapped Outer Electrode Configuration.	28
7. Effects of Frequency on Secondary Voltage at Various Primary Voltages, Ambient Air With a Copper Mesh Outer Electrode Configuration.	29
8. Effects of Frequency on Secondary Voltage at Various Primary Voltages, Nitrogen With a Copper Mesh Outer Electrode Configuration.	29
9. Effects of Frequency on Secondary Voltage at Various Primary Voltages, Propane With a Copper Mesh Outer Electrode Configuration.	30
10. Power Requirements For Reactor A Using Propane And Mesh Outer Electrode	31
11. Effects of Frequency on Secondary Voltage at Various Primary Voltages, Ambient Air With a Wrapped Outer Electrode Configuration.	32

Figure	Page
12. Effects of Frequency on Secondary Voltage at Various Primary Voltages, Ambient Air With a Copper Mesh Outer Electrode Configuration.	33
13. Effects of Frequency on Secondary Voltage at Various Primary Voltages, Nitrogen With a Copper Mesh Outer Electrode Configuration.	33
14. Effects of Frequency on Secondary Voltage at Various Primary Voltages, Propane With a Copper Mesh Outer Electrode Configuration.	34
15. Power Requirements For Reactor B Using Propane And Mesh Outer Electrode	35
16. Effects of Frequency on Secondary Voltage at Various Primary Voltages, Ambient Air With a Mesh Outer Electrode Configuration.	36
17. Effects of Frequency on Secondary Voltage at Various Primary Voltages, Nitrogen With a Mesh Outer Electrode Configuration.	36
18. Effects of Frequency on Secondary Voltage at Various Primary Voltages, Propane With a Mesh Outer Electrode Configuration.	37
19. Power Requirements For Reactor C Using Propane And Mesh Outer Electrode	37
20. Cross-Section View Of Reactor Annulus	41
21. Effects of Frequency on Secondary Voltage at Various Primary Voltages, Nitrogen With One Wrap 12 Gauge Wire	43
22. Effects of Frequency on Secondary Voltage at Various Primary Voltages, Nitrogen With 2.5 Inch Mesh Electrode	43
23. Effects of Frequency on Secondary Voltage at Various Primary Voltages, Nitrogen With 6.5 Inch Mesh Electrode	44

Figure	Page
24. Effects of Frequency on Secondary Voltage at Various Primary Voltages, Nitrogen With 12.5 Inch Mesh Electrode	44
25. Effects of Frequency on Secondary Voltage at Various Primary Voltages, Nitrogen With 17.75 Inch Mesh Electrode	45
26. Effects of Plasma Zone Length on Secondary Voltage at 30 Primary Volts	46
27. Effects of Plasma Zone Length on Secondary Voltage at 40 Primary Volts	46
28. Effects of Plasma Zone Length on Secondary Voltage at 50 Primary Volts	47
29. Effects of Plasma Zone Length on Secondary Voltage at 60 Primary Volts	47
30. Effects of Plasma Zone Length on Secondary Voltage at 70 Primary Volts	48
31. Effects of Plasma Zone Length on Secondary Voltage at 80 Primary Volts	48
32. Effects of Plasma Zone Length on Secondary Voltage at 90 Primary Volts	49
33. Effects of Plasma Zone Length on Secondary Voltage at 110 Primary Volts	49
34. Typical Plate Type Capacitor	52
35. Effects of Plasma Length on Secondary Voltages at First Class 4 Formation	56
36. Plasma Zone Orientation	60
37. Effects of Secondary Voltage on Product Distribution, Frequency 310 Hz Flow 64.89 ml/min	62
38. Compound Propyl Radical	63
39. Comparison of Flowrates on Group Contribution	64

Figure	Page
40. Comparison of Flowrates on Group Contribution	65
41. Effects of Frequency on Product Distribution, Secondary Voltage 19.2 kV Flow 64.89 ml/min	66
B1. Plot of Calculated Flowrate as a Function of Rotameter Settings	83
J1. Graphical Representation of Correction Values	125
M1. Chromatogram for run HR-015	135
M2. Chromatogram for run HR-016	135
M3. Chromatogram for Run D-1	136
M4. Chromatogram for Run D-2	136
M5. Chromatogram for Run D-3	137
M6. Chromatogram for Run D-4	137
M7. Chromatogram for Run D-5	138
M8. Chromatogram for Run D-6	138
M9. Chromatogram for Run D-8	139
M10. Chromatogram for Run D-9	139
M11. Chromatogram for Run D-10	140
M12. Chromatogram for Run D-12	140

NOMENCLATURE

A	Area, m ²
C	Capacitance, Farads
C _t	Total Effective Capacitance, Farads
d	Distance, m
D _i	Diameter Corresponding to Reactor Geometry, m
D _{ln}	Log mean Diameter, m
g	Empirical Constant
HAZ LAB	Hazardous Reaction Laboratory
K _a	Dielectric Constant of Reacting Fluid
K _e	Dielectric Constant For Plate Capacitor
K _g	Dielectric Constant of Reactor Material
PV	Primary Voltage, volts
r	Lead Resistance, ohms
R	Total Effective Resistance, ohms
SGDR	Silent Glow Discharge Reactor
SV	Secondary Voltage, kilovolts
x	Plasma zone length, cm
V _b	Breakdown Voltage, kilovolts
ε ₀	Permittivity of Free Space, Farads/meter

ω Frequency, Hz

CHAPTER I

INTRODUCTION

Hydrocarbon synthesis and rearrangement reactions have long been a major interest for the process industry. Recent interest in these areas have been revived due to the changing market structure and current trends for feed stock supplies. As crude oil, the main feed stock for the hydrocarbon industry, supplies are depleted and environmental regulations limit or restrict access, alternate methods of feed stock production are warranted.

One alternative is the pyrolysis of readily available hydrocarbons or undesired separation by-products. Interest in this method has increased dramatically over the past 25 years. Barker and Wang [1] report an increase in the number of publications from 8 in 1965 to over 160 in 1985 for pyrolysis studies. This increase demonstrates the widely recognized potential in pyrolysis reactions.

Pyrolysis is the cleavage of molecular bonds by energy introduction [19]. As energy is introduced to the molecules, the bonds of lower association strength begin cleaving. This process produces smaller stable molecules and carbon radicals [39]. It is the production of these radicals which is of primary interest in this research.

Hydrocarbon radicals are the basis for chain propagation or growth. As the radicals are formed they seek to fill the valence electron orbitals by one of two means. First by molecular bonding to an available radical, or second by removing a weakly

attached functional group from an existing hydrocarbon. These methods of reaction lead to the possibility for chain growth or molecular rearrangement.

Heating of the molecules is the primary method to supply the required energy for pyrolysis. Several types of reactors and apparatus have been used in the past with reasonable success [1]. It is the objective of this research to investigate a new energy transfer technique, frequency tuned capacitive discharge reactors. The use of this type of reactor will hopefully allow the chain propagation that is possible in pyrolysis, but has not been significantly observed in other reactors.

A disadvantage that accompanies most pyrolysis applications is the high product stream outlet temperatures. The required heating elevates the stream temperature to several hundred degrees Centigrade. A cooling mechanism is thus required. Unlike conventional heating, an electrically induced plasma provides energy to the electrons and not the nucleus of the molecules [35]. This behavior provokes an effective electron temperature, allowing pyrolysis, but maintains a reactor outlet stream temperature only slightly higher than ambient conditions.

Research on alternating current silent glow discharge reactors (SGDR) began at Oklahoma State University (OSU) as a cooperative effort with the Naval Research Laboratory in 1987. Earlier research [34,40] at OSU was focused at the destruction of airborne hydrocarbon contaminants. This work showed the potential for the cleavage of molecular bonds in the hydrocarbons. The work by Piatt [34], demonstrated the cleavage of the carbon-hydrogen bonds in a methane system. Tsai [40] again demonstrated the potential in the destruction of triethylenechloride. This work also demonstrated the effects of tuning the reactor by frequency variations. These variations are possibly the key to controlling the selectivity for bond cleavage in pyrolysis. With this work as the basis for the bond cleavage potential in a SGDR, research in the area of pyrolysis on high purity hydrocarbons is warranted.

The economic potential for this application on an industrial basis is staggering. As the availability of crude oil decreases through depletion and regulation, alternate sources of feed stocks and fuels will be mandated. Rearrangement and synthesis of abundant hydrocarbon sources, such as natural gas, prove economically favorable if conversion rates and product controls are established. Ethylene and propylene feed stocks and liquid fuels are but two possibilities for products. In addition to the numerous products that are possible, several current reactions requiring extreme temperatures or pressures could be initiated at reduced costs.

The advantages that could be realized in using a SGDR for pyrolysis are as follows:

- * enhanced chain propagation
- * molecular rearrangements without temperature elevation.
- * controlled bond cleavage by frequency tuning.
- * no catalysis is required within the reactor.
- * low pressure operations.
- * reduced energy requirements for existing reactions.

The preceding paragraphs sufficiently justify this research from an applied point of view. Economical justification is also seen in the potential of various products and energy savings of existing reactions.

Propane was chosen as the hydrocarbon used in this research. Several factors influenced this choice. First is the vast amount of data concerning propane pyrolysis. Over 100 references are listed in one article [42]. Second is the relative bond strength between the carbon-carbon and carbon-hydrogen bonds. Finally propane is a symmetrical molecule. This fact allows for easier product identification and chain propagation.

The objectives of this research are as follows:

- * To build a safe and operable experimental apparatus
- * To determine the possible products of chain propagation using SGDR pyrolysis
- * To determine the effects of reactor tuning on product distribution
- * To assess the possible scale up criterion for SGDRs
- * To assess future possibilities for SGDR pyrolysis.

A review of the literature on propane pyrolysis is given in Chapter II. The experimental design, safety considerations and operating procedures are given in Chapter III. Chapter IV details the operating conditions and observations of the various reactors and electrode configurations used under non-destructive test. Chapter V discusses the expansion of the current breakdown voltage prediction method. Chapter VI covers the rearrangement test and chain propagation observed under various reactor operating parameters. Finally Chapter VII gives a discussion of the relevant data obtained and possible implications for future studies.

CHAPTER II

LITERATURE SURVEY

Background Information

Pyrolysis, in the purest sense, is the transformation of a compound into another substance or substances through the addition of heat alone [19]. This definition applies to the majority of pyrolytic reactions. With SGDR induced pyrolysis this definition may need to be broadened. The actual temperature of the fluid, in our case propane, does not increase substantially in the reactor. Elevation of the effective electron temperature is physical governing the pyrolysis. This behavior will be discussed later in this section. It is this "transformation by heat" that will be used to evaluate the SGDR for pyrolysis rearrangement reactions.

Generalizations For Hydrocarbon Pyrolysis

Peytral's Rule of Least Molecular Deformation [33] states that the transformation caused by heat will follow the reaction which requires the least possible deformation of the molecule. At high temperatures the resulting compounds will have molecular bonds nearly identical to those in the original compound. Several reactions supporting this postulate are available but lie outside the scope of this research. This postulate fails to allow for the prediction of where scission will occur in the hydrocarbon chain or what path is the least

deforming. It emphasizes that a relation between the original compound and the products of its pyrolysis does exist and is often predictable.

Bredt's Rule [7], Blanc's Rule [5] and Haber's Rule [17] address the pyrolysis of cyclic rings. Bredt postulates that the meta and para positioning on various cyclic acids is a function of the ring carbons ability to form double bonds. Blanc suggested similar trends in cyclic anhydrides. Haber generalizes that the carbon-carbon linkage in the cyclic rings as more stable than the carbon-hydrogen bonds. This is reversed in the case of aliphatic hydrocarbon series.

Berthelot's Theory of Pyrogenic Reactions [4] is divided into three parts in an effort to explain the reaction mechanisms in general pyrogenic reactions. The three aspects to Berthelot's theory are as follows:

1. In addition to pyrolytic reactions of decomposition, there are also reactions of synthesis. In the latter, there is progressive hydrogen elimination, accompanied by the gradual formation of complex hydrocarbons, which eventually may result in the deposition of carbon.

2. The building-up and tearing-down processes are considered to limit each other. The long chain hydrocarbons produced decompose into smaller radicals, which recombine into higher chained molecules. This leads to a complicated equilibrium between an increasing number of hydrocarbons.

3. These reactions occur whether the hydrocarbon is in contact with hydrogen or other hydrocarbons.

Berthelot's theory met with a great deal of criticism. Haber [17] noted that at progressively higher temperatures graphite always appears in pyrolysis, and coke is never hydrogen free. Haber also criticized Berthelot's second statement in that no evidence is shown of an equilibrium being established due to external conditions.

Berthelot's theory, though not concrete in all areas, does contribute to the general pyrolysis reaction mechanisms. The idea of formation and deformation of a numerous

collection of hydrocarbons within the pyrolysis reactor is based on the radical formation possible on all hydrocarbons. Based on this, one should see a wide range of hydrocarbons formed during pyrolysis. Although previous work shows that the primary products of propane pyrolysis to be ethylene, methane, propylene and hydrogen [9], the application of the SGDR may alter the products and thus Berthelot's general thoughts on formation and deformation may be valid.

The ultimate in dissociation theories belongs to Nef [28]. Nef theorized that the original compound dissociates into an ephemeral molecule of bivalent carbons and thus reacts with itself or with other neighboring substances. This mechanism would tend to produce short chain hydrocarbons. As the hydrocarbons were formed, pyrolysis would occur on these new compounds. According to Nef's Theory, these in turn would dissociate into the bivalent carbon molecules. Actual formation of products would be restricted to the outlet portion of the reaction vessel where the dissociation is quenched due to temperature reduction.

Generalization Summary

Several theories have been represented in the above paragraphs. Although no single theory is without flaw or explains the complex mechanisms evolved in pyrolytic reactions, they serve as preliminary guidelines for the application of the SGDR pyrolysis. In all of the generalized theories one link is common, the reactions are controlled by the radical production by bond scission. This fact is the underlying control for pyrolysis reactions. The ability to predict and control which bond or bonds dissociate will govern the product formation. It is one objective of this research to investigate scission control through the frequency tuning in a SGDR

Propane Pyrolysis

The pyrolysis of propane has been studied using several reactors and techniques. Five different approaches that have been used previously will be discussed in this section.

Shock-tube pyrolysis conducted by Benson [3] in the temperature range of 830-1180 °C and atmospheric pressure showed a decomposition reaction. The products of ethylene, hydrogen, methane and ethylene were shown to follow two routes with approximately equal importance.



and



Benson further suggest that propylene reforms to yield acetylene. This first order mechanism is given in Appendix A.

Lifshitz and Frenklach [25] conducted similar tests using a temperature range of 800-1000 °C and a pressure of 200 Torr. The reaction in this range does not suggest the formation of allenes from either propylene or ethylene. It is theorized that this occurs at temperatures in excess of 1000 °C. The proposed reaction scheme for this mechanism is given in Appendix A.

Static system pyrolysis before 1960 followed approximately the same experimental design. A quartz vessel was used in which the temperature was controlled by a stainless steel block. Pease [31], Marek and McCluer [26], Paul and Marek [29], Pease and Durgan [32], Rice [35], Fery and Hepp [16], Dintess and Frost [13,14], Steacie and Puddington [38], Hobbs and Hinshelwood [18], and Ingold et al. [20] all conducted experiments over the temperature range of 25 - 400 °C using the static system. Collectively the conclusion was reached that the decomposition reactions are first order. Again free radicals formation was the governing factor in the reaction mechanism.

Laidler [24] studied propane pyrolysis over the temperature range of 530-670 °C and at pressures up to 600 mm Hg. Conclusions again showed free radical formation was the controlling mechanism. In this study one new development was considered, the reaction order increased to 3/2 at temperatures over 650 °C. Both mechanisms are given in Appendix A.

Propane pyrolysis utilizing photosynthesis techniques were studied by Steacie and Dewar [37], Darwent and Steacie [11] and Bywater and Steacie [10]. These studies were similar to the static system experiments with the exception that energy in the form of excited mercury atoms and/or light was used rather than heat. The reaction mechanism from the study of Bywater and Steacie [10] compares very similarly to previously proposed mechanisms. The mechanism is listed in Appendix A.

Back and Takamuku [2] studied the decomposition of propane using similar photosynthesis techniques in the temperature range of 300-400 °C. Verification that the propyl radicals formed propylene was confirmed. The mechanism of Bywater and Steacie [10] was used to describe the reaction.

Kunugi [23] studied the effects of propane pyrolysis in a tubular reactor. The experimental apparatus consisted of a transparent quartz tube at atmospheric pressure. Temperature ranges of 750-850 °C were investigated. The primary products were again methane, ethylene, hydrogen, propylene and ethane. Some C₄ and heavier hydrocarbons were also produced at very low rates. The reactions previously shown in equations 1 and 2 describe the overall reactions for this system. The decomposition rate was taken as that proposed by Laidler [24] at 3/2 order. The mechanism for this case is given in Appendix A.

Kershenbaum and Martin [22] studied non isothermal pyrolysis of propane in tubular reactors. Temperature ranges of 800-1000 °C were studied. This study used dilute propane mixtures with nitrogen in order to study the kinetics of the pyrolysis. The overall order was found to be between 1 and 1.2. This agrees well with previously

published results. The Laidler mechanism describes this pyrolysis and is given in Appendix A.

The above tubular reactor studies fail to detail the physical situation within the reactor on a molecular level. This information would be of particular interest in the development of a SGDR theory. Eggsgaard and Carlson [15] detail the steps of pyrolysis in two types of tubular reactors. Both Knudsen and Curie-point reactors were analyzed using a "random walk" approach of single molecules.

In Knudsen cylindrical reactors, the inside of the reactor wall is kept at a constant temperature by an arbitrary means. Either electrical heating or thermal combustion heating is adequate on the exterior of the reactor. The material of interest is then passed through the reactor vessel. It is the collision of the molecules with the heated walls that allows pyrolysis to take place. A relationship between reactor geometry, temperature and molecular weight of the substance was developed to allow estimation of the collision frequency. It is this collision frequency which governs the pyrolysis effects.

Curie-point reactors operate in a manner in which elements within the reactor are heated to the desired temperature, while the shell of the reactor remains at ambient temperature. In this case the molecular collisions with the elements increase the molecular energy to establish pyrolysis. Collisions with the exterior reactor wall deactivate the energy within the molecule and hinder pyrolysis.

An effective SGDR will avoid the requirements of these wall or element collisions. Within the reactor the elevated electron temperature is throughout the volume of the plasma zone. Localized areas for collision are restricted to the exterior reactor walls where some deactivation is probable. The efficiency of a SGDR of the same volume should be higher than either a Knudsen or Curie-point reactor due to the difference in physical collision requirements.

Plasma jet studies for propane pyrolysis by Nishimura [27] used an induction-coupled argon plasma jet. Two cases were studied, cocurrent and countercurrent propane

injection. Temperature ranges from 18,000-20,000 °K in the plasma center to 10,000-12,000 °K on the periphery were noted. Cocurrent products were carbon, hydrogen and a trace of acetylene. Carbon formation on the induction coils limited the duration times for this case. The countercurrent cases yielded products of acetylene, ethylene, hydrogen and soot. This reflects back to Benson's remarks [3] concerning propylene decomposition into acetylene at elevated temperatures. The reaction mechanism is given in Appendix A.

Propane Pyrolysis Summary

It is evident that the governing factor in pyrolysis is the production of free radicals. Throughout the previous paragraphs this has been the common mechanism of reaction. The ability of selective bond scission has been shown to be the key to control product distribution. Previous pyrolysis methods have been limited in the variables of control to temperature, retention time, reactor geometry and concentration. It is an objective of this research to investigate frequency tuning of a SGDR to assist in product distribution control and selectivity. During this research the products of interest will be limited to those supporting the chain growth portion of Bethelot's theory. More specifically hydrocarbons with a chain length of 4 carbons or more.

Plasma Origin And Definitions

Plasma origins date to the beginning of time and is the most abundant form of matter in existence. Star formations were the first sources of plasmas but were unrecognized as such for millions of years. Sir William Crookes [6] is honored for the first scientific reference to plasmas in 1879. Crookes' reference to plasmas was as a "fourth state of matter". Crookes' tube plasma was the first manmade plasma on record. Later in 1928, Langmuir [6] renamed Crookes "fourth state of matter" plasma.

Two types of plasma exist, thermal induced and electrically induced. Although both induction methods result in plasma formation, a marked difference exist between the two. In thermal induction, the plasma is isothermal. That is the electron temperature and the neutral species temperature are equivalent. In electrically induced plasmas this is not the case. A difference of several orders of magnitude can exist between the negative and neutral species temperatures.

A primary objective of this research is to study the effects of this difference on the pyrolysis of propane. All previous studies indicate the formation of radicals by bond scission as the governing mechanism of reaction. No deviation from this conclusion is anticipated in a SGDR. The mechanisms which govern formation of the radicals may possibly vary, but a detailed mechanism explanation is outside the scope of this research. The three possible mechanisms are: 1) direct kinetic transference from electron bombardment 2) vibrational effects from electrical field interference and 3) hydrogen removal by radical interaction. A comparison of products from the SGDR and previous pyrolysis applications will be given in the Conclusion section of this report.

Tsai [40] developed a relationship between the reactor geometries, density of the gas to be ionized and the dielectrics of the arrangement. Specific details are given in the Non-Destructive Test section of this report. This predicted "break-down" voltage is defined as "the effective value of the voltage required to start a visible corona."

This definition is only a qualitative perspective. The point at which a plasma becomes visible is dependent on several factors. Ambient light sources are the primary factor. Earlier experiments [19] in the absence of ambient light sources reveal the best conditions for plasma observation. Due to this lack of a precise definition for a visible plasma, the following qualitative measures were established.

A class 1 plasma denotes the first visible signs of plasma formation in the reactor annulus. In class 2 formations, the plasma extends across the annulus and covers at least one-half the reactor circumference. Class 3 plasmas extend this area to approximately

75% of the available plasma generation zone. A class 4 plasma is fully developed through the reactor zone with no visible voids. Because plasma intensity can increase after full formation occurs, plasmas above a fully developed state will be classified as 4+. Although these are arbitrary classifications, they serve as a qualitative means for description.

General Plasma Mechanisms

Reactions taking place within an induced plasma are believed to follow the same general pyrolysis mechanisms that were discussed previously in this section. By supplying energy to the electrons of the molecules, scission, or bond separation, occurs. This bond cleavage results in radical production of both negatively and positively charged species. This results in most plasma reactions being first order for decomposition and second order for recombination reactions.

This radical formation is not limited to the initial compound introduced in the reactor. In hydrocarbons carbon-carbon, carbon-hydrogen and carbon-functional group bonds can be cleaved in any existing compound. Two factors control the order of bond cleavage, association strength and radical stability [30]. Estimation of bond scission is somewhat predictable based on these factors. The order of bond-dissociation energies is listed in Table I.

The decreasing order of radical stability is tertiary radical > secondary radical > primary radical > methyl radical [39].

Hydrocarbons are normally good insulators, especially in the gas phase. However under the influence of a sufficient electrical field, these molecules are ionized. It is the ionization effects that allow the plasma formation within the SGDR. As ionization occurs current passes from the outer electrode through the gas in the reactor to the inner electrode. Details for this SGDR will be given in the Experimental Design section.

TABLE I

BOND DISSOCIATION ENERGIES
FOR A-B BONDS (KCAL/MOLE) [39]

Component , A	B ->	H	Cl	Br	I	OH	NH ₂	CH ₃	CN
CH ₃ -		105	85	71	57	93	85	90	122
C ₂ H ₅ -		98	80	68	53	91.5	82	86	118
i-C ₃ H ₇ -		95	81	68	53.5	93	82	86	NA
t-C ₄ H ₉ -		93	81	67	52	93	82	84	NA
C ₆ H ₅ -		111	96	80.5	65	111	102	102	131
C ₆ H ₅ CH ₂ -		88	72	58	48	81	71	76	NA
CH ₂ CHCH ₂ -		86	68	54	41	78	NA	81	NA
CH ₃ CO-		86	81	66	49	107	NA	81	NA
C ₂ H ₅ O-		104	NA	NA	NA	44	NA	83	NA
CH ₂ CH-		110	90	78	NA	NA	NA	100	130
H-		104.2	103.2	87.5	71.3	119	107	105	125

Literature Survey Summary

The literature cited in the preceding paragraphs provide sufficient background information for mechanisms and reactions of propane pyrolysis. Although no specific information on the use of a SGDR is given, the mechanisms involved are expected to be very similar. Radical formation by bond scission has been shown to be the controlling mechanism in all studies. The application of the plasma jet pyrolysis shows the effectiveness of high temperature plasmas for decomposition. It is an objective of this research to investigate the application of a SGDR using the mechanisms and general pyrolysis theories of this survey.

CHAPTER III

EXPERIMENTAL DESIGN

This section is devoted to the topics of experimental apparatus design, materials used, safety considerations, sample collection and analytical techniques used. Each topic will be discussed on an individual basis within this section.

Safety Considerations

The first step in designing this, or any, experimental apparatus is the consideration for safe equipment operation. This is especially important in studies involving flammable or explosive substances. Due to the flammability of the material used several steps to ensure minimal risks to persons or property were taken. These steps are listed as follows:

- 1) The reactor, collection vessels, waste gas flare and material containment cylinders were located in an exterior explosion proof bay.
- 2) Power sources and controls were located within the Hazardous Reaction Laboratory (HAZ LAB). This isolates the power source from the flammable material.
- 3) Work performed on the test material was conducted while two persons were present in the HAZ LAB.

A schematic drawing showing the location of the reaction apparatus, waste gas flare, flow control, containment cylinders and power/control sources is given in Figure 1.

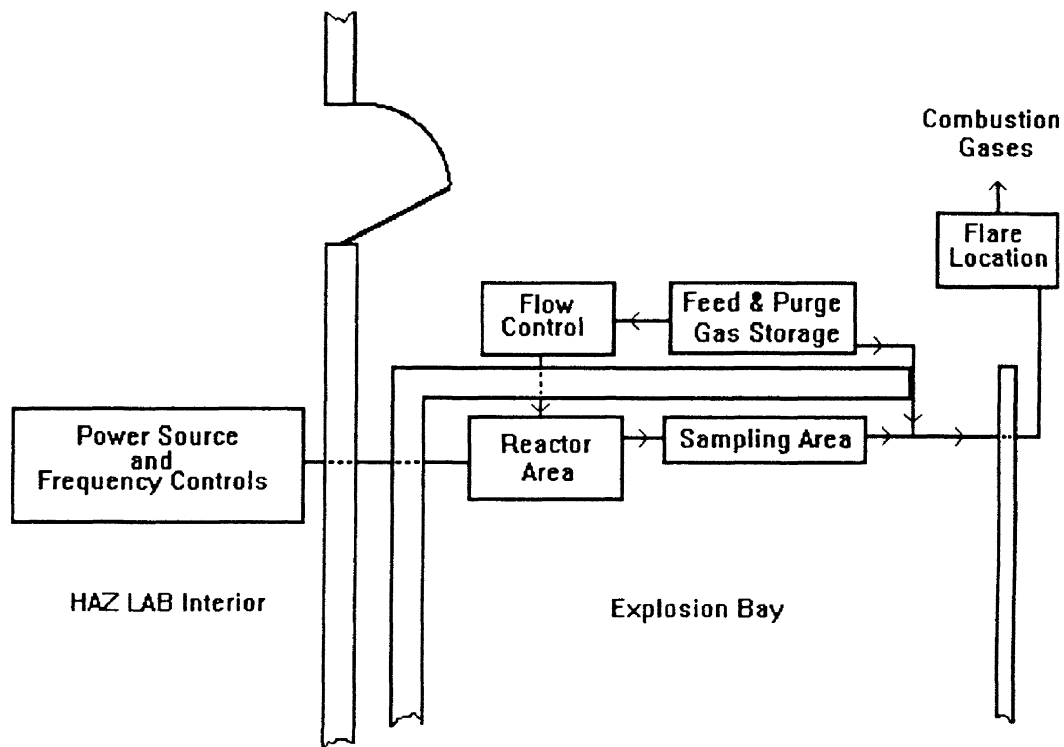


Figure 1. Location of Experimental Equipment

Experimental Apparatus Description

The experimental apparatus is composed of five distinct areas of concern. These are the power and control source, the reactor, feed gas storage and rate control, sample collection and waste gas incineration. Each area will be discussed separately. An equipment list is also provided in Table III. A schematic of the experimental apparatus is shown in Figure 3.

The electrical system in the apparatus consisted of an AC power supply, an oscillator for frequency adjustment, a transformer for voltage increase, a multimeter, and a watt meter for total power consumption measurement. The only piece of electrical equipment not located within the HAZ LAB was the transformer. This was located in the

explosion bay. Power from the 110V wall outlet was passed through the adjustable AC power supply and frequency tuner to the transformer for voltage increase. The watt meter was positioned between the wall outlet and the power supply. Multimeter readings allowed for the monitoring of the secondary voltage potential across the reactor.

The reactors used in this study consisted of two concentric glass cylinders to form an annulus for gas flow. Electrodes were placed around the outer cylinder and within the inner cylinder. The dielectric effects of the glass cause diffusion of the current into the annulus when a potential is applied. The plasma then forms within the annulus. The construction of this reactor configuration allows for complete separation of the gas and plasma flow from the electrodes. Various reactors and electrode configurations were used. Table II list the reactor specifications. Electrode configurations applied will be detailed for each study case. Figure 2 shows a schematic of the reactors used with the two types of electrode configurations.

TABLE II.

REACTOR SPECIFICATIONS
FOR REACTORS USED

Reactor	Material	I.D. Outer Tube (cm)	O.D. Inner Tube (cm)	Length (cm)	Annular Gap (cm)
A	Quartz	2.78	1.80	25.400	0.490
B	Pyrex	4.80	3.00	44.132	0.900
C	Pyrex	4.80	3.00	91.440	0.900
D	Pyrex	4.80	3.00	121.25	0.900
E	Quartz	4.80	2.80	121.90	1.000

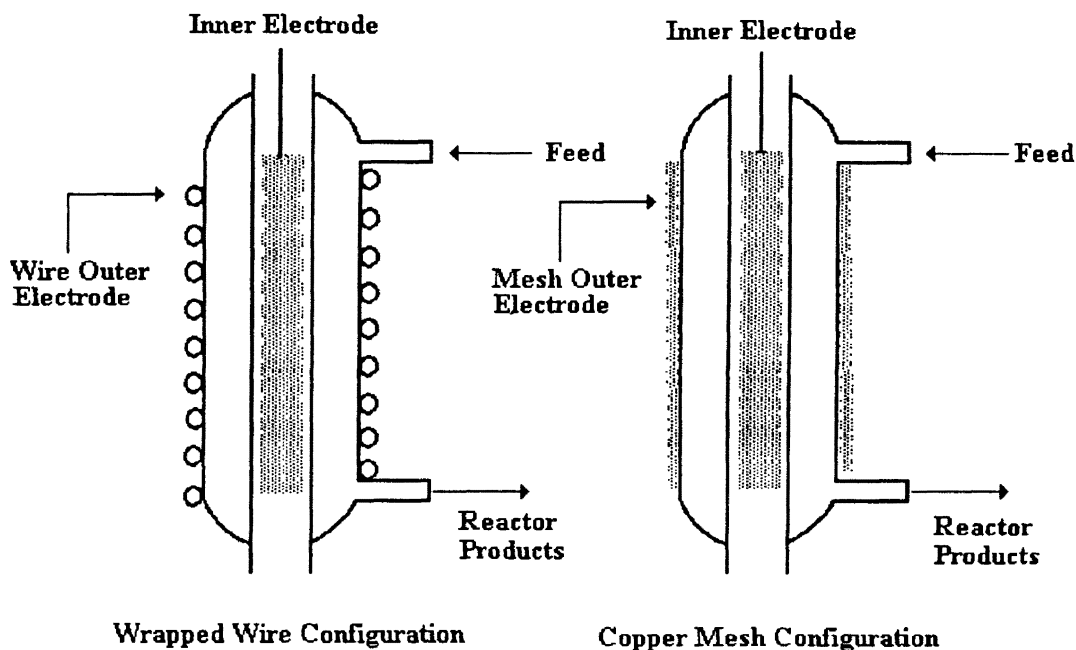


Figure 2. Lateral Cross-Section of Reactor Configurations

Feed gas storage consisted of high pressure containment cylinders with appropriate regulators. This allowed for the line pressure of the feed and purge gases to be adjustable. Installation of a pressure fluctuation dampener was required upstream from the flow control. Slight changes in flow were caused by pressure fluctuations at the propane regulator. These fluctuations were due to the temperature drop of the propane as it passed through the regulator. The flow was controlled by a calibrated rotameter in line prior to the reactor. Calibration was done using a "bubble flow meter" to measure the flowrate as a function of time. Regression analysis on the data points yielded the following correlation

$$Y = 9.2749X - 27.855 \quad (3)$$

Supporting calculations and data are given in Appendix B.

Sample collection was conducted on the assumption that products of interest could exist in two phases. Hydrocarbons of a chain length greater than 16 will exist as a solid at room temperature. Chains between 5 and 16 carbons in length exist in a liquid phase, while lesser chains exist as a gas. Thus two methods of sample collection were employed. The reactor was cleaned before and after each run to determine the material residue solidified within the reactor. This residue was removed from the reactor walls with solvent for product analysis. Liquid phase products were collected in a ice water trap. This cold trap allowed collection of all hydrocarbons with a chain length of 5 or greater. Removal of the sample vessel from the trap allowed the remaining liquid sample to be analyzed by gas chromatography.

Excess gas was incinerated in a low volume flare located away from the building and explosion bay. Waste gas from the reactor was fed into an additional propane stream for incineration. Oxygen for combustion was supplied with ambient air via a natural convection force within the flare.

Materials used were restricted to the feed gas, purge gas and solvent for residue removal. Nitrogen, used as the purge gas, was Linde Specialty Gases, dry grade, at 99.9%. Feed gas was Linde Specialty Gases CP grade propane Stock No. UN1075, 99.6%. Analysis for the feed gas is given in Appendix C. Solvent for residue removal was Fisher Analytical Grade methylene chloride, Stock # 23566.

TABLE III
EQUIPMENT LIST FOR
EXPERIMENTAL APPARATUS

ITEM	Specification
AC Power Supply	California Instruments, Model 101 TC
Oscillator	California Instruments, Model 850 T
Flow Meter	Rotameter, Fischer & Porter Co. Model No. 10A6, 32N, Tube Specifications, FP-1/8-16-G-5/448 D009U01
Watt Meter	General Electric, Model No. 3720341, Amp-5/10 Volts-100/200, Watts 500/1000/2000
Multimeter	John Fluke Mfg. Co., Model No. 8050 A
High Voltage Probe	John Fluke Mfg. Co., Model 80K6
High Voltage Wiring	Taylor Pro-Wire, 8mm Silicone core
Transformer	Jefferson Luminous Tube Transformer, Cat. No. 721-411, Primary voltage 120V, 60 Hz, Secondary voltage 15,000V, 60 MA, Mid Point Grounding
Flare	Bunsen Burner, Model No. 124

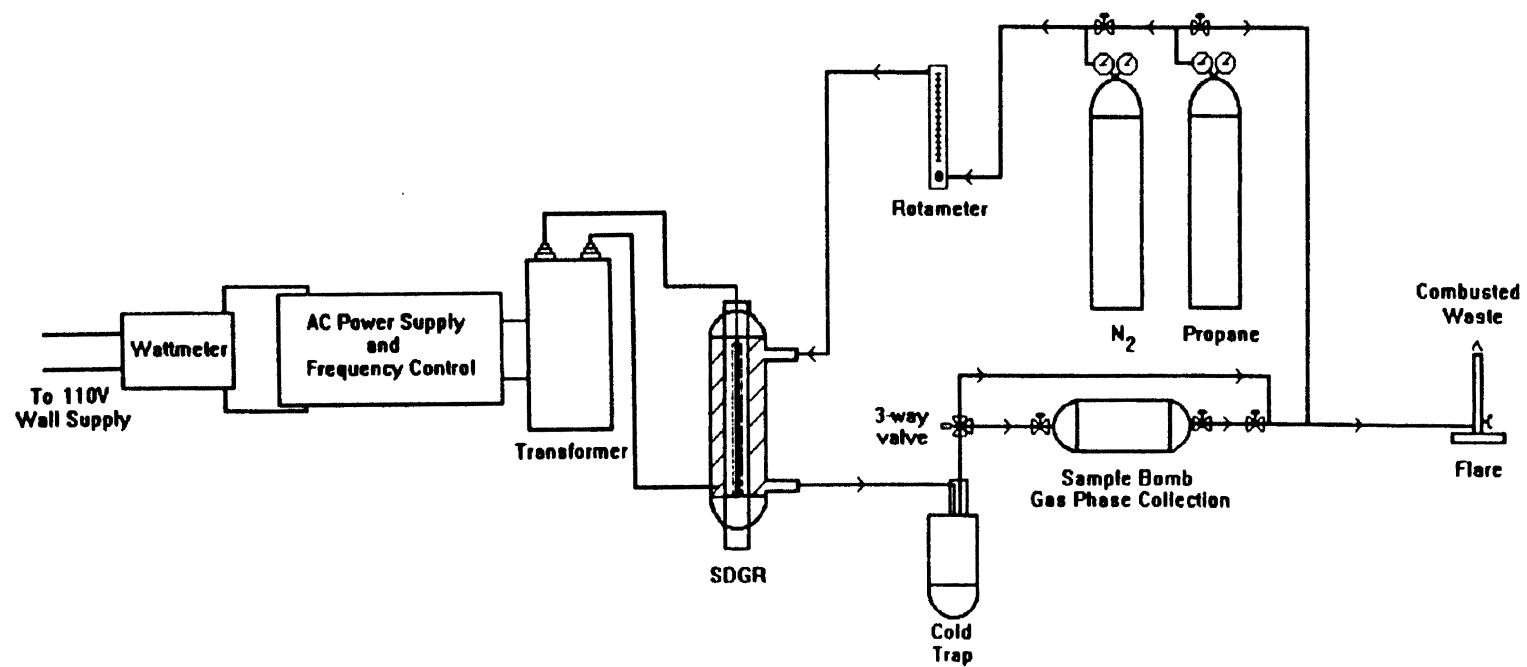


Figure 3. Experimental Apparatus for SGDR

Procedure

The following procedure outlines the basic steps taken in the experimental runs.

- 1) Sample collection vessels were placed in the apparatus.
- 2) Nitrogen flow was established and connections were checked for leaks.
- 3) Coolant was added to the cold trap as required.
- 4) After all leaks were corrected, nitrogen was allowed to flow for 5 minutes to insure system purging.
- 5) Propane flow was established at 10 psig line pressure. The flare was ignited.
- 6) Propane was allowed to flow for 3 minutes throughout the system.
- 7) Reactor was started and adjusted to desired settings.
- 8) Reaction was allowed to run for a minimum of 60 minutes to insure steady state plasma operation and system conditions.
- 9) Power to the SGDR was terminated.
- 10) Liquid phase sample removed from the nitrogen trap.
- 11) Residue within reactor removed by solvent washing.
- 12) Analytical procedures were conducted on individual samples.

This basic procedure was followed in an effort to establish experimental consistency within the data set. Various reactor configurations, operating conditions and feed flow rates are noted on Run Data Sheets. An example of this sheet as completed for run number HR-04 is given in Appendix D.

Analytical Procedure

Due to the number of possible compounds in reactions of this nature, individual component identification and compositions were not determined. Trends in production composition were broken into groups of components by approximate chain length and retention times in the liquid product.

Gas Phase Analysis

The main objective of this research was to investigate chain propagation. Therefore analysis of components that exist in the gas phase at room temperatures was not conducted.

Liquid Phase Analysis

Liquid phase components recovered from the cold trap, after reaching ambient temperature, were analyzed using gas chromatography. Gas chromatograph specifications are listed in Table IV.

Several components were analyzed under these operating conditions. Retention times of these components were recorded. Table V list the component and corresponding retention times.

Three groups were developed in classifying the liquid products. Group 1 consisted of components whose retention times are between n-pentane and n-octane. Group 2 retention times are between n-octane and n-decane. Group 3 retention times follow n-decane. This classification allows for group product distribution and the shifting of such groups under various reactor operating parameters

TABLE IV

GAS CHROMATOGRAPH SPECIFICATIONS
FOR LIQUID PHASE SAMPLES

Parameter	Specification
GC Make and Model	Hewlett-Packard Model # 8090A
Column Type and Cat. #	Alltech Cap. Cat. # 13638
Carrier Gas and Flow Rate	He 190 ml/min
Detector Type and Temp.	TCD, 250 °C
Injector Temp.	250 °C
Oven Ramp Rate	Ramp A 8 °C/min Ramp B 25°C/min
Injection Amount	1 microliter

TABLE V

COMPONENT RETENTION TIMES

Component	Retention Time (minutes)
Pentane	0.98 to 1.00
Hexane	1.44 to 1.48
Heptane	2.39 to 2.41
Octane	4.53 to 4.55
Decane	9.39 to 9.42
Dodecane	13.66 to 13.79

A mixture of the six components, used as retention time determinates, was analyzed in a matrix of methylene chloride solvent. The chromatogram for this mixture is given in Appendix M. The separation seen allows for the detection of various components with alternate retention times. The chromatograms of the actual liquid samples and

percent conversions will be given in Chapter VII. Conversions will be estimated on a mass basis from the collected sample.

Solid Phase Analysis

Residue remaining in the reactor as solid phase components were removed via solvent washing. The solvent containing the residue was placed in pre-weighed sample containers and allowed to evaporate. A net mass of the residue was then determined for conversion calculations.

CHAPTER IV

REACTOR EVALUATIONS UNDER NON-DESTRUCTIVE TEST

Previous work using SGDRs [12,40] characterized various reactors using non-destructive tests. Although these tests gave some general trends of the reactors, they were limited. Both Desai [12] and Tsai [40] limited their non-destructive observations to dry air only. Desai [12] further limited his observations to only one reactor and electrode configuration. Tsai, while developing a prediction model for breakdown voltage and frequency, did not alter the electrode configuration or effective plasma length in any reactor studied. It is one objective of this research to expand this previous work by altering the effective plasma length and observe the changes that result.

Procedure

The procedure for non-destructive test is as follows:

- 1) The reactor was placed in the experimental apparatus with the desired electrode configuration.
- 2) All required flow connections were made and checked for leakage. Sample collection vessels were by-passed.
- 3) All electrical connections were made.
- 4) Flow of the test fluid was established and set to desired flowrate.

- 5) Primary voltage to the reactor was set.
- 6) Frequency was increased from the initial setting to the final frequency by 20 Hz increments.
- 7) Operating conditions for each frequency point were recorded.

Reactor A

Non-destructive test for reactor A using three test fluids and the two electrode configurations yielded the data collected in Tables E1 through E7 listed in Appendix E. Figures 4, 5 and 6 graphically represent the relationship between secondary voltage and frequency at various primary voltages for ambient air, nitrogen and propane using a wrapped outer electrode configuration. Figures 7, 8 and 9 represent the data for the same test fluids and flow rates utilizing a mesh outer electrode configuration.

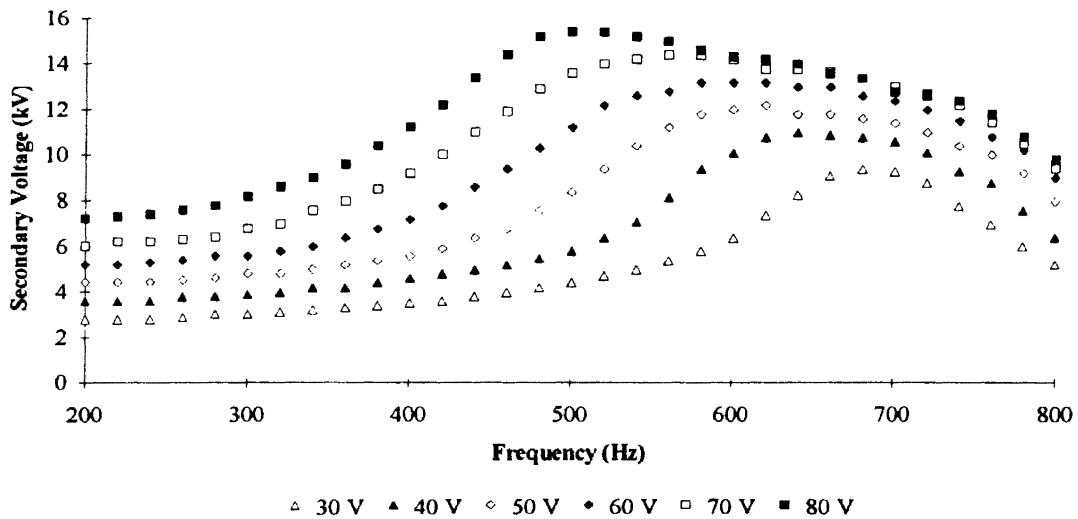


Figure 4. Effects of Frequency on Secondary Voltage at Various Primary Voltages, Ambient Air With A Wrapped Outer Electrode Configuration

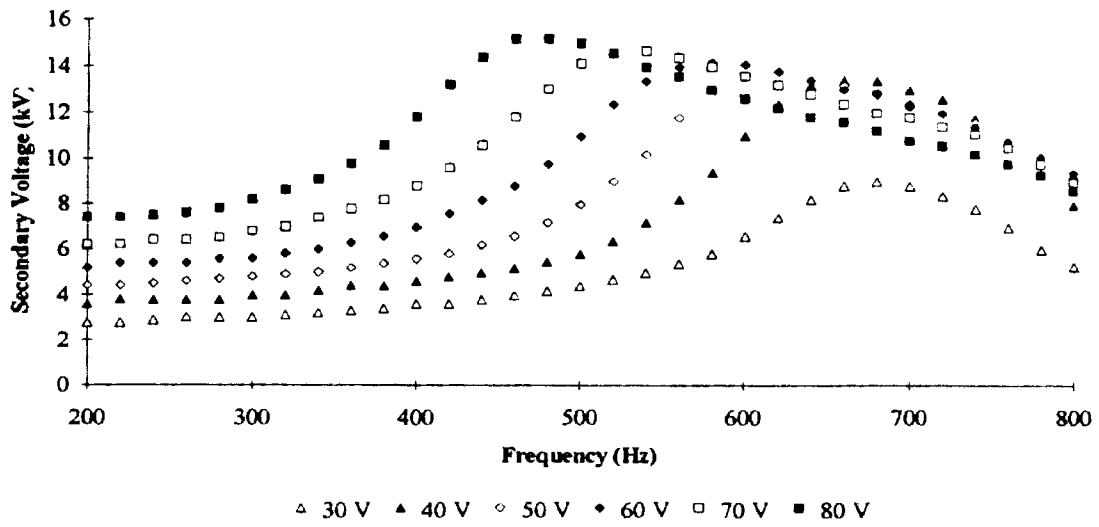


Figure 5. Effects of Frequency on Secondary Voltage at Various Primary Voltages, Nitrogen With A Wrapped Outer Electrode Configuration

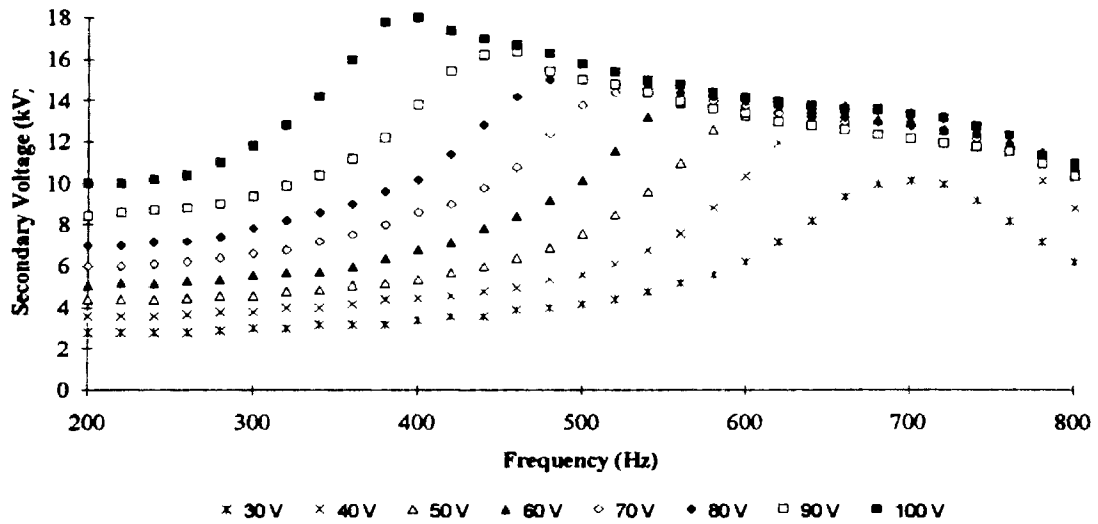


Figure 6. Effects of Frequency on Secondary Voltage at Various Primary Voltages, Propane With A Wrapped Outer Electrode Configuration

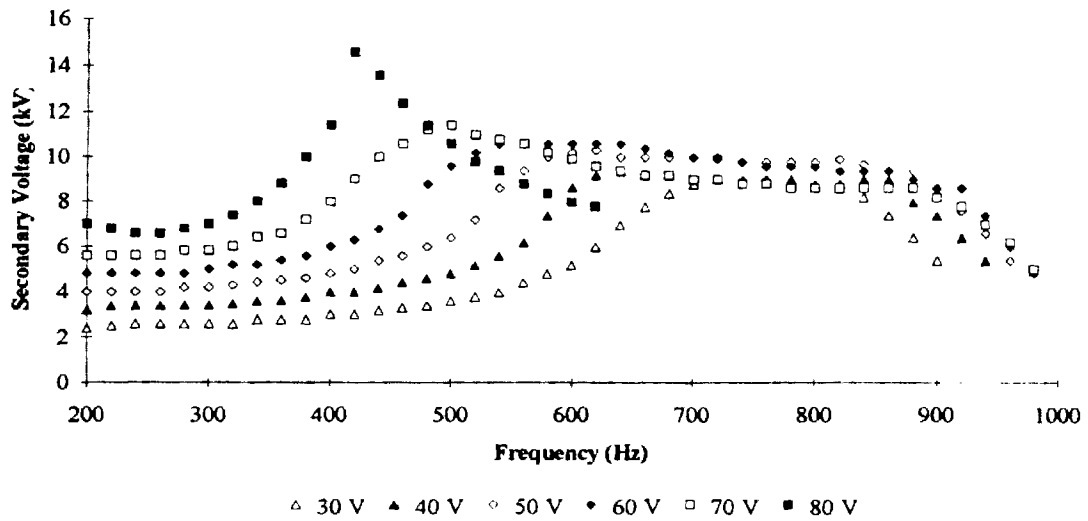


Figure 7. Effects of Frequency on Secondary Voltage at Various Primary Voltages, Ambient Air With A Copper Mesh Outer Electrode Configuration

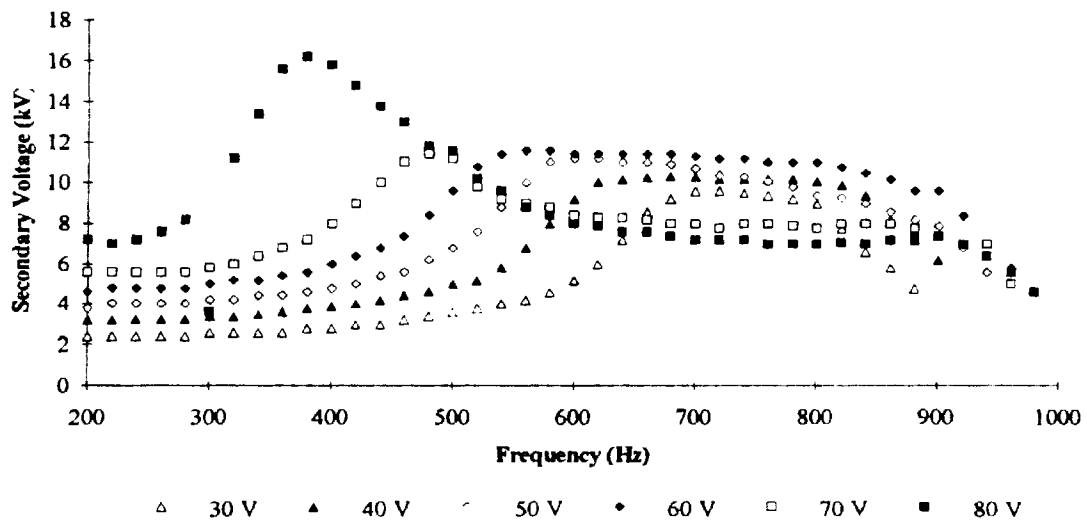


Figure 8. Effects of Frequency on Secondary Voltage at Various Primary Voltages, Nitrogen With A Copper Mesh Outer Electrode Configuration

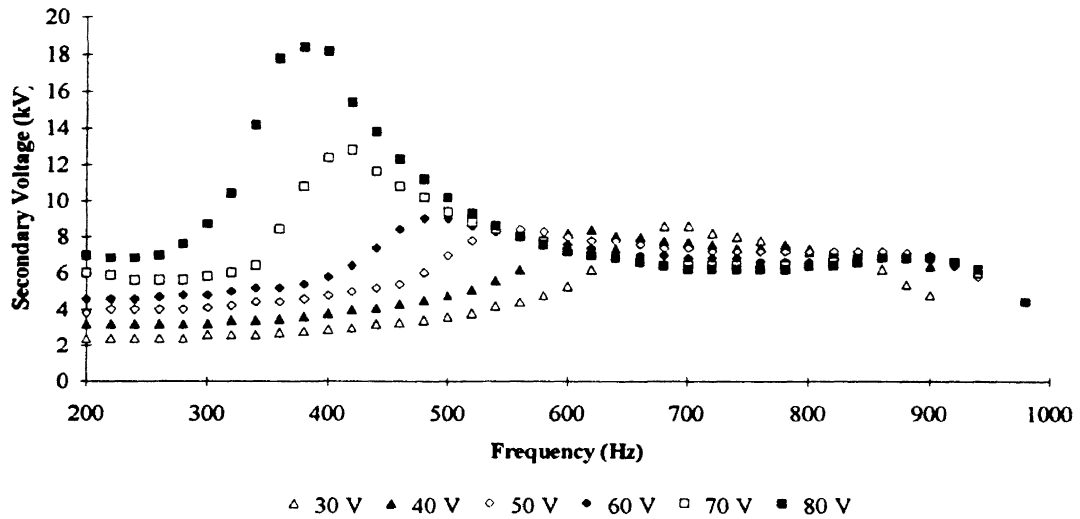


Figure 9. Effects of Frequency on Secondary Voltage at Various Primary Voltages, Propane With A Copper Mesh Outer Electrode Configuration

As frequency is altered, the secondary voltage passes through a maximum. Earlier work of Tsai and Desai concluded the same general trends existed, but only dry air was used as the test fluid. As seen in Figures 4, 5 and 6 the location for maximum secondary voltage varies by changing fluids. As an example, using a primary voltage of 80 volts the frequencies at which the maximums occur are 500-520 Hz for air, 460-480 Hz for nitrogen and 480-500 for propane with the mesh electrode configuration. It is evident that secondary voltage is a weak function of the physical properties of the fluid. Tsai [40] included this in the prediction model, but failed to show any data application due to the one fluid approach.

Outer electrode configuration also effected secondary voltage. As seen in Figures 7, 8 and 9 the rate of secondary voltage loss is decreased with the mesh outer electrode after the maximum was reached. This trend deviates in the highest primary voltage applications where a reversed effect is noted as the rate of loss is increased after the maximum. Secondary voltage maximums also shifted with this electrode configuration.

Comparison of the same fluid, reactor geometry and primary voltage show this change. As an example using propane and a primary voltage of 80 volts the shift is from 400-500 Hz using the wrapped outer electrode to 380-400 with the mesh outer electrode.

In all cases power consumption for the system increased as the maximum secondary voltage was approached. Power levels varied as the primary voltage was increased. This change in power requirement was a decrease at the lower frequencies, but an increase at the maximum secondary voltages. Figure 10 displays the power requirements for the propane test using the mesh outer electrode configuration. All experiments using reactor A have similar trends. Data for the power consumption is listed in Table E7 in Appendix E.

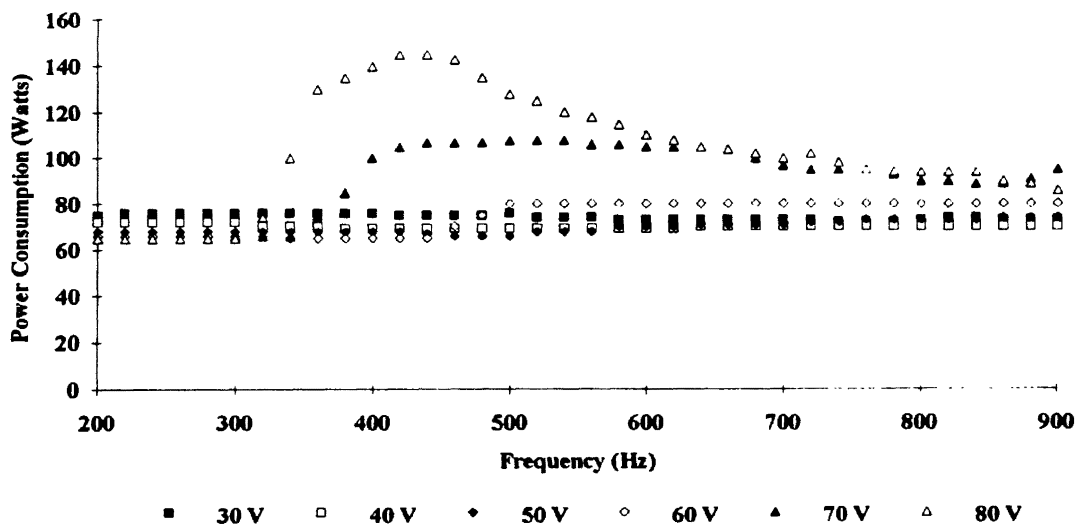


Figure 10. Power Requirements For Reactor A Using Propane And Mesh Outer Electrode

Reactor B

A similar approach was applied to reactor B using the same test fluids, flowrates and operating parameters. Figure 11 displays the data collected using ambient air and a wrapped outer electrode configuration. Figure 12 displays the same operating parameters using the mesh electrode configuration.

The same trends seen in reactor A also were developed in reactor B when comparing air for both electrode configurations. Tests using nitrogen and propane were conducted with only the mesh electrode configuration. Figures 13 and 14 display the effects of frequency on secondary voltage for nitrogen and propane tests, respectively. Data from these test are given in Tables F1 through F4 located in Appendix F.

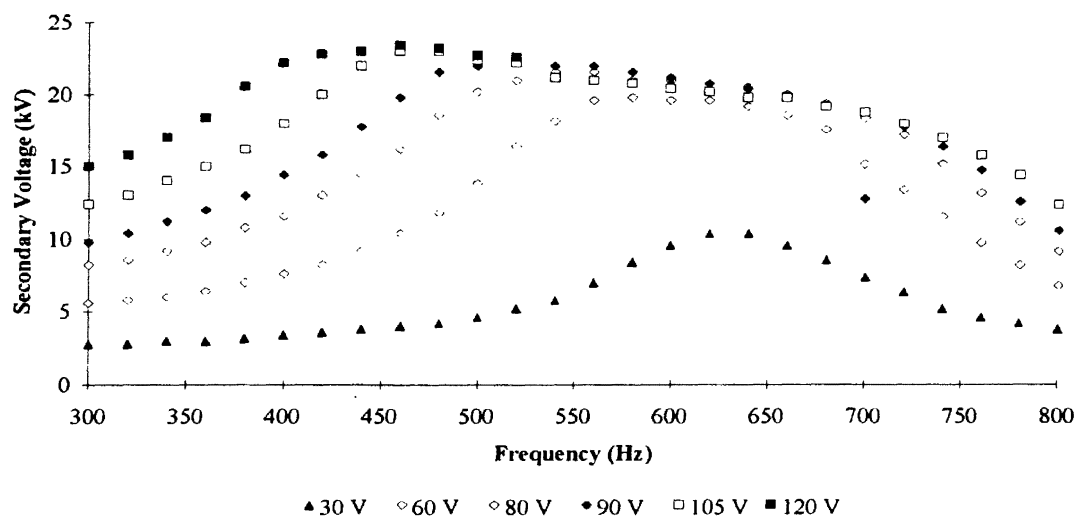


Figure 11. Effects of Frequency on Secondary Voltage at Various Primary Voltages, Ambient Air With A Wrapped Outer Electrode Configuration

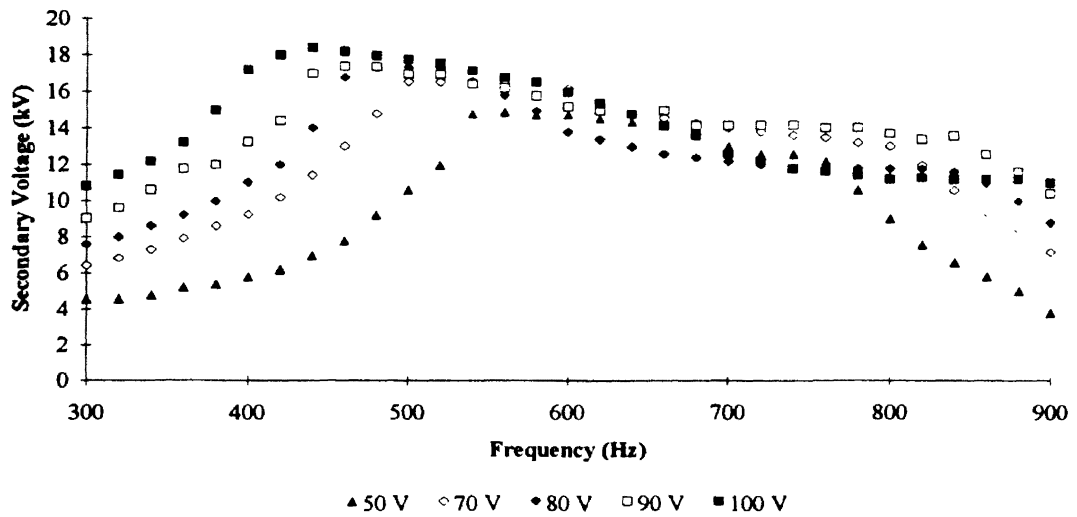


Figure 12. Effects of Frequency on Secondary Voltage at Various Primary Voltages, Ambient Air With A Mesh Outer Electrode Configuration

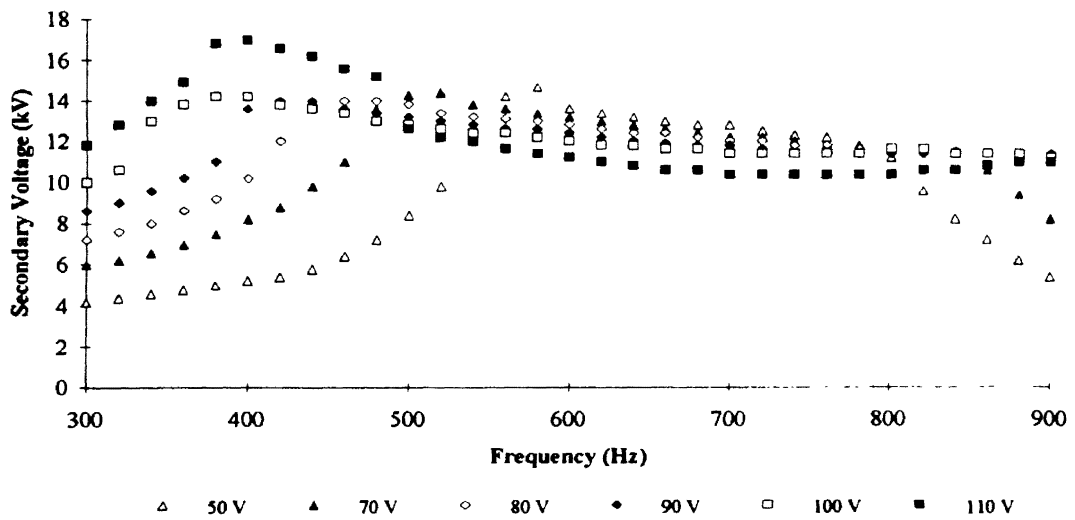


Figure 13. Effects of Frequency on Secondary Voltage at Various Primary Voltages, Nitrogen With A Mesh Outer Electrode Configuration

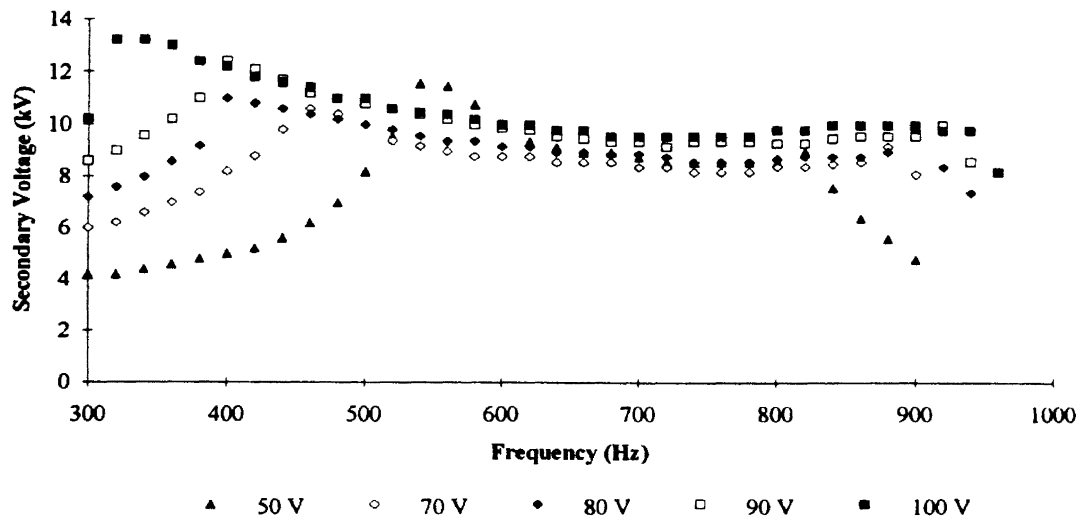


Figure 14. Effects of Frequency on Secondary Voltage at Various Primary Voltages, Propane With A Mesh Outer Electrode Configuration

The same effects in fluid and electrode changes are seen in reactor B that were observed in reactor A. Changes in the frequency required to obtain the maximum secondary voltage are again noted as functions of fluid type, electrode configuration and reactor geometry.

Power consumption also followed the same trends as in reactor A. Increases in required power is evident near the maximum secondary voltages. Figure 15 displays the power requirements using propane with a mesh outer electrode configuration.

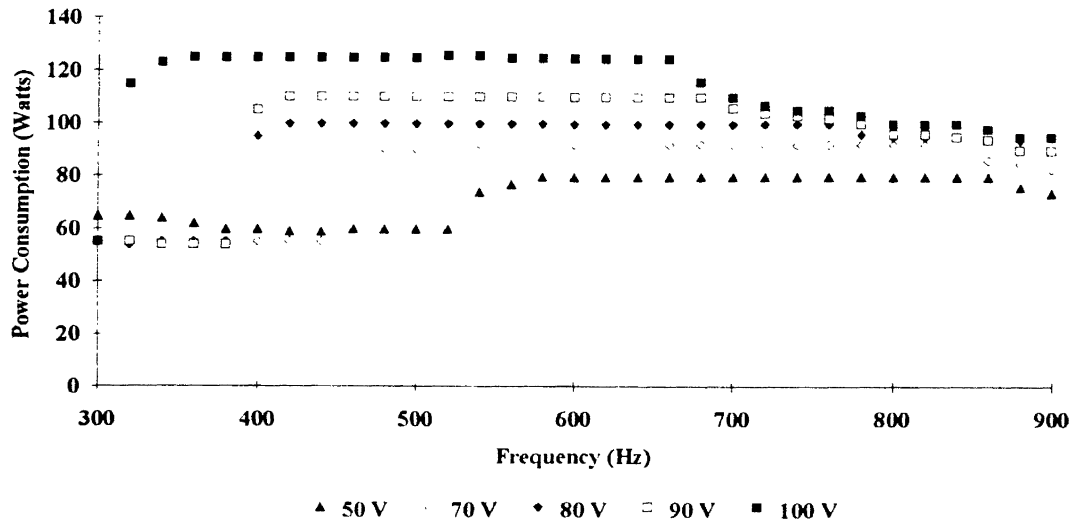


Figure 15. Power Requirements For Reactor A Using Propane And Mesh Outer Electrode

Reactor C

Reactor C has the same geometry as reactor B, but is increased in length. An effective plasma length of 36 inches can be observed with this reactor. Figures 16, 17 and 18 display the effects of frequency on secondary voltage for reactor C using a mesh outer electrode configuration on air, nitrogen and propane, respectively. Power consumption again follows the general trends as seen in reactors A and B. Figure 19 displays the data from the propane analysis. Data from these analysis are given in Table G1 through G4 in Appendix G.

In addition to the runs for reactor characterization, reactor C was also used to study the effects of plasma zone lengths on secondary voltage and power requirements. This reactor was chosen due to the 36 inch available zone length and geometry similarities to reactor B. Details concerning trends caused by this variable will be discussed at the end of this section.

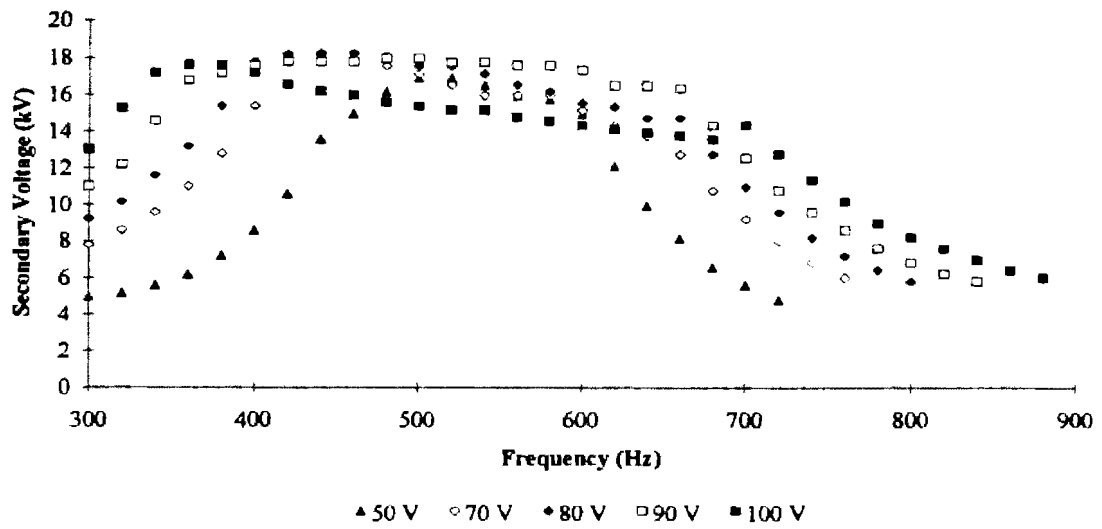


Figure 16. Effects of Frequency on Secondary Voltage at Various Primary Voltages, Ambient Air With A Mesh Outer Electrode Configuration

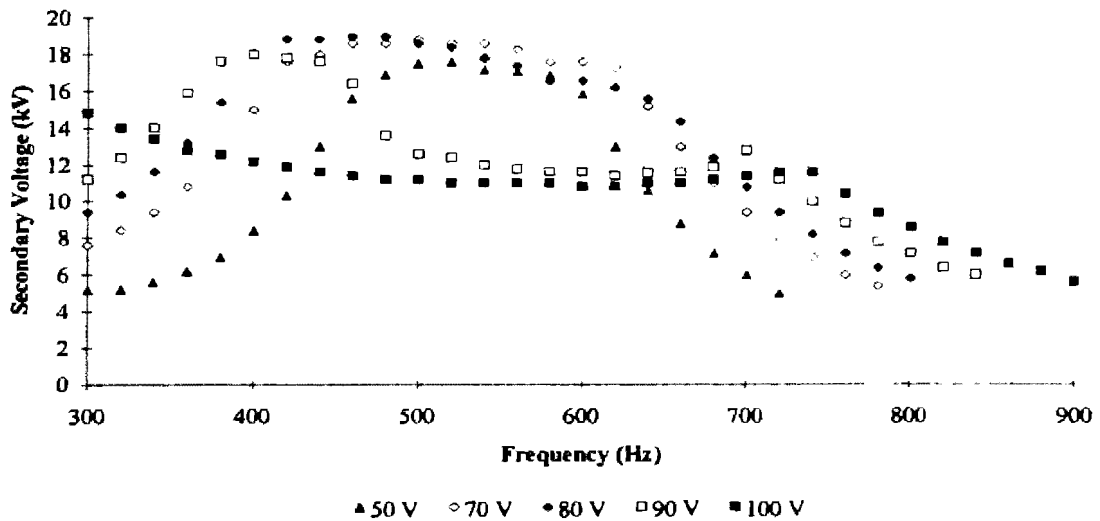


Figure 17. Effects of Frequency on Secondary Voltage at Various Primary Voltages, Nitrogen With A Mesh Outer Electrode Configuration

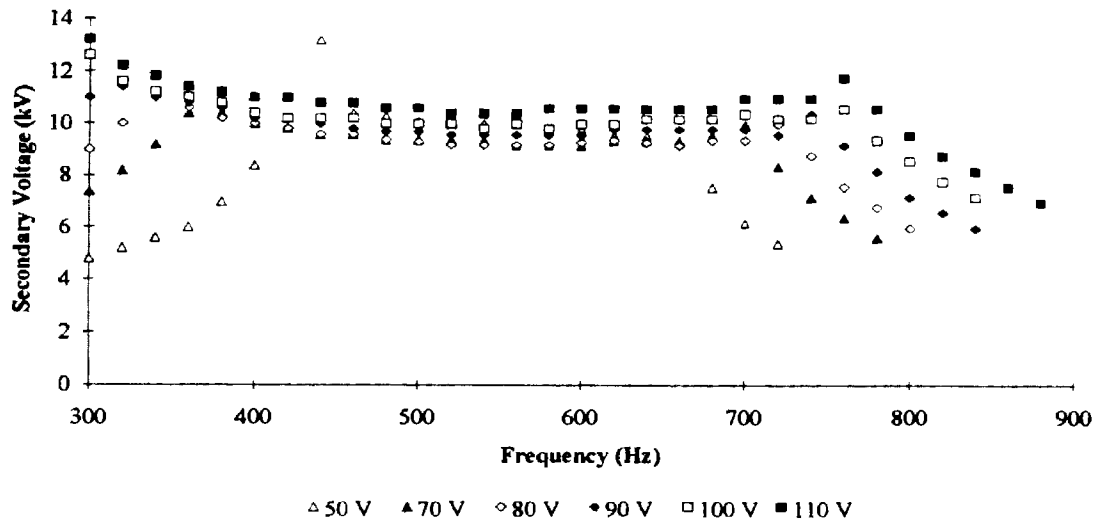


Figure 18. Effects of Frequency on Secondary Voltage at Various Primary Voltages, Propane With A Mesh Outer Electrode Configuration

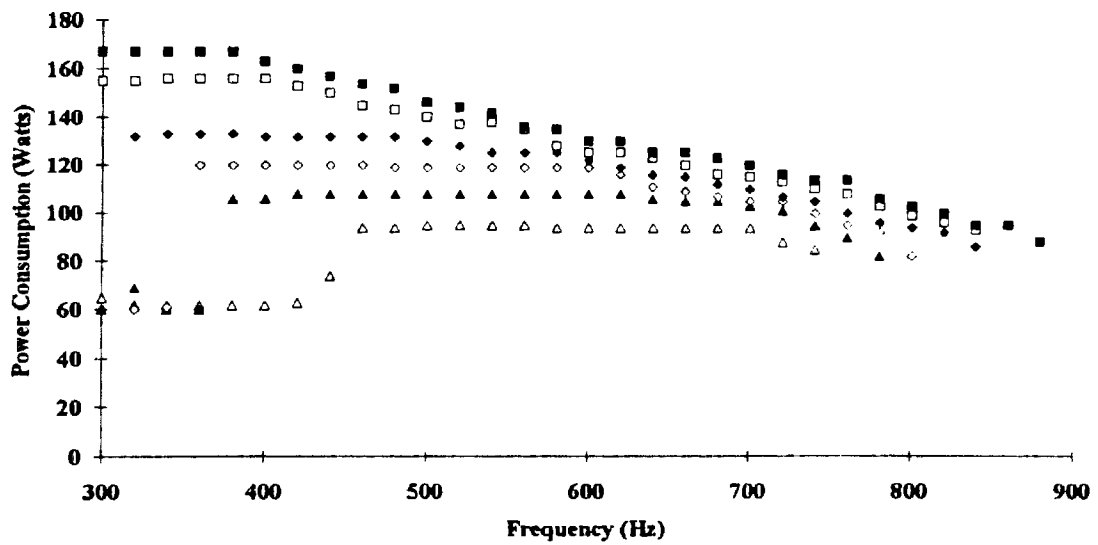


Figure 19. Power Requirements For Reactor C Using Propane And Mesh Outer Electrode

Trends in the power requirements for reactor C follow those previously observed. Comparisons of Figures 10, 15 and 19 all show that maximum power requirements are at the maximum secondary voltages. This trend holds for all reactors, electrode configurations and fluids studied.

Trends in the secondary voltage follow the same basic pattern in all reactors. In reactor A, B and C a maximum is reached at or through a narrow range of controlled frequencies. This maximum then decreases as the frequency deviates from the optimum. Although this decrease is seen in all applications, the rate varies as outer electrode configuration was altered. Comparison of Figures 4 & 7, 5 & 8 and 6 & 9 show the application of the mesh configuration slows the rate of secondary voltage loss when all other variables were held constant. This lengthening of the optimum frequency range will allow a more detailed study of frequency effects on bond cleavage in the rearrangement tests.

By applying a least squares fit to the data after the maximum secondary voltage, a statistical comparison of the rate losses was obtained. This method is not intended to fit the data, but allows comparison. Table VI gives these calculated rates for reactor A configurations. Supporting data are given in Appendix H.

It is also noted that as the electrode configuration was changed, maximum secondary voltages decreased. This effect may be contributed to the increase in plasma volume within the reactor. In applications using the wrapped electrode configuration the visible plasma was confined to the areas extending from the outer electrode to the inner mesh electrode. This produced a spiral shaped plasma within the reactor annulus. Applications of the mesh outer electrode configuration eliminated this effect. Mesh outer electrode configurations produced a fully developed plasma volume within the annulus. It is believed that this increase in plasma volume is responsible for the secondary voltage decrease. As required plasma volume is increased, by increases in the outer electrode surface area, the volume of gas being ionized also increases. This increases the

capacitance of the reactor. Details will be discussed in the model modification section.

Table VII show a comparison of the secondary voltages for reactor A at various primary voltages using the two outer electrode configurations. Reactor B shows the same trend for air. Data for this comparison is given in Appendix H.

TABLE VI

COMPARISON OF SECONDARY VOLTAGE
LOSS RATE FOR REACTOR A

Fluid	Primary Voltage (Volts)	Frequency (Hz)	Electrode Configuration	Rate Loss (Δ SV/ Δ Freq.)
Air	40	640-800	wrapped wire	0.014
Air	40	640-800	wire mesh	0.0028
N ₂	40	660-800	wrapped wire	0.019
N ₂	40	660-800	wire mesh	0.00065
C ₃ H ₈	40	680-800	wrapped wire	0.021
C ₃ H ₈	40	620-800	wire mesh	0.0031
Air	70	580-800	wrapped wire	0.010
Air	70	500-800	wire mesh	0.0046
N ₂	70	540-800	wrapped wire	0.010
N ₂	70	480-800	wire mesh	0.0051
C ₃ H ₈	70	560-800	wrapped wire	0.0055
C ₃ H ₈	70	420-860	wire mesh	0.0058

TABLE VII

COMPARISON OF SECONDARY VOLTAGES
FOR REACTOR A AT VARIOUS PRIMARY
VOLTAGES AND ELECTRODE
CONFIGURATIONS

Fluid	Primary Voltage (Volts)	Frequency (Hz)	Electrode Configuration	Secondary Voltage (kV)
Air	30	680	wrapped wire	9.4
Air	30	720	mesh electrode	9.0
Air	40	660	wrapped wire	11.0
Air	40	640	mesh electrode	9.4
Air	50	620	wrapped wire	12.2
Air	50	600	mesh electrode	10.2
Air	60	600	wrapped wire	13.2
Air	60	540	mesh electrode	10.6
Air	70	560	wrapped wire	14.4
Air	70	500	mesh electrode	11.4
Air	80	500	wrapped wire	15.4
Air	80	420	mesh electrode	14.6

It is these deviations that warrant the further investigation of Tsai's [40] prediction model. Under the current model, Tsai uses a relationship between the dielectric constants of the reactor walls and gas and reactor geometry. Equation (4) shows this predicted relationship as:

$$V_b = 10.96D_2\rho_f\left(1 + \frac{0.308}{(\rho_f D_2)^5}\right)\left(\frac{\ln(D_2/D_1)}{K_g} + \frac{\ln(D_3/D_2)}{K_a} + \frac{\ln(D_4/D_3)}{K_g}\right) \text{ kV} \quad (4)$$

where V_b = Predicted Breakdown Voltage, kV

K_g = dielectric constant of the reactor walls

K_a = dielectric constant of the gas in the annulus

ρ_r = relative density of gas in the annulus, g/cm³

D_i = corresponding diameters as shown in Figure 20., cm

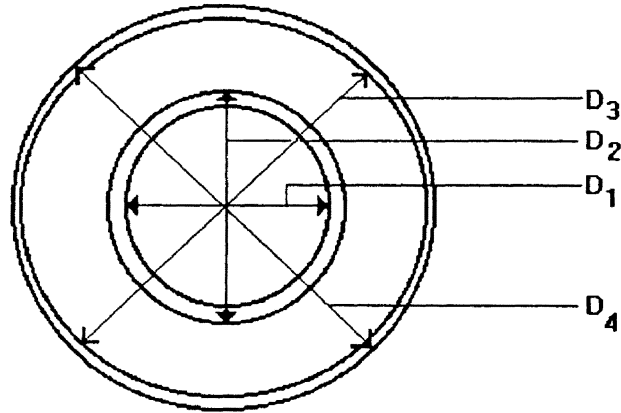


Figure 20. Cross-section View of Reactor Annulus

Although this model predicts the breakdown voltage for the reactors in Tsai's studies, the effects of plasma length in the reactors were not considered. This effect is one objective of this research and will be observed in applications of reactor C as discussed.

The changes in operational parameters have shown to produce similar effects on all the reactors observed. This observation is the basis for studying the effects of plasma zone length using only one reactor diameter ratio. It has also been shown from the previous non-destructive operations that the application of the copper mesh electrode provides plasma formation in a more uniform manner. Therefore, only reactor C with a copper mesh outer electrode configuration will be used in the observation of length effects.

Length Effects on Plasma Formation

Effects which are caused by the length of the plasma were studied in the following manner. By varying the effective lengths of the outer electrode and holding all other variables constant, the effects of length are isolated. Initially one wrap of 12 gauge wire was used as an outer electrode. The range of operating frequencies and primary voltages were reproduced as in the non-destructive testing. Secondary voltage and power requirements were recorded for each condition. The length of the outer electrode was then increased and the procedure repeated. Five lengths were used for data collection. Figures 21 through 25 display the effects of varying the outer electrode length on secondary voltage at various primary voltages and frequencies. Tables I1 through I5 in Appendix I list the collected data.

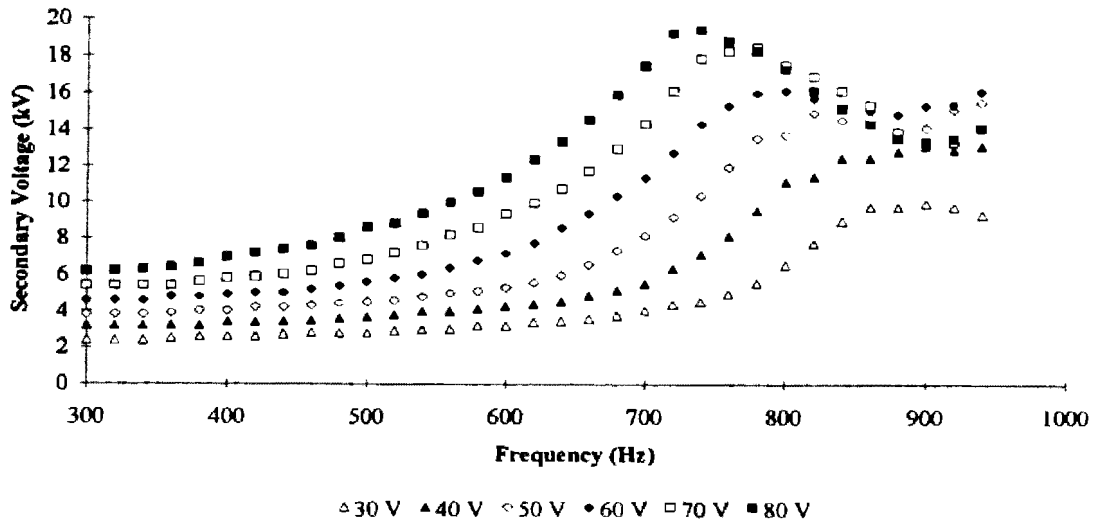


Figure 21. Effects of Frequency on Secondary Voltage at Various Primary Voltages, Nitrogen With One Wrap 12 Gauge Wire Electrode

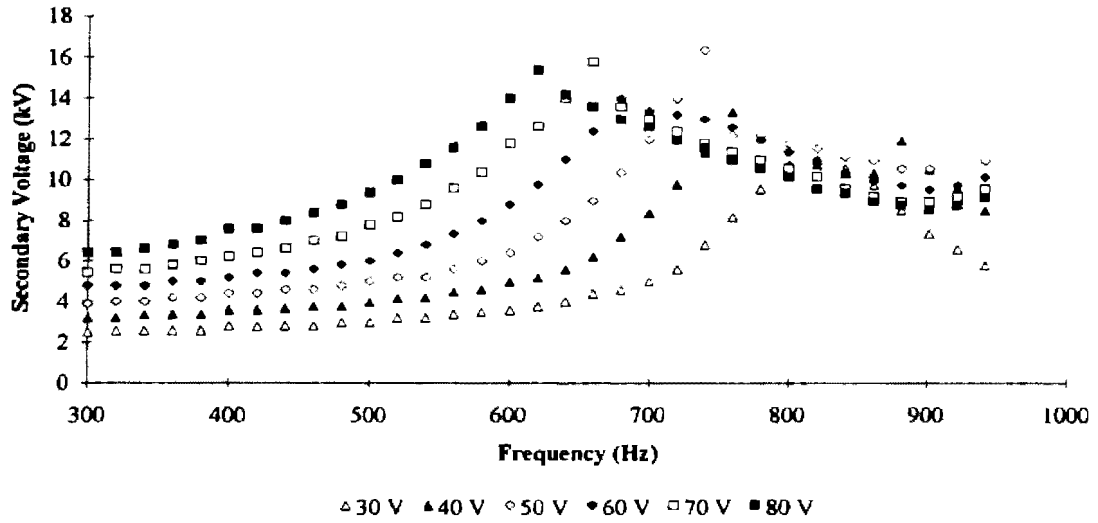


Figure 22. Effects of Frequency on Secondary Voltage at Various Primary Voltages, Nitrogen With 2.5 Inch Mesh Electrode

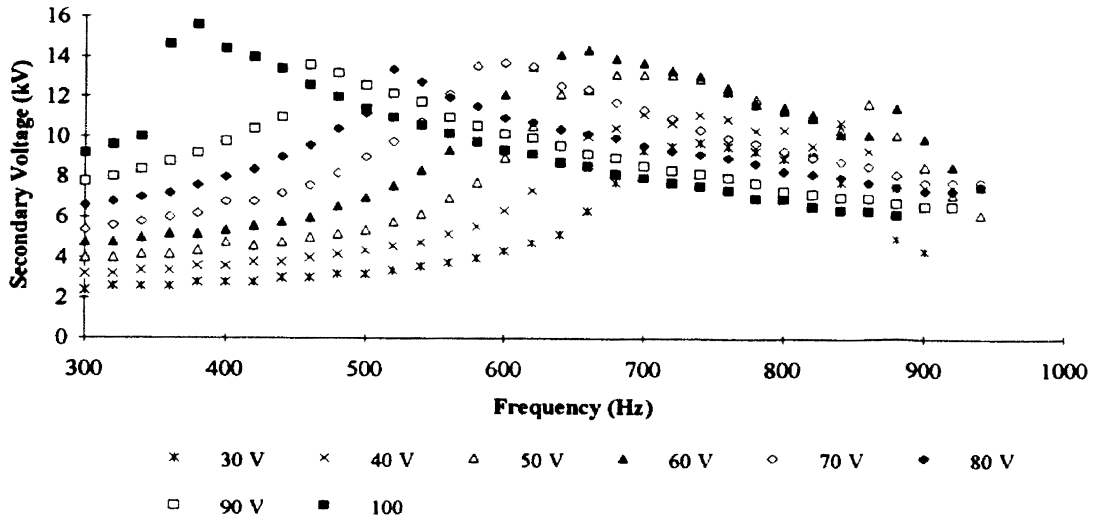


Figure 23. Effects of Frequency on Secondary Voltage at Various Primary Voltages, Nitrogen With 6.5 Inch Mesh Electrode

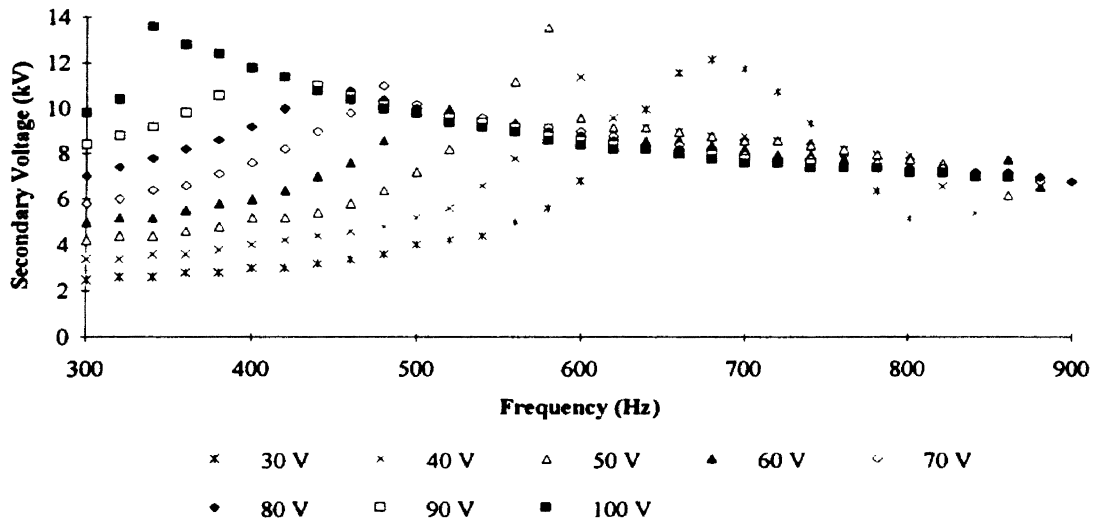


Figure 24. Effects of Frequency on Secondary Voltage at Various Primary Voltages, Nitrogen With 12.5 Inch Mesh Electrode

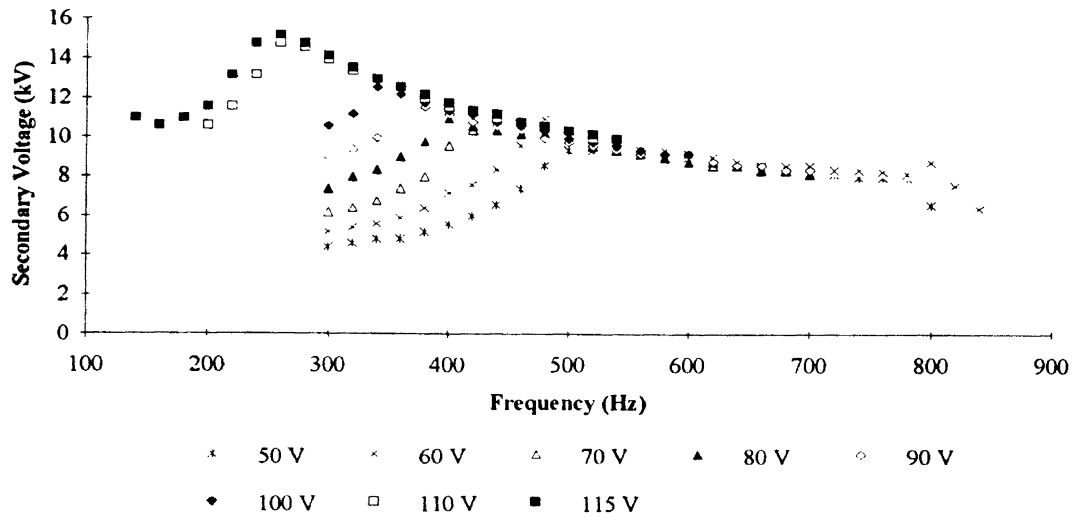


Figure 25. Effects of Frequency on Secondary Voltage at Various Primary Voltages, Nitrogen With 17.75 Inch Mesh Electrode

The trends seen in experiments using these reactor configurations follow those seen in the non-destructive test for reactors A, B and C. Secondary voltage reaches a maximum at some specific frequency for each primary voltage tested. Comparison of Figures 21 through 25 show a deviation in this location and maximum value that is dependent on plasma zone length only. As the plasma zone length was increased, secondary voltage decreased and maximum location was shifted to a lower frequency. This trend holds for all cases except at a primary voltage of 30 V where plasma formation was difficult to establish. Figures 26 through 33 display these effects. Collected data are listed in Tables I6 through I13 in Appendix I.

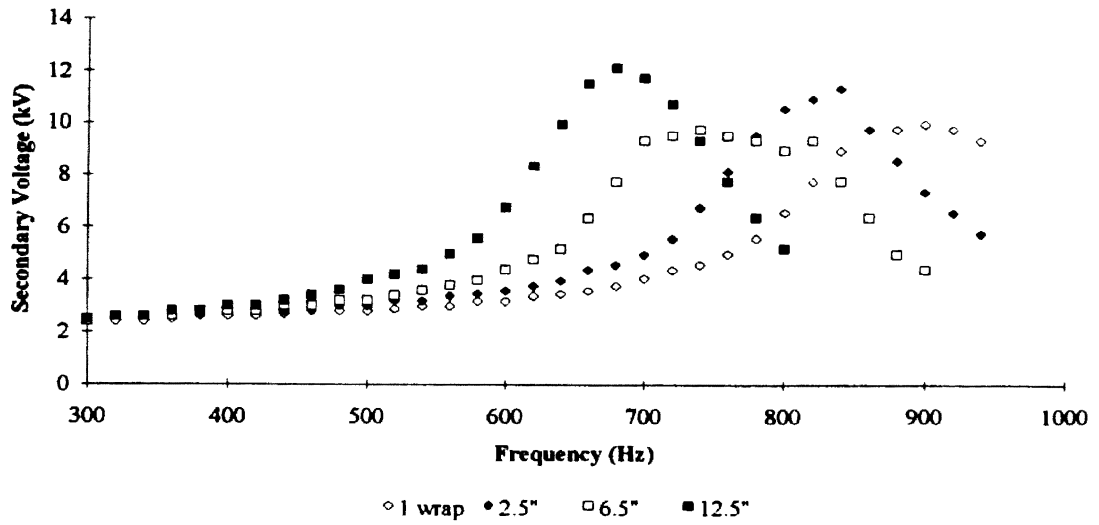


Figure 26. Effects of Plasma Zone Length on Secondary Voltage at 30 Primary Volts

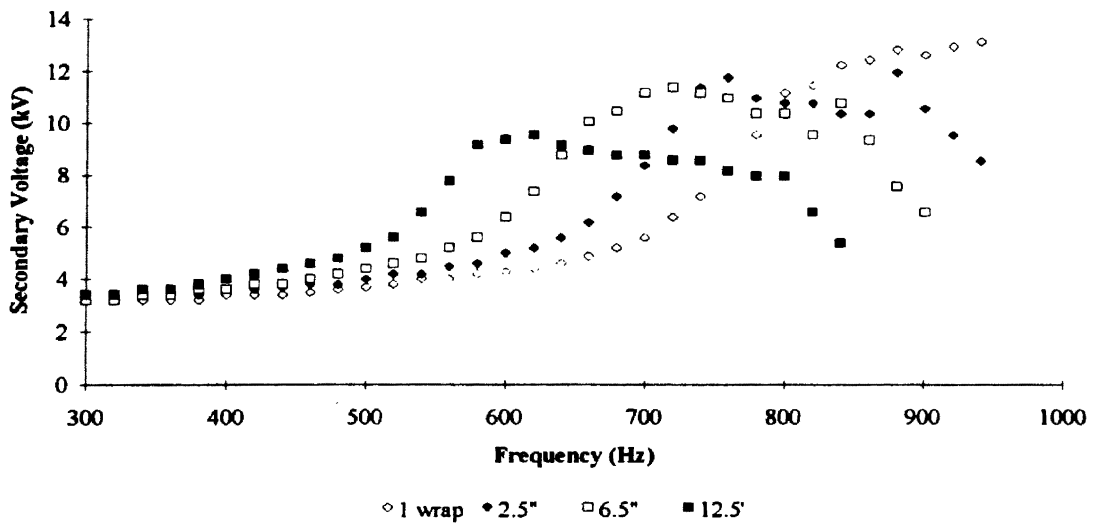


Figure 27. Effects of Plasma Zone Length on Secondary Voltage at 40 Primary Volts

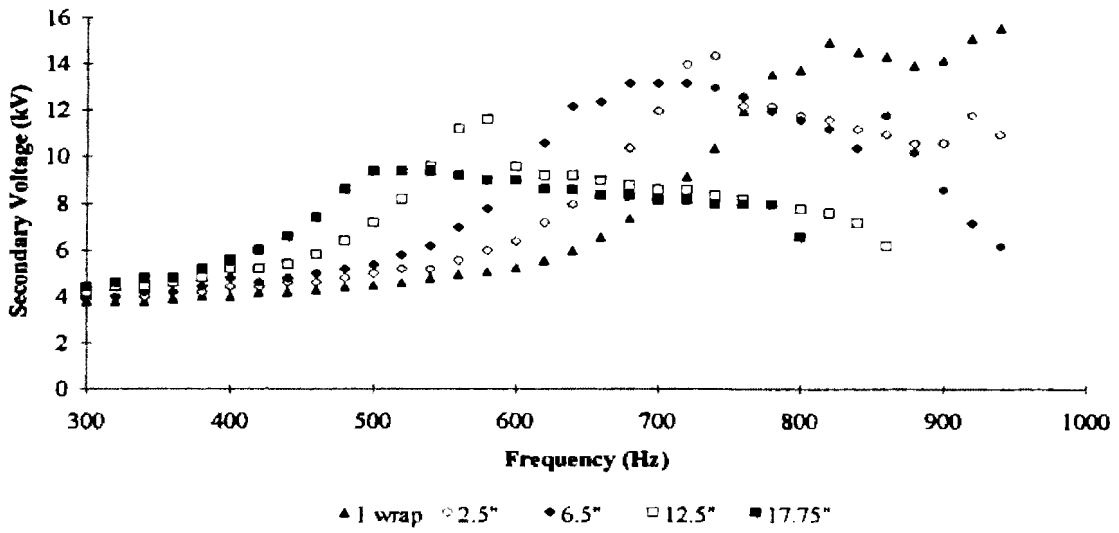


Figure 28. Effects of Plasma Zone Length on Secondary Voltage at 50 Primary Volts

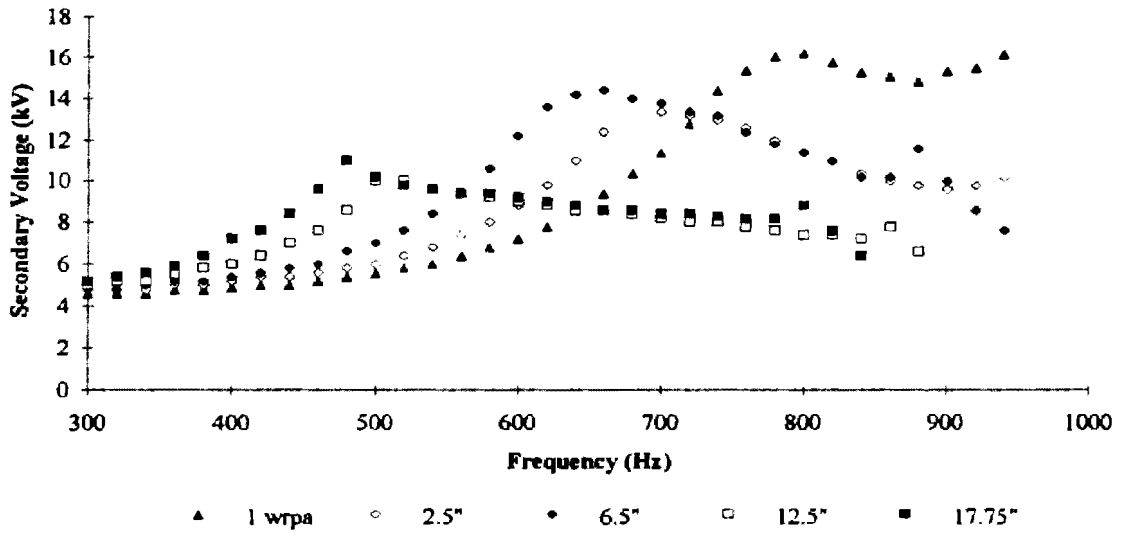


Figure 29. Effects of Plasma Zone Length on Secondary Voltage at 60 Primary Volts

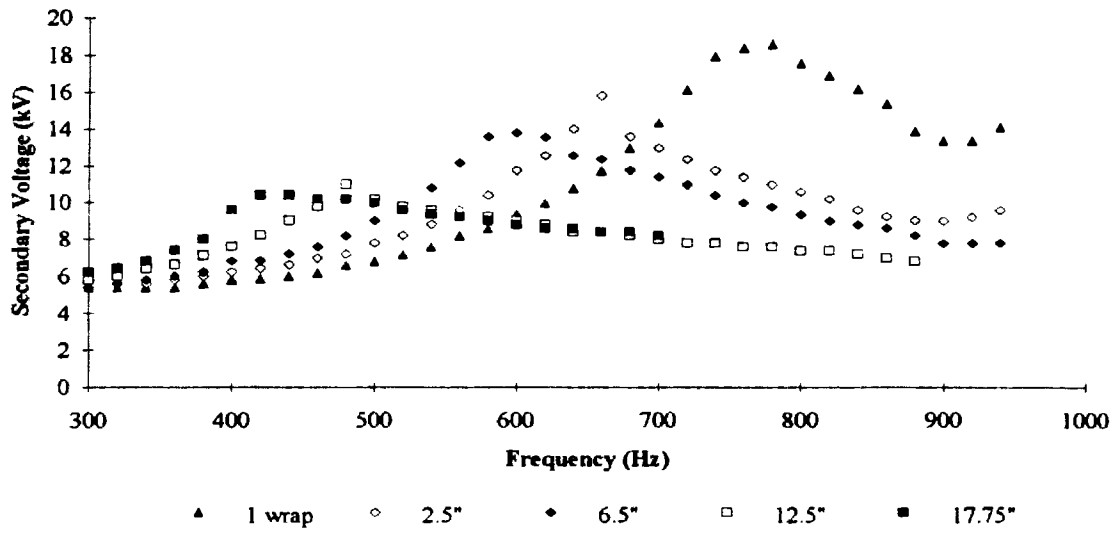


Figure 30. Effects of Plasma Zone Length on Secondary Voltage at 70 Primary Volts

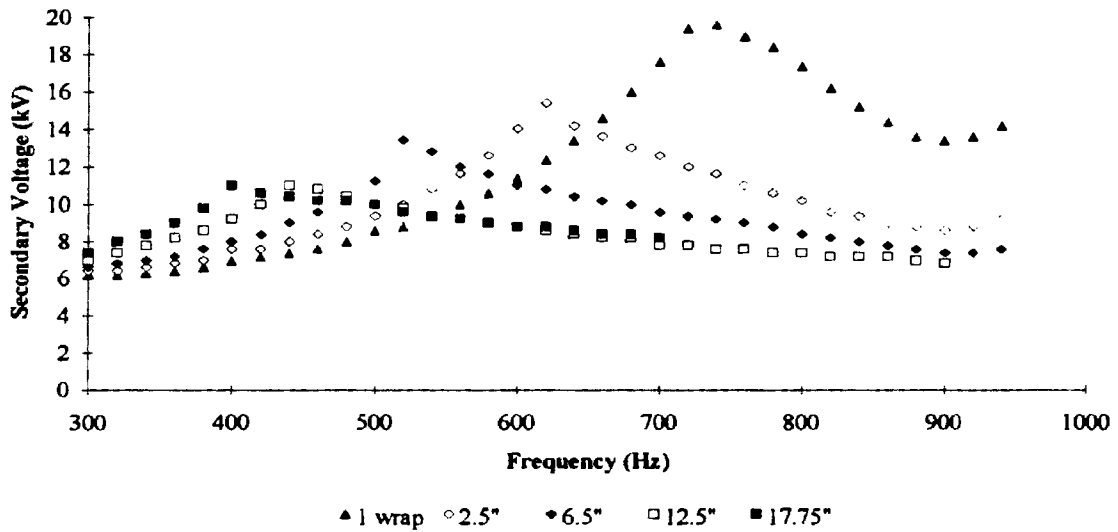


Figure 31. Effects of Plasma Zone Length on Secondary Voltage at 80 Primary Volts

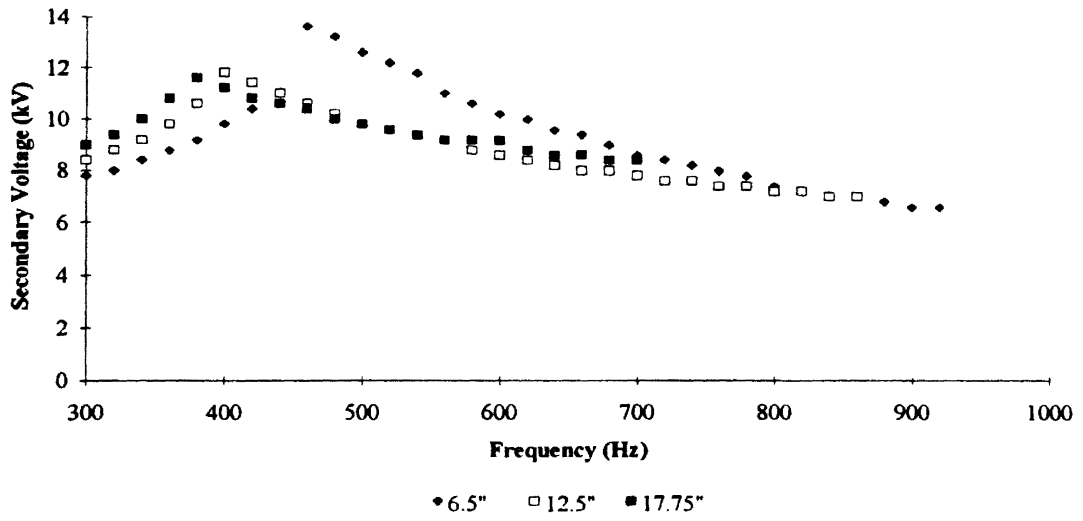


Figure 32. Effects of Plasma Zone Length on Secondary Voltage at 90 Primary Volts

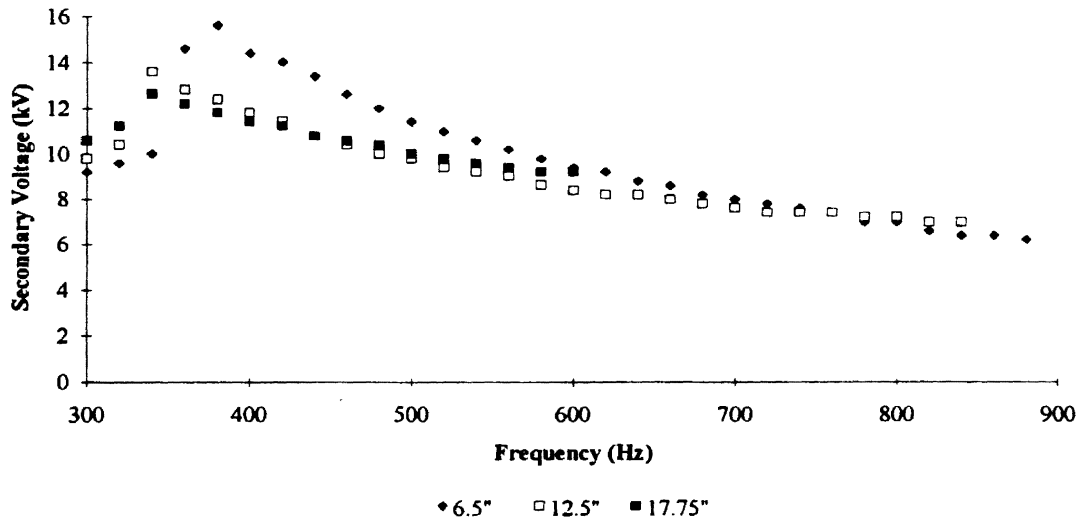


Figure 33. Effects of Plasma Zone Length on Secondary Voltage at 100 Primary Volts

The data collected is sufficient to establish the need for modifications in the prediction model. Prediction of the required breakdown voltage using Tasi's model will not allow for length deviations. Further problems arise from the definition of breakdown voltage. The actual magnitude of the visual plasma is not defined. The first visual plasma, class 1 by definition, occurs at a much lower secondary voltage than a fully developed plasma, class 4 by definition. Modification of this model will be in an effort to relate plasma length, reactor geometry and required dielectric values to the development of the first visible class 4 plasma in each reactor geometry.

Chapter V details the model modification.

CHAPTER V

MODEL MODIFICATIONS

Examination of Figures 26 through 33 reveal the length effects in the required breakdown voltage. As the length was increased the secondary voltage decreased for the formation of a class four plasma. Tsai failed to investigate this variable in his prediction model. The prediction model, equation 4, was applied to the reactors used in Tsai's research [40] with acceptable results. Deviation ranged from 0.1 to 9.2 % in the reactors studied. Development of a more accurate prediction method for the formation of a class four plasma was required after application of the previous model to reactors used in this portion of study. Deviation between the predicted values and those experimentally obtained, using equation 4, are listed in Table VIII.

This data shows that as the length decreases from the value used in Tsai's research the deviation increases. This trend can be explained by examination of the capacitance of the reactors.

In general, capacitors consist of charged plates separated by a dielectric. Figure 34 displays the typical capacitor arrangement using two flat plates.

TABLE VIII

DEVIATIONS OF PREDICTED BREAKTHROUGH
VOLTAGES AS COMPARED TO
EXPERIMENTAL VALUES

Reactor Configuration (mesh outer electrodes)	Predicted Value (kV)	Experimental Value (kV)	Deviation (%)
Reactor B, 44.13 cm	13.22	13.2	0.0
Reactor C, 0.1 cm	13.22	18.4	28.2
Reactor C, 6.35, cm	13.22	15.2	13.1
Reactor C, 16.51 cm	13.22	14.6	9.5
Reactor C, 31.75 cm	13.22	13.6	2.9
Reactor C, 44.13 cm	13.22	13.2	0.0
Reactor E, 44.13 cm	14.34	14.4	0.05



Figure 34. Typical Plate Type Capacitor

Kantor [21] develops the governing equation for capacitance calculation of plate type capacitor as:

$$C = K_e \epsilon_o \frac{A}{d} \quad (5)$$

where

C = Capacitance, Farads

K_e = Dielectric constant of substance between plates

ϵ_o = The permittivity of free space, 8.85×10^{-12} Farads/meter

A = Area of plates, m

d = Distance between plates, m

This equation is the basis of the reactor capacitance estimation.

Two factors were considered in the derivation for reactor capacitance estimation. First three dielectrics were used. The two reactor walls and the fluid in the annulus. Second was the tubular shape of the reactor. For composite dielectric layers the total value is sum of the dielectric contributions. Using equation 5 as the basis the following derivation was completed.

For a cylinder

$$A = \pi DL \quad (6)$$

on each surface. Thus the surface area changes as it travels through the dielectric. A more correct area of consideration would be substituting the log-mean diameter into equation 6. This is given by

$$D_{\ln} = \frac{D_o - D_i}{\ln \frac{D_o}{D_i}} \quad (7)$$

where D_o and D_i are the outside and inside diameters of the cylindrical dielectric layer, respectively.

thus equation 6 becomes

$$A = \pi L \frac{D_o - D_i}{\ln \frac{D_o}{D_i}} \quad (8)$$

d is the effective distance between the plates. This distance between two concentric cylindrical electrodes is determined by the difference of the diameters. Thus

$$d = D_o - D_i \quad (9)$$

and equation 5 is now written as

$$C = \varepsilon_o \pi L K_e \left(\frac{D_o - D_i}{\ln \frac{D_o}{D_i}} \right) \quad (10)$$

This allows calculation of the capacitance for a cylindrical shaped capacitor. In the reactor geometry three layers exist with varying dielectric constants. The interface of these dielectric layers act as an effective conducting medium between each dielectric. It is therefore possible to estimate the effective capacitance of the reactor as three cylindrical capacitors in series. Total effective capacitance is thus summed as

$$\frac{1}{C_t} = \frac{1}{C_1} + \frac{1}{C_2} + \frac{1}{C_3} \quad (11)$$

Substituting equation 10 for each layer into equation 11 the total effective capacitance is estimated by

$$C_t = \varepsilon_o \pi L \left[\frac{\ln\left(\frac{D_2}{D_1}\right)}{K_1} + \frac{\ln\left(\frac{D_3}{D_2}\right)}{K_2} + \frac{\ln\left(\frac{D_4}{D_3}\right)}{K_3} \right]^{-1} \quad (12)$$

where C_t = Total effective capacitance, Farads
 ε_o = Permittivity of free space, 8.85×10^{-12} Farads/meter
 L = Length of plasma zone in meters
 K_i = Dielectric constant of substance in layer i
 D_i = Respective diameters of dielectric layer i

This relationship was then applied to the various reactor geometries listed in Table II. Table IX list the calculated capacitance of each geometry.

Brotherton [8] relates the effects of capacitance on resistance by the relation

$$R = r + \frac{g}{\omega^2 C^2} \quad (13)$$

where R = Total effective resistance, ohms
 g = Empirical constant based on capacitor geometry
 ω = Frequency, Hz
 C = Total capacitance, Farads
 r = Resistance of leads and conductors, ohms

This relation shows the logarithmic effects of capacitance on resistance. This change in resistance directly alters the voltage across the reactor. Ohm's Law [8] shows this change as

$$V = IR \quad (14)$$

Because of the low current through the transformer, 0.62 mA, the resistance changes have the controlling effects on voltage.

In the reactors studied the length changes were responsible for the changes in capacitance. Thus the changes in length altered the resistance of the reactor. Surprisingly as the length was increased the resistance decreases exponentially. This accounts for the increases in required secondary voltage as the length decreased. Figure 34 shows the logarithmic effects of length on secondary voltages for class 4 plasma development.

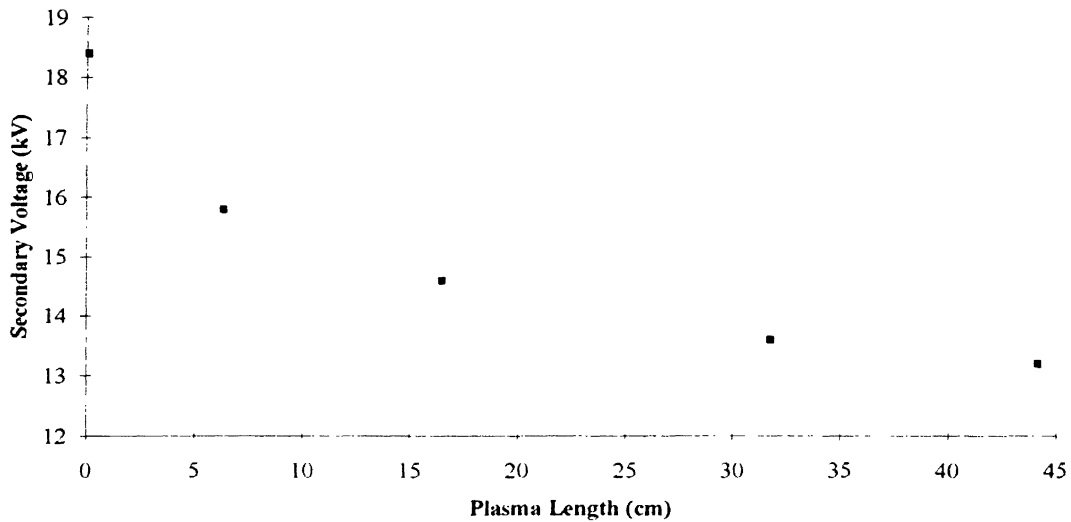


Figure 35. Effects of Plasma Length on Secondary Voltages At First Class 4 Formation

Inspection of the prediction model in equation 4 reveals a close comparison to the capacitance relation of equation 13. Correction values were determined from the experimental secondary voltages and the predicted values from equation 4. These correction values were then plotted against the length of each plasma for an empirical development correction. Table Curve™ [40] was incorporated for this procedure. Appendix J contains the plotted data and statistical information from this application. The results lead to a correction of equation 4 for length changes as

$$V_b = \frac{10.96}{(0.709 + 0.046x^5)} D_2 \rho_f \left(1 + \frac{0.308}{(\rho_f D_2)^5} \right) \left(\frac{\ln(D_2/D_1)}{K_g} + \frac{\ln(D_3/D_2)}{K_a} + \frac{\ln(D_4/D_3)}{K_g} \right) \quad (15)$$

where V_b = Predicted "Breakdown Voltage," kV

x = Length of the plasma formation zone, cm

All other variables remain as in equation 4.

This modified model allows more accurate prediction of the required secondary voltages in class 4 formations with zones up to 45 cm. It is not recommended for application outside the configurations of a mesh or solid outer electrode. Lengths of the application are also limited to those observed.

TABLE IX

CALCULATED CAPACITANCE OF REACTORS
USING EQUATION 11

Reactor Configuration	Capacitance (10^7) (Farads)
Reactor A, mesh outer	15.4
Reactor B, mesh outer	24.8
Reactor C, mesh outer	51.5
Reactor C, one wrap	0.056
Reactor C, 6.35 cm	3.57
Reactor C, 16.51 cm	4.68
Reactor C, 31.75 cm	17.9
Reactor C, 44.13 cm	24.8
Reactor D, mesh outer	68.6
Reactor E, mesh outer	68.6

CHAPTER VI

DESTRUCTIVE TEST

The main thrust of this research is the investigation of SGDR applications to propane pyrolysis. It is predicted this application will result in the production of various hydrocarbons due to chain length alterations and various isomer formations during radical controlled rearrangements. Chain propagation to the liquid phase components is the major area of interest.

Due to the qualitative nature of this research, visual observations describe currently unexplained phenomena. These observations are detailed through the chapter.

Initial Observations

The first trials were an effort to investigate the transfer of energy by means of the SGDR. Piatt [34] and Tsai [40] both demonstrated the ability of a SGDR to aid in the oxidation of hydrocarbons, however radical formation of a pure substance was not investigated. This lack of application warranted a short preliminary study.

Using reactor A, three rearrangement experiments were conducted. See Appendix K for operation parameters of runs HR-004, HR-005 and HR-006. In these preliminary test no liquid sample collection was attempted. Samples of the gas phase product were collected in stainless steel sample bombs and analyzed. Analysis of the individual samples was conducted by Phillips Analytical Services in Bartesville, OK. Analytical specifications

are unavailable. Results, listed in Appendix K, show the products as a mixture of various hydrocarbons ranging in size to above a six carbon length compound. This preliminary investigation confirmed the possibilities of chain propagation and rearrangement using a SGDR.

The corona formed during these initial test appeared as a blue tint. No noticeable extended chain hydrocarbons were seen condensing along the reactor walls. After run HR-006 was completed, visual inspection of the reactor showed slight deposits of residue along the reactor walls. No sample was obtained.

Initial Rearrangement Test

Reactors B, C, and D were used in the initial detailed study, but failed during operation. Reactor D was operable for experimental runs HR-015 and HR-016. Investigation in the cause of these failures revealed a weakness in the physical properties of Pyrex for these applications. As the runs were longer in duration than the non-destructive test, heating of the reactor walls were more pronounced. This heating was restricted to the plasma zone. Expansion of the reactor in the zone due to heating was greater than the expansion of the non-effective zone causing thermal stresses in the reactor walls. As these stress fractures would widen under heating, a reduction in the dielectric effects occurred in that area. This in turn increased the plasma strength causing extreme temperatures at point locations in the reactor walls. Pin holes in the reactor walls normal to the surface of the wall resulted from thermal decomposition of the Pyrex. Similar observations were seen in earlier tests [12] under higher pressures in various Pyrex reactors.

Experimental runs HR-015 and HR-016 yielded the first collectable liquid sample. Operating parameters are listed in Appendix K. Plasma location was altered between the two runs and is shown in Figure 36. This had significant effects from both a qualitative visual observation and a quantitative sample analysis.

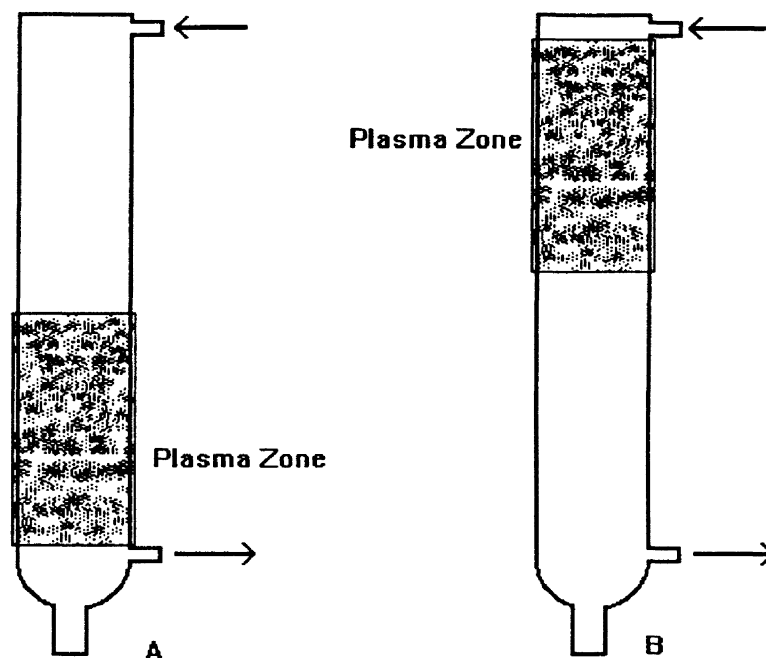


Figure 36. Plasma Zone Orientation

Visual observations for run HR-015, reactor geometry in Figure 36 A, noted the formation of an aerosol within the annulus of the reactor. This formation developed above the reactor zone. The turbulence of the plasma was also demonstrated by the back mixing effects in the aerosol. Residue collection on the reactor walls was also seen in this run for the first time. Liquid phase hydrocarbon formation condensed on the reactor annulus above the plasma zone. Gravity effects caused the liquid phase to be returned to the plasma zone where vaporization appeared to occur. Small amounts of liquid were seen condensing in the area below the plasma zone. Again a blue tint plasma was visible at the beginning of the run. This tint changed to a very faint greenish tint at the inner annulus boundary.

Sample collection in the liquid cold trap yielded a collection amount of 0.05 g. GC analysis of the collected sample showed a distribution of 98.068% less than C₈, 1.091%

between C₈ and C₁₀ and 0.843% greater than C₁₀. Sample chromatogram is listed in Appendix M.

Zone location to that in Figure 36 B was used for run HR-016. This altered both visual effects and quantitative results. The formation of the aerosol shifted to the area below the plasma zone. This had two positive effects on the reaction. The first was the elimination of the backmixing effects. This elimination allowed the complete formation of a compound without re-exposure to the destruction zone. Second was the allowance of the liquid residue to move away from the plasma zone. This allowed for the residue to remain in the liquid phase during the run. Again the tint of the plasma was initially blue, changing to a greenish tint along the walls. This was more evident in this run.

Sample collection netted 0.09 g of liquid. GC analysis yielded the following distribution. Less than C₈ 72.691% , between C₈ and C₁₀ 27.198% and 0.111% greater than C₁₀. Sample chromatograph is given in Appendix M.

Conversion for each test is based on the procedure given in the experimental section of this report. Run HR-015 yielded 0.50% while run HR-016 yielded 0.91% conversion to liquid product.

Rearrangement Test Using Reactor E

Reactor E was used for the remaining rearrangement test and showed no visible signs of stress or thermal failure. The location of the plasma zone was placed as that in Figure 36 B. Three distinct series of runs were made to evaluate the effects of the adjustable parameters. These parameters were secondary voltage, frequency and retention time of the fluid in the plasma zone. It is a major objective of these studies to see the effects of frequency control on both product conversion and distribution.

Secondary Voltage Effects

Effects of secondary voltage were isolated by holding both frequency and retention time constant while adjusting primary voltage. Five secondary voltages were used to establish trends in operational changes. Individual run data is listed in Appendix L in Table LI. Table LII in Appendix L list the analysis results of the samples in relation to the applied secondary voltages. Chromatographs for this series are given in Appendix M. Figure 36 graphically displays this data.

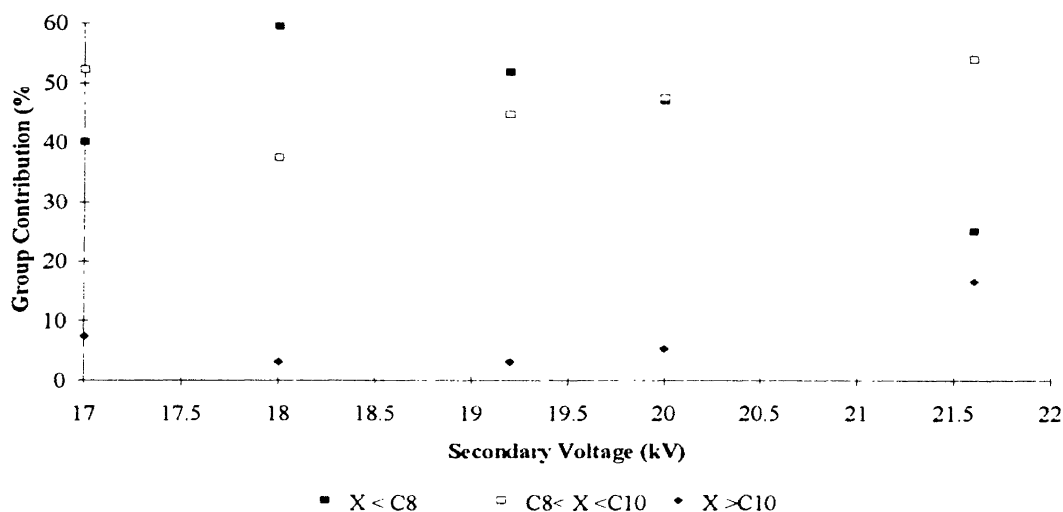


Figure 37. Effects of Secondary Voltage on Product Distribution
Frequency 310 Hz, Flow 64.89 ml/min

As seen in Figure 37, alterations of secondary voltage cause shifts in group contribution. The shift in the amount of product to higher molecular weight compounds at the lowest and highest applied secondary voltages can be described in an energy comparison. At lower settings the available energy to cleave molecular bonds decreases. This decrease causes a bond selectivity process to begin. Higher chained and branched hydrocarbons require less energy for bond separation than smaller n-chained compounds. Therefore more large radicals are produced. As the concentration of these larger radicals increase the probability of long chain coupling is enhanced.

At the other extreme, the highest secondary voltage, the energy in the system is sufficient to sustain heavier compounds from reaching the reactor walls. This creates a carry-over effect forcing larger chained compounds further down the reactor. Some possibly reach the end of the reactor to the collection trap. It is also possible that at these high energy levels compound radicals are formed. A compound propyl radical is shown in Figure 38. This type of formation would then react very aggressively at both ends, thus enhancing chain propagation.

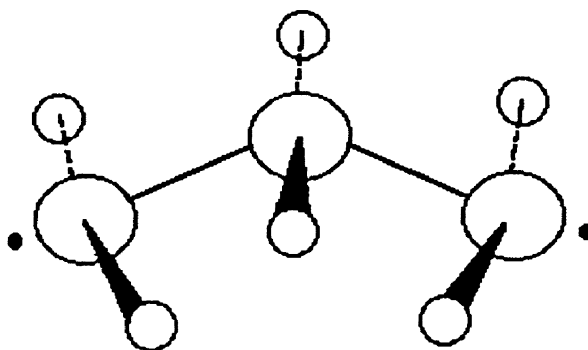


Figure 38. Compound Propyl Radical

Total sample amounts collected for the low and high secondary voltages vary only 0.01 gram in favor of the lower setting.

Visual observations during this series of tests revealed an increase in the intensity of green tint in the reactor. This can be attributed to the increased carbon-carbon bond cleavage taking place. Other visual effects were an increase in the amount of aerosol production at the intermediate voltages when compared to the low and high operations. This aids in substantiating the proposed reasoning for group shifting.

Residence Time Effects on Group Distribution

Effects of residence time on product distribution follow a predictable pattern. As the residence time is decreased, the total energy transfer to the molecules is not sufficient to enhance bond cleavage thus a minimum time is required. Residence times below this value will result in very limited amounts of liquid phase products being produced. Increasing residence time would also cause a shift in the amount of liquid phase product due to an over propagation of chain length. This would be characterized by increasing solid residue along the reactor wall.

Four tests were conducted to evaluate the proposed effects. Table LI in Appendix L list the operation parameters for the individual runs. Table LII in Appendix list the sample analysis results. Chromatograms for this series are given in Appendix M. Figure 39 and 40 displays these graphically.

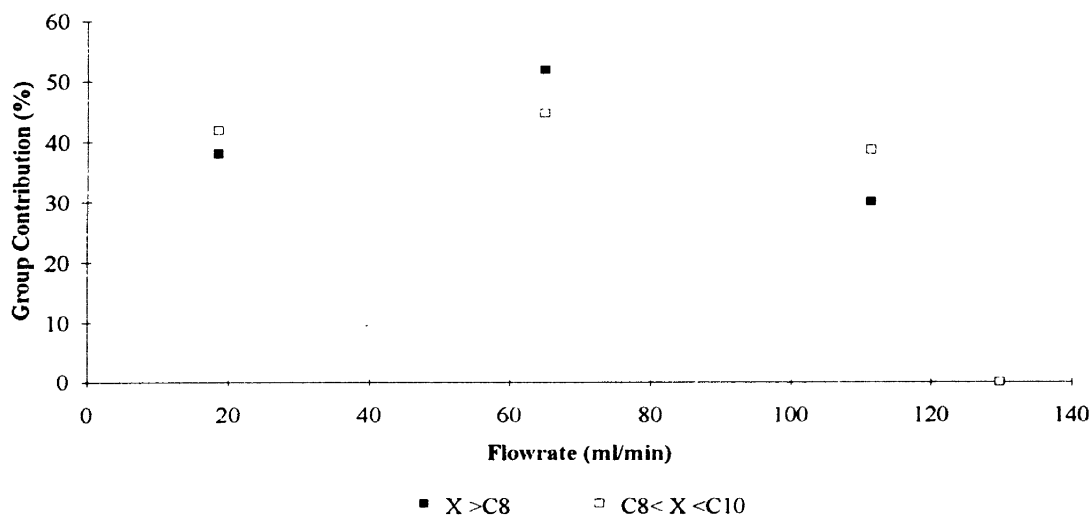


Figure 39. Comparison of Flowrates on Group Contribution

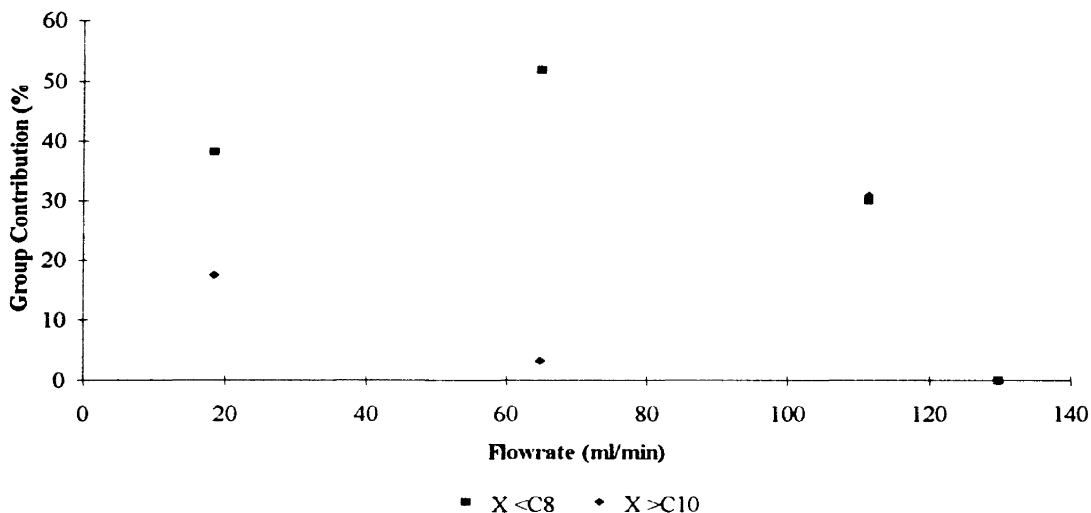


Figure 40. Comparison of Flowrates on Group Contribution

Effects from altering residence time follow the expected trends. Visual observations also aided in studying the effects. At the upper flowrate, no aerosol was visible within the annulus. At the lowest flowrate two observations were noted: 1) the extreme collection of residue on the reactor walls and 2) the color change from the previously observed green tint to a pink coloration along the walls.

Total conversion to liquid phase samples deviated from the moderate flowrate as expected. The highest conversion of 6.09% was bonded by the extremes of 2.02% and 2.72% at the lower and upper flowrates respectively.

Frequency Effects on Group Distribution

The last variable in the operation parameters is of the greatest interest in this research. By changing the frequency and causing shifts in the group distribution a new technique for hydrocarbon reaction control is opened.

Five test were conducted at a constant flowrate and secondary voltage while frequency was altered. The minimum, maximum and optimum frequencies were located

for this geometry and used as reference frequencies. Two additional settings were then chosen between the optimum and the end points of operation. Table LI in Appendix L list the operation parameters for the series test. Analysis of individual samples is listed in Table LII also in Appendix L. Chromatograms for this series are given in Appendix M. Figure 41 graphically displays these effects.

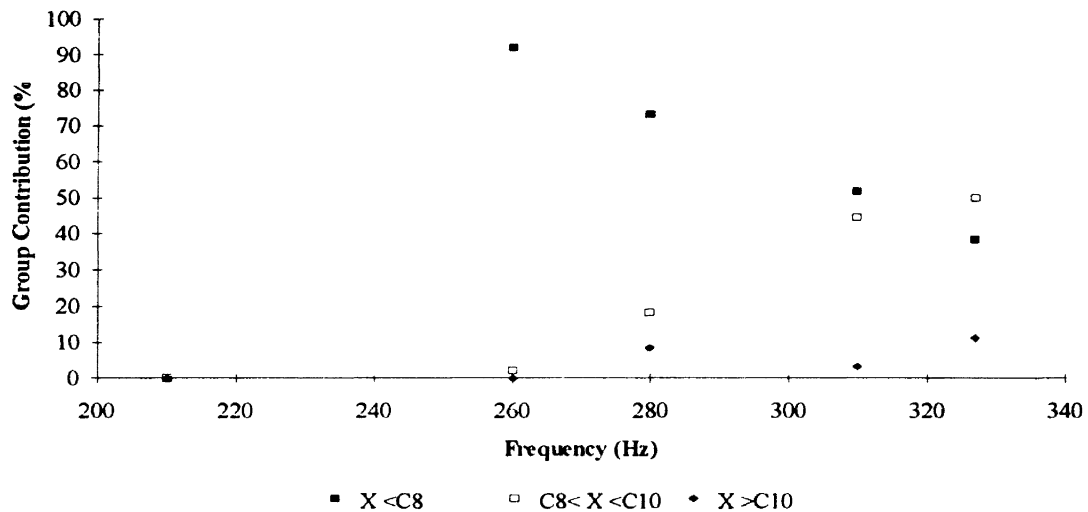


Figure 41. Effects of Frequency on Product Distribution
Secondary Voltage 19.2 (kV),
Flow 64.89 ml/min

Figure 41 dramatically displays the trends seen in product distribution as frequency was altered. As frequency was increased, contribution to total composition was altered by a decreasing value for Group 1 and an increasing value for Group 2. Group 3 does not show a clear trend at this time. The lowest frequency of 210 Hz yielded no liquid phase product.

Conversions were also effected by the frequency changes. The highest conversion of 6.09% was established at 310 Hz. Deviation from this frequency in either direction lowered the total conversion to liquid phase components.

The visual observations during this series were similar to those of previous runs. The initial color of the plasma formation carried a blue tint changing to a greenish tint

along the reactor walls during operation. One key observation was the formation of a plasma at the minimum frequency setting with no liquid product collected. During this test the production of the aerosol was not visible, nor was any residue seen collecting on the reactor walls. This change from previous test suggest two possible explanations. First the reactions within the plasma are limited to only gas phase products, or no reactions were present. The formation of the plasma carried no green tint during operation. It is therefore possible that the plasma formation is visible only by electron transfers from elevated energy shells back to their ground state yielding energy releases in the form of photons.

Conversion Results From Residue Production

Component analysis of residue in the reactor was unable to be accomplished due to limited analytical capabilities currently available through the Chemical Engineering Department. Thus only an estimated total conversion for all test was calculated. A conversion of 5.56% to the solid phase was obtained.

SUMMARY

From the experimental data collected changes in frequency, secondary voltage and residence time all effected the product distribution. The most significant trend is the effect of frequency variation to group contribution for the liquid phase. Although total conversion to liquid phase components is small, trends were observed to establish product control. By controlling the residence time, secondary voltage and frequency a narrow band of products should be feasible.

CHAPTER VII

CONCLUSIONS AND RECOMMENDATIONS

It has been shown that several distinct facts can be concluded from the data collection and analysis in this study. These are listed in Table XI and will be discussed on an individual basis. Like wise several recommendations for further research and improvements on methods used in this study are listed in Table XII and are discussed individually.

TABLE XI

CONCLUSIONS FROM PROPANE PYROLYSIS USING A SGDR FOR ENERGY TRANSFER

Numerical Assignment	Brief Description
1	Prediction of required secondary voltage is a function of reactor capacitance.
2	Hydrocarbon pyrolysis is possible utilizing a SGDR for energy transfer.
3	Product distribution is controlled by secondary voltage, residence time and frequency.

TABLE XII

RECOMMENDATIONS FOR FUTURE
RESEARCH

Numerical Assignment	Brief Description
1	Reduction of reactor energy losses to the atmosphere.
2	Development of prediction method as function of sine wave and primary voltage.
3	Alternate arrangements of power source.
4	Effects of decreasing plasma strength throughout plasma zone.
5	Complete sample group analysis.
6	Accurate analysis of fluid in the annulus.

Prediction of the required secondary voltage to establish a class 4 plasma is a function of the capacitance in the reactor. As the capacitance was increased, due to length increases, the resistance of the reactor decreased exponentially. This decrease was seen in the changes required to establish the corona in various reactor zone lengths.

Pyrolysis of hydrocarbons using a SGDR was evident through the various test conducted. Although conversions to the liquid phase components were small, sufficient sample collections were made to provide analysis. This analysis showed qualitatively that rearrangement was present and controllable. This strengthen Bethelot's theory of equilibrium [4] in pyrolytic reactions. If some type of equilibrium was not reached, then according to Nef [28] only short chain products would have been produced. Likewise Peytral's rearrangement theory of similarity [33] does not seem conclusive. By inspecting the GC analysis of samples taken, it is seen that some isomerization and multiple bond formation had to occur. This is demonstrated by the multiple peaks between the standard component retention times.

Perhaps the most dramatic conclusion is the control of pyrolytic reactions in a SGDR. As proved in the data analysis secondary voltage, retention time and frequency play important roles in product distribution. Energy transfer rates and residence time can also be altered in thermally induced pyrolysis, thus secondary voltage and residence times in this research offer no breakthrough in distribution control. Frequency alterations do offer an alternative control variable. This variable has shown to be bond selective by changing product distribution. As the frequency increases it is theorized that cleavage of the tertiary and secondary carbon-carbon bonds are preferred. The shift to higher chained and more complex hydrocarbons in the collected liquid sample support this hypothesis.

Recommendations to reduce the energy losses come from observing the formation of coronas along the outer electrodes and leads. A possible solution is to immerse the reactor in a liquid dielectric. Transformer oil available from various sources could provide the addition insulation for exterior corona quenching.

Development of the sine wave formation and primary voltage prediction theory arises from the observation that at lower primary voltages an increased frequency was required to initiate the corona. Because energy to the system is the integral of the sine wave formed over the frequency, total energy estimation is possible. By definition capacitance in the availability to store energy. It is logical that once the capacitance of the reactor is exceeded then the excess energy is used for ionization of the fluid within the reactor.

This leads to the next recommendation of power supply. If the relation between capacitance and total energy is valid then phasing the power supply would aid in corona formation. In the current system peak voltages, for the same current sign, are reached every 360 degrees. By rearrangement of the power supply to three phase coupling then the peaks would be obtained every 120 degrees. The area under the sine curve would be increased for the same frequency and primary voltage. Corona formation should then be produced at a lower primary voltage and frequency than currently available.

Decreasing plasma strength along the reactor length could possibly increase the conversion to more complex hydrocarbon chains in the following manner. As the energy transfer is decreased the higher association bonds are less effected. This shifts the bond cleavage to lower associated bonds which are located in the more complex and branched chains. More branched radicals increase the probability of chain propagation.

Complete analysis of all phases are required to fully understand the effects of SGDR applications for several reasons. The conversion of propane to ethylene and propylene is a desired reaction. Both are used as feed stocks in plastics production. This may prove to be more economically feasible than production to liquid products. Residue in the reactor is undetermined in this study. It is desired to evaluate this product for similar reasons.

The last recommendation is a complete analysis of the gas phase directly from an operational SGDR. Equilibrium could be investigated at various operating parameters by analysis of the reacting phase. Shifts in frequency could then be examined immediately for possible trends in equilibrium shifts.

LIST OF REFERENCES

1. Barker, C.; Wang, L; "Applications of Pyrolysis in Petroleum Geochemistry: A Bibliography" *J. Anal. Appl. Pyrolysis*, 1983, 13, 9-16
2. Back, R.A.; Takamuku, S., "The Mercury-Photosensitized Decomposition of Propane at Temperatures Above 300", *J Am.Chem. Soc.*, 1964, 86, 2558
3. Benson, A. M., "Pyrolysis of Propane in a Shock Tube", *AIChE J.*, 1967, 13, 9.0
4. Berthelot, *Ann. Chim. Phys.*, 1867, Vol. 12, 143-187, Hurd, C. D., The Pyrolysis of Carbon Compounds, Amer. Chem. Soc., Monograph Series, Chemical Catalog Co., New York, 1929, p 16
5. Blanc, *Compt. Rend.*, 1907, 144, 1356, Hurd, C. D., The Pyrolysis of Carbon Compounds, Amer. Chem. Soc., Monograph Series, Chemical Catalog Co., New York, 1929, p 14
6. Boenig, H. W., Fundamentals of Plasma Chemistry and Technology, Technimoc Publication Co., 1988, 192-199
7. Bredt; Thovet; Schmitz; *Ann. Chim.*, 1924, 1, 437, Hurd, C. D., The Pyrolysis of Carbon Compounds, Amer. Chem. Soc., Monograph Series, Chemical Catalog Co., New York, 1929, p 12
8. Brotheren, M., Capacitors, Their Use in Electrical Circuits, D. Van Nostrend Co. Inc., 1946, 32-35
9. Buekens, A. G.; Froment, G. F., "Thermal Cracking of Propane", *Ind. Eng. Process Des. Dev.*, 1968, 7, 3
10. Bywater, S.; Steacie, E. R., "The Mercury (3P_1) Photosensitized Decomposition of Propane at High Temperatures", *J. Chem. Phys.*, 1951, 19, 319
11. Darwent, de B. B.; Steacie, E. R., "The Mercury Photosensitized Reactions of Propane at Low Pressures", *J. Chem. Phys.*, 1945, 13, 563

12. Desai, V., Decomposition of Hydrogen Sulfide in an Alternating Current, Frequency Tuned Plasma Reactor, Oklahoma State University
13. Dintess, A. I.; Frost, A. V., Roy. Acad. Sci. (USSR), 1934, 5, 513, Volkan, A. G.; April, G. C., "Survey of Propane Pyrolysis Literature", Ind. Eng. Chem. Process Des. Dev., 16, 430
14. Dintess, A. I., Frost, A. V., Roy. Acad. Sci. (USSR), 1935, 4, 153, Volkan, A. G.; April, G. C., "Survey of Propane Pyrolysis Literature", Ind. Eng. Chem. Process Des. Dev., 16, 430
15. Egsgaard, H.; Carlson, L., "Techniques in Gas-Phase Themolysis, The Fate of Molecules in Low-Pressure Pyrolysis Reactors. A Theorectial Study.", J. Annal. App. Pyrolysis, 1987, 11, 25-38
16. Fery, H. M.; Hepp, H. E., "Thermal Decompositions of Simple Paraffins", Ind. Eng. Chem., 1933, 25, 441
17. Haber, Ber Bunsenges. Phys. Chem., 1896, Vol. 29, 2694, Hurd, C. D., The Pyrolysis of Carbon Compounds, Amer. Chem. Soc., Monograph Series, Chemical Catalog Co., New York, 1929, p 15
18. Hobbs, J. E.; Hinshelwood, C. N., Proc. Roy. Soc., Ser. A., 1938, 167, 447, Volkan, A. G.; April, G. C., "Survey of Propane Pyrolysis Literature", Ind. Eng. Chem. Process Des. Dev., 16, 430
19. Hurd, C. D., The Pyrolysis of Carbon Compounds, Amer. Chem. Soc., Monograph Series, Chemical Catalog Co., New York, 1929, 9-10
20. Ingold, K. U., et al., Proc. Roy. Soc., Ser. A, 1950, 203, 486, Volkan, A. G.; April, G. C., "Survey of Propane Pyrolysis Literature", Ind. Eng. Chem. Process Des. Dev., 16, 430
21. Kantor, R.H., Capacitance and Capacitors, Varian Associates, 1962, 26-37
22. Kershenbaum, L. S.; Martin, J. J., "Kinetics of the Nonisothermal Pyrolysis of Propane", AIChE J., 1967, 13, 148
23. Kunugi, T., et al., Ind. Chem. Eng., 1967, 7, 550, Volkan, A. G.; April, G. C., "Survey of Propane Pyrolysis Literature", Ind. Eng. Chem. Process Des. Dev., 16, 431
24. Laidler, K. J., Wojciechowski, B. W., "Propane Pyrolysis at High Temperature and Low Pressure", Proc. Roy. Soc., Ser. A, 1962, 270, 242

25. Lifshitz, A.; Frenklach, M., "Mechanisms of the High Temperature Decomposition of Propane", *J. Phys. Chem.*, 1975, 79, 686
26. Marek, L. F., McCluer, W. B., "Velocity Constants for the Thermal Dissociation of Ethane and Propane", *Ind. Eng. Chem.*, 1933, 23, 878
27. Nishimura, Y., Nakashio, F., Sakai, W., "Pyrolysis of Propane in an Induction-Coupled Argon Plasma Jet", *Int. Chem. Eng.*, 1970, 10 (1), 133-137
28. Nef, *Ann. Chem.*, 1901, 318, 14, Hurd, C. D., The Pyrolysis of Carbon Compounds, Amer. Chem. Soc., Monograph Series, Chemical Catalog Co., New York, 1929, p 17
29. Paul, R. E.; Marek, L. F., "Primary Thermal Dissociation", *Ind. Eng. Chem.*, 1934, 26, 454
30. Pavlis, R. L., Pittsburg State University, Pittsburg, KS, Personal Communication, 1991
31. Pease, R. N., "Equilibrium and Kinetics of Gas Reactions", *J. Am. Chem. Soc.*, 1928, 50, 1779
32. Pease, R. N.; Durgan, E. S., "The Kinetics of the Dissociation of Propane and the Butanes", *J. Am. Chem. Soc.*, 1930, 52, 1262
33. Peytral, *Bull. Soc. Chem.*, 1920, 27, 34, Hurd, C. D., The Pyrolysis of Carbon Compounds, Amer. Chem. Soc., Monograph Series, Chemical Catalog Co., New York, 1929, p 11
34. Piatt, M. A., Methane Destruction in an Alternating Current Plasma Reactor, Oklahoma State University, 1988
35. Rice, F. O., "The Thermal Decomposition of Organic Compounds from the Standpoint of Free Radicals. I. Saturated Hydrocarbons", *J. Am. Chem. Soc.*, 1931, 53, 1959
36. Shaw, M. A., Eagle-Picher Research and Development Laboratories, Personal Communication, Miami, OK, 1993
37. Steacie, E. R.; Dewar, D. J., "Mercury Photosensitized Reactions of Propane", *J. Chem. Phys.*, 1949, 8, 571
38. Steacie, E. R.; Puddington, "The Kinetics of Gas-Phase Reactions Involving Atoms and Organic Radicals", *Can. J. Res. Sect. B*, 1938, 16, 176

39. Streitwiser, A.; Heathcock, C. H., Introduction to Organic Chemistry, 3rd Ed., M^cMillian Publishing Co., New York, NY, 1985, 1153, 1188
40. Tsai, V. Y., Conceptual Design and Performance Analysis of Frequency Tuned Capacitive Discharge Reactors, Oklahoma State University, 1990
41. Table Curve TM, Copywrite Jandel Scientific, 1998-1992
42. Volkan, A. G.; April, G. C., " Survey of Propane Pyrolysis Literature", Ind. Eng. Chem. Process Des. Dev., 16, 429-436

APPENDIX A
REACTION MECHANISMS

FIRST ORDER MECHANISM AS
PROPOSED BY BENSON [3]

- 1) $C_3H_8 \longrightarrow CH_3 \bullet + C_2H_5 \bullet$
- 2) $C_3H_8 \longrightarrow C_3H_7 \bullet + H \bullet$
- 3) $CH_3 \bullet + C_3H_8 \longrightarrow C_3H_7 \bullet + CH_4$
- 4) $C_3H_7 \longrightarrow C_2H_4 + CH_3 \bullet$
- 5) $C_3H_7 \longrightarrow C_3H_6 + H \bullet$
- 7) $H \bullet + C_3H_6 \longrightarrow C_2H_4 + CH_3 \bullet$ (in many steps)
- 8) $C_3H_6 \longrightarrow C_2H_4$ (in many steps)

FIRST ORDER MECHANISIM AS
PROPOSED BY LIFSHITZ [25]

- 1) $C_3H_8 \longrightarrow C_2H_5 \bullet + CH_3 \bullet$
- 2) $H \bullet + C_3H_8 \longrightarrow {}^i\text{-}C_3H_7 \bullet + CH_4$
- 3) $H \bullet + C_3H_8 \longrightarrow {}^n\text{-}C_3H_7 \bullet + H_2$
- 4) ${}^i\text{-}C_3H_7 \bullet \longrightarrow C_2H_4 + CH_3 \bullet$
- 5) ${}^n\text{-}C_3H_7 \bullet \longrightarrow C_2H_4 + CH_3 \bullet$
- 6) ${}^i\text{-}C_3H_7 \bullet \longrightarrow H \bullet + C_3H_6$
- 7) ${}^n\text{-}C_3H_7 \bullet \longrightarrow H \bullet + C_3H_6$
- 8) $C_2H_5 \bullet \longrightarrow C_2H_4 + H \bullet$
- 9) $CH_3 \bullet + CH_3 \bullet \longleftrightarrow C_2H_6$

FIRST ORDER MECHANISIM AS
PROPOSED BY LAIDLER [24]

- 1) $C_3H_8 \longrightarrow CH_3 \bullet + C_2H_5 \bullet$
- 2) $X + C_3H_8 \longrightarrow CH_3 \bullet + C_2H_5 \bullet + X^{\#}$
- 3) $C_2H_5 \bullet + C_3H_8 \longrightarrow C_2H_6 + C_3H_7 \bullet$
- 4) $H \bullet + C_3H_8 \longrightarrow H_2 + C_3H_7 \bullet$
- 5) $CH_3 \bullet + C_3H_8 \longrightarrow CH_4 + C_3H_7 \bullet$
- 6) $C_3H_7 \bullet \longrightarrow CH_3 \bullet + C_2H_4$
- 7) $C_3H_7 \bullet \longrightarrow H \bullet + C_3H_6$
- 8) $CH_3 \bullet + C_3H_7 \bullet^{\#} \longrightarrow CH_4 + C_3H_6$ or
- 9) $CH_3 \bullet + CH_3 \bullet \longrightarrow C_2H_6$

1.2-1.3 ORDER MECHANISIM AS
PROPOSED BY BYWATER AND STEACIE [10]

- 1) $Hg(^1So) + hv \longrightarrow Hg(^3P_1)$
- 2) $Hg(^3P_1) + C_3H_8 \longrightarrow C_3H_7 \bullet + H \bullet + Hg(^1So)$
- 3) $H \bullet + C_3H_8 \longrightarrow H_2 + C_3H_7 \bullet$
- 4) $2C_3H_7 \longrightarrow C_3H_6 + C_3H_8$
- 5) $H \bullet + C_3H_6 \longrightarrow C_3H_7 \bullet$
- 6) $C_3H_7 \bullet \longrightarrow C_3H_6 + H \bullet$
- 7) $C_3H_7 \bullet \longrightarrow C_2H_4 + CH_3 \bullet$
- 8) $CH_3 \bullet + C_3H_8 \longrightarrow CH_4 + C_3H_7 \bullet$

APPENDIX B
REGRESSION ANALYSIS
FOR FLOWMETER
CALIBRATION

The procedure for calibration of the rotameter is summarized for familiarity. A bubble flowmeter was used to measure the volume of fluid passing through the rotameter in a set period of time. Measurements were taken at 8 rotameter settings. The recorded time and measured volume were then used to calculate the actual volumetric flow rate of the fluid. Table BI list the collected data and calculated flowrates.

TABLE BI
DATA FOR REGRESSIONAL ANALYSIS

Rotameter Setting	Volume Measured (cc)	Time Measured (sec)	Calculated Flowrate (cc/min)
0	0	0	0.0
5.0	10.0	30.51	19.66
5.0	10.0	30.53	19.65
5.0	10.0	30.34	19.78
5.0	10.0	32.40	18.52
5.0	10.0	31.28	19.18
5.0	10.0	31.35	19.14
5.0	10.0	31.63	18.97
5.0	10.0	31.77	18.88
5.0	10.0	32.09	18.70
10.0	10.0	11.97	50.12
10.0	10.0	11.90	50.42
10.0	10.0	11.82	50.76
10.0	20.0	23.46	51.15
10.0	20.0	23.64	50.76
10.0	20.0	23.27	51.57
10.0	20.0	23.63	50.78
10.0	30.0	35.38	50.88
10.0	30.0	35.20	51.34
10.0	40.0	47.16	50.89
15.0	10.0	6.21	96.62
15.0	10.0	6.26	95.85
15.0	10.0	6.19	96.90
15.0	20.0	12.34	97.24
15.0	20.0	12.41	96.70
15.0	20.0	12.41	96.70
15.0	30.0	18.70	96.26

TABLE BI
(continued)

Rotameter Setting	Volume Measured (cc)	Time Measured (sec)	Calculated Flowrate (cc/min)
15.0	30.0	18.52	97.19
15.0	30.0	18.49	97.35
15.0	40.0	24.77	96.89
20.0	20.0	8.22	145.98
20.0	20.0	8.16	147.06
20.0	20.0	8.26	145.28
20.0	30.0	12.28	146.58
20.0	30.0	12.26	146.82
20.0	30.0	12.27	146.70
20.0	30.0	12.27	146.70
20.0	40.0	16.45	145.90
20.0	40.0	16.34	146.88
20.0	40.0	16.20	148.15
20.0	40.0	16.26	147.60
25.0	30.0	8.93	201.56
25.0	30.0	9.00	200.00
25.0	30.0	8.88	202.70
25.0	40.0	11.83	202.87
25.0	40.0	11.88	202.02
25.0	40.0	11.69	205.30
25.0	50.0	14.77	203.11
25.0	50.0	15.03	199.60
25.0	50.0	14.99	200.13
25.0	50.0	14.94	200.80
30.0	40.0	9.60	250.00
30.0	40.0	9.55	251.31
30.0	40.0	9.56	251.05
30.0	50.0	12.07	248.55
30.0	50.0	12.01	249.79
30.0	50.0	12.01	249.79
30.0	60.0	14.27	252.28
30.0	60.0	14.31	251.57
30.0	60.0	14.25	252.63
30.0	60.0	14.36	250.70
40.0	30.0	5.24	343.51
40.0	30.0	5.18	347.49
40.0	30.0	5.13	350.88
40.0	40.0	6.91	347.32

TABLE B1
(continued)

Rotameter Setting	Volume Measured (cc)	Time Measured (sec)	Calculated Flowrate (cc/min)
40.0	40.0	6.87	349.34
40.0	40.0	7.06	339.94
40.0	40.0	6.86	349.85
40.0	50.0	8.74	343.25
40.0	50.0	8.75	342.86
40.0	60.0	10.47	343.84
50.0	50.0	6.79	441.83
50.0	50.0	6.70	447.76
50.0	50.0	6.75	444.44
50.0	60.0	8.07	446.10
50.0	60.0	8.10	444.44
50.0	60.0	8.06	446.65
50.0	60.0	8.02	448.88
50.0	70.0	9.38	447.76
50.0	70.0	9.47	443.50
50.0	70.0	9.35	449.20

A linear regression analysis on this data yielded the correlation:

$$Y = 9.274X - 27.855$$

The correlation coefficient for this regression is calculated to be 0.99618. Figure B1 displays this graphically.

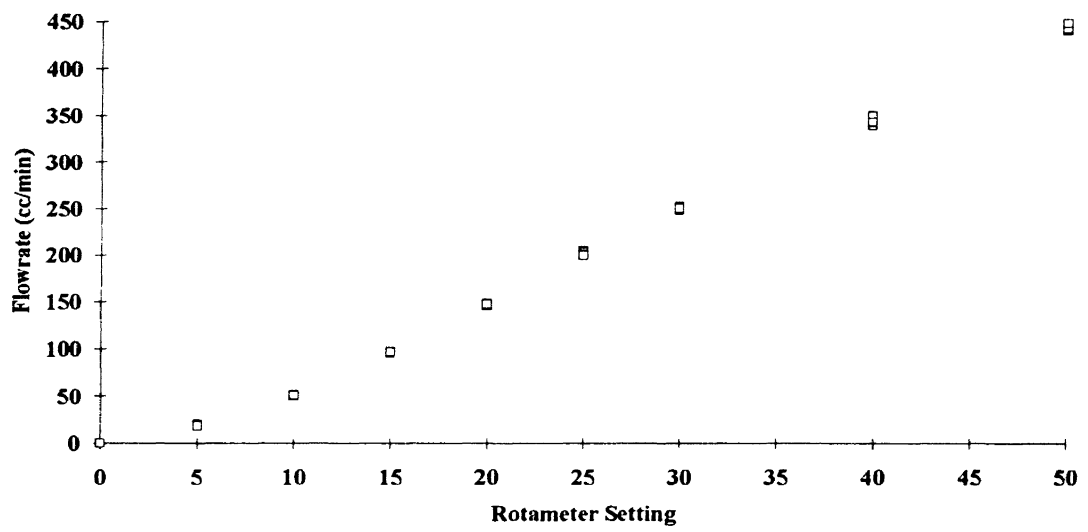


Figure B1. Plot of Calculated Flowrate as a Function of Rotameter Settings

APPENDIX C
ANALYSIS OF PROPANE
FEED STOCK

Analysis of the feed stock was conducted by Phillips Petroleum Company. Specific procedures for the gas phase analysis were left to the discretion of the analytical personnel at that facility. The following percentages listed in Table C1 reflect the details of that analysis.

TABLE C1

PERCENTAGES OF COMPONENTS FOUND
IN PROPANE FEED STOCK

Component	Percent Composition
Ethane & Ethylene	0.266
Isobutane	0.076
Air, H ₂ and Methane	0.000
Propane	99.658
	Totals 100.00

APPENDIX D

**EXAMPLE OF RUN DATA SHEET FOR HYDROCARBON
REARRANGEMENT TESTING**

PLASMA REACTOR HYDROCARBON REARRANGEMENT RUN DATA

Run ID. Number: HR-004
Date: 6-28-93
Ambient Temperature: 31.5 C

Reactor Data:

Inner Electrode: Length 25 cm
Material: Copper mesh
Outer Electrode: Length 25.4 cm
Material: Copper mesh

Effective Plasma Length: 25.4 cm

Inner Diameter (D_2): 1.80 cm

Outer Diameter (D_3): 2.78 cm

Gap Length: 0.490 cm

Plasma Formation Volume: 89.5 cm³

Operating Conditions:

Primary Voltage: 40 V
Frequency: 620 Hz
Secondary Voltage: 3.0 kV
Fluid Used: Propane
Flowrate: 10 setting; 65 cc/min

Comments:

Using reactor A with mesh outer electrode, from non-destructive test data with this configuration max secondary voltage @ 620 Hz. Will try to optimize around this setting.

C₃H₈ flow started at 8:43 pm

Plasma started at 8:45 pm, Sec. Volt 3.4, smooth plasma, class 3.7

Time	Secondary Voltage	Power
8:50	3.1	63
8:55	3.0	63
9:00	2.9	63
9:05	2.9	63
9:10	2.95	63
9:15	3.0	63

Samples collected at 9:15, small amount of liquid located in bottom of reactor. Will analyze with reactor residue. Removed reactor residue with acetone and placed in clean sample vile. Analysis not performed.

APPENDIX E
EXPERIMENTAL DATA FOR
NON-DESTRUCTIVE TEST
IN REACTOR A

TABLE E1

EXPERIMENTAL DATA CORRESPONDING
TO FIGURE 4

Reactor A with wrapped outer electrode configuration

Ambient Air

Temperature 9 °C

Reactor Volume: 87.5 cm³

PRIM. VOLT	30	40	50	60	70	80
FREQUENCY	SC. VOLT	SC. VOLT	SC. VOLT	SC. VOLT	SC. VOLT	SC. VOLT
200	2.8	3.6	4.4	5.2	6	7.2
220	2.8	3.6	4.4	5.2	6.2	7.3
240	2.8	3.6	4.4	5.3	6.2	7.4
260	2.9	3.8	4.5	5.4	6.3	7.6
280	3	3.8	4.6	5.6	6.4	7.8
300	3	3.9	4.8	5.6	3.8	8.2
320	3.1	4	4.8	5.8	7	8.6
340	3.2	4.2	5.1	6	7.6	9
360	3.3	4.2	5.2	6.4	8	9.6
380	3.4	4.4	5.4	6.8	8.5	10.4
400	3.5	4.6	5.6	7.2	9.2	11.2
420	3.6	4.8	5.9	7.8	10	12.2
440	3.8	5	6.4	8.6	10.1	13.4
460	4	5.2	6.8	8.4	11.9	14.4
480	4.2	5.25	7.6	10.3	12.9	15.2
500	4.4	5.8	8.4	11.2	13.6	15.4
520	4.7	6.4	9.4	12.2	14	15.4
540	5	7.1	10.4	12.6	14.2	15.2
560	5.4	8.2	11.2	12.8	14.2	15
580	5.8	9.4	11.8	13.2	14.2	14.6
600	6.4	10.1	12	13.2	14.2	14.3
620	7.4	10.8	12.2	13.2	13.8	14.2
640	8.3	11	11.8	13	13.8	14
660	9.1	10.09	11.8	13	13.5	13.6
680	9.4	10.4	11.6	12.6	13	13.4
700	9.3	10.6	11.4	12.4	13	13.4
720	8.8	10.1	11	12	12.7	12.6
740	7.8	9.3	10.4	11.5	12.2	12.4
760	7	8.8	10	10.8	11.7	11.8
780	6	7.6	9.2	10.2	10.5	10.8
800	5.2	6.4	8	9	9.4	9.8

TABLE E2

EXPERIMENTAL DATA CORRESPONDING
TO FIGURE 5

Reactor A with wrapped outer electrode configuration
 Nitrogen with flowrate of 10 setting, 65 cc³/min
 Temperature 9 °C
 Reactor Volume: 87.5 cm³

PRIM. VOLT FREQUENCY	30 Sc. VOLT	40 Sc. VOLT	50 Sc. VOLT	60 Sc. VOLT	70 Sc. VOLT	80 Sc. VOLT
200	2.8	3.6	4.4	5.2	6.2	7.4
220	2.8	3.8	4.4	5.4	6.2	7.4
240	2.9	3.8	4.5	5.4	6.4	7.5
260	3	3.8	4.6	5.7	6.4	7.6
280	3	3.8	4.7	5.6	6.5	7.8
300	3	4	4.8	2.6	6.8	8.2
320	3.1	4	4.9	5.8	7	8.6
340	3.2	4.2	5	6	7.4	9.1
360	3.3	4.4	5.2	6.3	7.8	9.8
380	3.4	4.4	5.4	6.6	8.2	10.6
400	3.6	4.6	5.6	7	8.8	11.8
420	3.6	4.8	5.8	7.6	9.6	13.2
440	3.8	5	6.2	8.2	10.6	14.4
460	4	5.2	6.6	8.8	11.8	15.2
480	4.2	5.5	7.2	9.8	13	15.2
500	4.4	5.8	8	11	14.1	15
520	4.7	6.4	9	12.2	14.6	14.6
540	5	7.2	10.2	13.4	14.7	14
560	5.4	8.2	11.8	14	14.4	13.6
580	5.8	9.6	13	14.2	14	13
600	6.6	11	13.6	14.1	13.6	12.6
620	7.4	12.4	13.8	13.8	13.2	12.2
640	2	13.2	13.4	13.4	12.8	11.8
660	8.8	13.4	13.2	13	12.4	11.6
680	9	13.4	12.9	12.8	12	11.2
700	8.8	13	12.4	12.3	11.8	10.8
720	8.4	12.6	12	12	11.4	10.6
740	7.8	11.8	11.6	11.4	11.1	10.2
760	7	10.8	10.8	10.8	10.5	9.8
780	6	9.4	10.1	10.1	9.8	9.3
800	5.3	8	9.2	9.4	9	8.6

TABLE E3

EXPERIMENTAL DATA CORRESPONDING
TO FIGURE 6

Reactor A with wrapped outer electrode configuration
Propane with flowrate of 10 setting, 65 cc³/min
Temperature 9 °C
Reactor Volume: 87.5 cm³

PRIM. VOLT FREQUENCY	30 Sc. VOLT	40 Sc. VOLT	50 Sc. VOLT	60 Sc. VOLT	70 Sc. VOLT	80 Sc. VOLT	90 Sc. VOLT	100 Sc. VOLT
200	2.8	3.6	4.4	5.1	6	7	8.4	5
220	2.8	3.6	4.4	5.2	6	7	8.6	5
240	2.8	3.6	4.4	5.2	6.1	7.2	8.7	5.1
260	2.8	3.7	4.5	5.5	6.2	7.2	8.8	5.2
280	2.9	3.8	4.6	5.4	6.4	7.4	9	5.5
300	3	3.8	4.8	5.6	6.6	7.8	9.4	5.9
320	3	4	4.8	5.7	6.8	8.2	9.7	6.4
340	3.2	4	4.9	5.8	7.2	8.6	10.4	7.1
360	3.2	4.2	5.1	6	7.5	9	11.2	8
380	3.2	4.4	5.2	6.4	8	9.6	12.2	8.9
400	3.4	4.5	5.4	6.8	8.6	10.2	13.8	9
420	3.6	4.6	5.7	7.2	9	11.4	15.4	8.7
440	3.6	4.8	6	7.8	9.8	12.8	16.2	8.5
460	3.9	5	6.4	8.4	10.8	14.2	16.4	8.35
480	4	5.4	6.9	9.2	12.4	15	15.4	8.15
500	4.2	5.6	7.6	10.2	13.8	15	15	7.9
520	4.4	6.1	8.5	11.6	14.4	14.8	14.8	7.7
540	4.8	6.8	9.6	13.2	14.4	14.8	14.4	7.5
560	5.2	7.6	11	13.9	14.4	14.4	14	7.4
580	5.6	8.8	12.6	14.2	14	14.2	15.6	7.2
600	6.2	10.4	13.3	14.2	13.9	14	15.4	7.1
620	7.2	12	13.6	13.9	13.4	13.8	13	7
640	8.2	13	13.8	13.6	13.3	13.4	12.8	6.9
660	9.4	13.6	13.9	13.4	13	13.2	12.6	6.8
680	10	13.8	13.6	13.1	13	13	12.4	6.8
700	10.2	13.6	13.2	13	12.8	12.8	12.2	6.7
720	10	13.2	12.8	12.6	12.6	12.6	12	6.6
740	9.2	12.6	12.6	12.4	12.2	12.4	11.8	6.4
760	8.2	11.6	12	12	11.8	12	11.6	6.2
780	7.2	10.2	11.4	11.6	11.4	11.4	11	5.7
800	6.2	8.8	11.5	10.8	10.6	10.8	10.4	5.5

TABLE E4

EXPERIMENTAL DATA CORRESPONDING
TO FIGURE 7

Reactor A with mesh outer electrode configuration

Ambient Air

Temperature 21 °C

Reactor Volume: 87.5 cm³

PRIM. VOLT FREQUENCY	30 Sc. VOLT	40 Sc. VOLT	50 Sc. VOLT	60 Sc. VOLT	70 Sc. VOLT	80 Sc. VOLT
200	2.4	3.2	4	4.8	5.6	7
220	2.5	3.4	4	4.8	5.6	6.8
240	2.6	3.4	4	4.8	5.6	6.6
260	2.6	3.4	4	4.8	5.6	6.6
280	2.6	3.4	4.2	4.8	5.8	6.8
300	2.6	3.4	4.2	5	5.8	7
320	2.6	3.5	4.3	5.2	6	7.4
340	2.8	3.6	4.4	5.2	6.4	8
360	2.8	3.6	4.5	5.4	6.6	8.8
380	2.8	3.8	4.6	5.6	7.2	10
400	3	4	4.8	6	8	11.4
420	3	4	5	6.3	9	14.6
440	3.2	4.2	5.4	6.8	10	13.6
460	3.3	4.4	5.6	7.4	10.6	12.4
480	3.7	4.6	6	8.8	10.7	11.4
500	3.6	4.8	6.4	9.6	10.8	11.6
520	3.8	5.2	7.2	10.2	11	9.8
540	4	5.6	8.6	10.6	10.8	9.4
560	4.4	6.2	9.4	10.6	10.6	8.8
580	4.8	7.4	10	10.6	10.2	8.4
600	5.2	8.6	10.2	10.6	9.9	8
620	6	9.2	10.3	10.6	9.6	7.8
640	7	9.4	10	10.6	9.4	
660	7.8	9.2	10	10.4	9.6	
680	8.4	9.2	10	10.2	9.6	
700	8.8	9	10	10	9	
720	9	9	4.9	10	9	
740	9	9	9.8	9.8	8.8	
760	9	9	9.8	9.6	8.8	
780	8.8	9	9.8	9.6	8.6	
800	8.7	8.8	9.8	9.6	8.6	

TABLE E5

EXPERIMENTAL DATA CORRESPONDING
TO FIGURE 8

Reactor A with mesh outer electrode configuration

Nitrogen with flowrate set at 10 setting

Temperature 21 °C

Reactor Volume: 87.5 cm³

PRIM. VOLT	30	40	50	60	70	80
FREQUENCY	SE. VOLT	SE. VOLT	SE. VOLT	SE. VOLT	SE. VOLT	SE. VOLT
200	2.4	3.2	3.8	4.6	5.6	7.2
220	2.4	3.2	4	4.8	5.6	7
240	2.4	3.2	4	4.8	5.6	7.2
260	2.4	3.2	4	4.8	5.6	7.6
280	2.4	3.2	4	4.8	5.6	8.4
300	2.6	3.4	4.2	5	5.8	10.8
320	2.6	3.4	4.2	5.2	6	11.2
340	2.6	3.5	4.4	5.2	6.4	13.4
360	2.6	3.6	4.4	5.4	6.8	15.6
380	2.8	3.8	4.6	5.6	7.2	16.2
400	2.8	3.9	4.8	6	8	15.8
420	3	4	5	6.4	9	14.8
440	3	4.2	5.4	6.8	10	13.8
460	3.2	4.4	5.6	7.4	11	13
480	3.4	4.6	6.2	8.4	11.4	11.8
500	3.6	5	6.8	9.6	11.2	11.8
520	3.8	5.2	7.6	10.8	9.8	10.2
540	4	5.8	8.8	11.4	9.2	9.6
560	4.2	6.8	10	11.6	9	8.8
580	4.6	8	11	11.6	8.8	8.4
600	5.2	9.2	11.2	11.4	8.4	8
620	6	10	11.2	11.4	8.3	7.9
640	7.2	10.2	11	11.4	8.3	7.6
660	8.6	10.3	11	11.4	8.2	7.6
680	9.2	10.3	10.9	11.4	8	7.4
700	9.6	10.3	10.7	11.3	8	7.2
720	9.6	10.2	10.4	11.2	7.8	7.2
740	9.5	10.2	10.3	11.2	8	2
760	9.7	10.2	10.1	11	8	7
780	9.2	10.2	9.8	11	7.8	7
800	9	10.1	9.4	11	7.8	7

TABLE E6

EXPERIMENTAL DATA CORRESPONDING
TO FIGURE 9

Reactor A with mesh outer electrode configuration
Propane flowrate set at 10 setting Temperature 21 °C Reactor Volume: 87.5 cm³

PRIM. VOLT FREQUENCY	30	40	50	60	70	80
	SE. VOLT	SE. VOLT	SE. VOLT	SE. VOLT	SE. VOLT	SE. VOLT
200	2.4	3.2	3.8	4.6	6	7
220	2.4	3.2	4	4.6	5.9	6.8
240	2.4	3.2	4	4.6	5.6	6.8
260	2.4	3.2	4	4.7	5.6	7
280	2.4	3.2	4	4.8	5.6	7.6
300	2.6	3.2	4.1	4.8	5.8	8.7
320	2.6	3.4	4.2	5.2	6	10.4
340	2.6	3.4	4.4	5.2	6.4	14.2
360	2.7	3.7	4.4	5.2	8.4	19.8
380	2.8	3.6	4.6	5.4	10.8	18.4
400	2.9	3.8	4.8	5.8	12.4	18.2
420	3	4	5	6.4	12.4	15.4
440	3.2	4.1	5.6	7.4	11.6	13.8
460	3.3	4.3	5.4	8.4	10.8	12.3
480	3.4	4.5	6	9	10.2	11.2
500	3.6	4.8	7	9	9.4	10.2
520	3.8	5.1	7.8	8.6	8.8	8.7
540	4.2	5.6	8.2	8.4	8.4	8.6
560	4.4	6.2	8.4	8	8	8
580	4.4	7.6	8.3	7.8	7.6	7.6
600	5.3	8.2	8	7.6	7.2	7.2
620	6.2	8.4	7.8	7.4	7	7
640	7.4	8.1	7.8	7.2	6.8	6.8
660	8	8	7.6	7	6.6	6.6
680	8.6	7.8	7.4	7	6.4	6.4
700	8.6	7.7	7.4	6.8	6.4	6.2
720	8.2	7.6	7.2	6.8	6.4	6.2
740	8	7.4	7.2	6.8	6.4	6.2
760	7.8	7.4	7.2	6.6	6.2	6.2
780	7.6	7.4	7.2	6.6	6.4	6.2
800	7.4	7.2	7.2	6.6	6.4	6.4
820	7	7.2	7.2	6.8	6.6	6.4
840	6.6	7.2	7.2	6.8	6.6	6.6
860	6.2	7	7.2	6.8	6.8	6.8
880	5.4	6.8	7.1	6.8	6.8	6.8
900	4.4	6.4	7	6.8	6.8	6.8
920			6.6	6.4	6.6	6.6
940			6	6	6	6.2
980			4.4	4.4	4.4	4.4

TABLE E7

EXPERIMENTAL DATA CORRESPONDING
TO FIGURE 10

Reactor A with mesh outer electrode configuration
Propane flowrate set at 10 setting Temperature 21 °C Reactor Volume: 87.5 cm³

PRIM. VOLT FREQUENCY	30 POWER	40 POWER	50 POWER	60 POWER	70 POWER	80 POWER
200	75	72	68	66	65	65
220	76	72	68	66	65	65
240	76	72	68	66	65	65
260	76	72	68	66	65	65
280	76	72	68	66	65	65
300	76	72	68	66	66	65
320	76	70	68	66	66	74
340	76	70	68	65	66	100
360	76	70	68	65	75	130
380	76	69	68	65	85	135
400	76	69	68	65	100	140
420	75	69	68	65	105	145
440	75	69	67	65	107	145
460	75	69	66	70	107	143
480	75	69	66	75	107	135
500	76	69	66	80	108	128
520	74	69	68	80	108	125
540	74	69	68	80	108	120
560	74	69	68	80	106	118
580	73	69	70	80	106	115
600	73	69	70	80	105	110
620	73	69	70	80	105	108
640	73	70	71	80	105	105
660	73	70	71	80	104	104
680	73	70	71	80	100	102
700	73	70	71	80	97	100
720	73	70	72	80	95	102
740	72	70	72	80	95	98
760	72	70	73	80	95	95
780	72	70	73	80	93	94
800	73	70	73	80	90	94
820	74	70	73	80	90	94
840	74	70	73	80	89	94
860	73	70	74	80	89	90
880	73	70	74	80	91	89
900	73	70	74	80	95	86
920			74	80	90	86
940			74	80	90	85
980			75	80	90	83

APPENDIX F
EXPERIMENTAL DATA FOR
NON-DESTRUCTIVE TEST IN
REACTOR B

TABLE F1

EXPERIMENTAL DATA CORRESPONDING
TO FIGURE 11

Reactor B with wrapped outer electrode configuration
Ambient Air
Temperature 24 °C

PRIM. VOLT FREQUENCY	30 SC.VOLT	60 SC.VOLT	80 SC.VOLT	90 SC.VOLT	105 SC.VOLT	120 SC.VOLT
300	2.8	5.6	8.2	9.8	12.4	7.5
320	2.8	5.8	8.6	10.4	13	7.9
340	3	6	9.2	11.2	14	8.5
360	3	6.4	9.8	12	15	9.2
380	3.2	7	10.8	13	16.2	10.3
400	3.4	7.6	11.6	14.4	18	11.1
420	3.6	8.2	13	16.8	10	11.4
440	3.8	9.6	14.4	17.6	11	11.5
460	4	10.4	16.2	19.8	23	11.7
480	4.2	11.8	18.6	21.6	23	11.6
500	4.6	13.8	20.2	22	22.4	11.35
520	5.2	16.4	21	22.4	22.2	11.3
540	5.8	19.2	21.6	22	21.6	
560	7	19.6	21.6	22	21	
580	8.4	19.8	21	21.8	20.8	
600	9.6	19.6	21	21.2	20.4	
620	10.4	19.6	20.8	20.8	20.2	
640	10.4	19.2	20.6	20.8	19.8	
660	9.6	18.6	20	19.8	19.8	
680	8.6	17.6	19.4	19.2	19.2	
700	3.4	15.2	18.4	18.8	18.8	
720	7.2	13.4	17.6	17.8	18	
740	6.2	11.6	15.2	16.4	17	
760	4.3	9.2	13.2	14.8	15.8	
780	4.2	8.2	11.2	12.6	14.4	
800	3.8	6.8	9.6	10.6	12.4	

TABLE F2
 EXPERIMENTAL DATA CORRESPONDING
 TO FIGURE 12

Reactor B with mesh outer electrode configuration
 Ambient Air Temperature 28 °C

PRIM. VOLT FREQUENCY	50 SC.VOLT	70 SC.VOLT	80 SC.VOLT	90 SC.VOLT	100 SC.VOLT
300	4.6	6.4	7.6	9	10.8
320	4.6	6.8	8	9.6	11.4
340	4.8	7.3	8.6	10.6	12.2
360	5.2	7.9	9.6	11.8	13.2
380	5.4	8.6	10	12	15
400	5.8	9.2	11	13.2	18.2
420	6.2	10.2	12	14.8	18
440	7	11.4	14	17	18.4
460	7.9	13	16.8	17.4	18.2
480	9.2	14.8	17.6	17.4	18
500	10.6	16.6	17.4	17	17.8
520	12	16.6	17.4	17	17.6
540	14.8	16.6	16.6	16.4	17.6
560	14.9	16.6	15.8	16.2	17.6
580	14.8	16.6	15	15.8	17.6
600	14.8	16.2	13.8	15.2	16
620	14.6	14.9	13.4	14.8	15.4
640	14.4	14.8	13	15	14.8
660	14.2	14.6	12.6	15	14.2
680	14	14.3	12.4	14.2	13.6
700	13	14	12.2	14.2	12.6
720	12.6	13.8	12	14.2	12.2
740	12.6	13.6	11.8	14.2	11.8
760	12.2	13.5	11.8	14	11.6
780	10.6	13.2	11.8	14	11.4
800	9	13	11.8	13.7	11.6
820	7.6	12	11.8	13.4	11.3
840	6.6	10.6	11.6	13.2	11.2
860	5.8	9.4	11	12.6	11.2
880	5	8.4	10	11.6	11.2
900	3.8	7.2	8.8	10.4	11

TABLE F3

EXPERIMENTAL DATA CORRESPONDING
TO FIGURE 13

Reactor B with mesh outer electrode configuration
Nitrogen at flowrate of 10 setting
Temperature 28 °C

PRIM. VOLT	50	70	80	90	100	110
FREQUENCY	SC. VOLT	SC. VOLT	SC. VOLT	SC. VOLT	SC. VOLT	SC. VOLT
300	4.2	6	7.2	8.6	10	11.8
320	4.4	6.2	7.6	9	10.6	12.8
340	4.6	6.6	8	9.6	13	14
360	4.8	7	8.6	10.2	13.8	14.9
380	5	7.5	9.2	11	14.2	16.8
400	5.2	8.2	10.2	13.6	14.2	17
420	5.4	8.8	12	14	13.4	16.6
440	5.8	9.8	13.6	14	13.6	16.2
460	6.4	11	14	13.6	13.4	15.6
480	7.2	13.6	14	13.4	13	15.2
500	8.4	14.3	13.8	13.2	12.8	12.6
520	8.8	14.4	13.4	13	12.6	12.2
540	12	13.8	13.2	12.8	12.4	12
560	14.2	13.6	13.1	12.6	12.4	11.6
580	14.7	13.4	13	12.6	12.2	11.4
600	13.6	13.2	12.8	12.4	12	11.2
620	13.4	13	12.6	12.2	11.8	11
640	13.2	12.8	12.4	12	11.8	10.8
660	13	12.6	12.4	11.9	11.6	10.6
680	12.8	12.4	12.2	11.8	11.6	10.6
700	12.8	12.2	12	11.8	11.4	10.4
720	12.5	12.2	12	11.6	11.4	10.4
740	12.3	12	11.8	11.4	11.4	10.4
760	12.2	11.8	11.8	11.4	11.4	10.4
780	11.8	11.8	11.6	11.4	11.4	10.4
800	11.2	11.6	11.6	11.4	11.6	10.4
820	9.6	11.6	11.6	11.4	11.6	10.6
840	8.2	11.5	11.5	11.4	11.4	10.6
860	7.2	10.6	11.4	11.4	11.4	10.8
880	6.2	9.4	11	11.2	11.4	11
900	5.4	8.2	9.8	11.4	11.2	11

TABLE F4

EXPERIMENTAL DATA CORRESPONDING
TO FIGURE 14

Reactor B with mesh outer electrode configuration
Nitrogen at flowrate of 10 setting
Temperature 28 °C

PRIM. VOLT FREQUENCY	50 SC. VOLT	70 SC. VOLT	80 SC. VOLT	90 SC. VOLT	100 SC. VOLT
300	4.2	6	7.2	8.6	10.2
320	4.2	6.2	7.6	9	13.2
340	4.4	6.6	8	9.6	13.2
360	4.6	7	8.6	10.2	13
380	4.8	7.4	9.2	11	12.4
400	5	8.2	11	12.4	12.2
420	5.2	8.8	10.8	12.1	11.8
440	5.6	9.8	10.6	11.7	11.6
460	6.2	10.6	10.4	11.2	11.4
480	7	10.4	10.2	11	11
500	8.2	10	10	10.4	11
520	9.6	9.4	9.8	10.6	10.6
540	11.6	9.2	9.6	10.4	10.5
560	11.5	9	9.4	10.2	10.2
580	10.8	8.8	9.4	10	10.2
600	10	8.8	9.2	9.9	10
620	9.4	8.8	9.6	9.8	10
640	9.2	8.6	9	9.6	9.8
660	9	8.6	9	9.5	9.8
680	9	8.6	8.9	9.4	9.6
700	8.8	8.4	8.9	9.4	9.6
720	8.6	8.4	8.8	9.2	9.6
740	8.6	8.2	8.6	9.4	9.6
760	8.6	8.2	8.6	9.4	9.6
780	8.6	8.2	8.6	9.4	9.6
800	8.6	8.4	8.7	9.3	9.8
820	8	8.4	8.8	9.3	9.8
840	7.6	8.5	8.8	9.7	10
860	6.4	8.6	8.8	9.6	10
880	5.6	9.2	9	9.6	10
900	4.8	8.1	8.8	9.6	10
920			8.4	10	9.8
940			7.4	8.6	9.8
960					8.2

TABLE F5

EXPERIMENTAL DATA CORRESPONDING
TO FIGURE 15

Reactor B with mesh outer electrode configuration
Nitrogen at flowrate of 10 setting
Temperature 28 °C

PRIM. VOLT FREQUENCY	50 POWER	70 POWER	80 POWER	90 POWER	100 POWER
300	65	55	55	55	55
320	65	55	54	55	115
340	64	55	55	54	123
360	62	54	55	54	125
380	60	54	55	54	125
400	60	55	95	105	125
420	59	55	100	110	125
440	59	55	100	110	125
460	60	81	100	110	125
480	60	90	100	110	125
500	60	90	100	110	125
520	60	92	100	110	126
540	74	92	100	110	126
560	77	92	100	110	125
580	80	92	100	110	125
600	80	92	100	110	125
620	80	92	100	110	125
640	80	92	100	110	125
660	80	92	100	110	125
680	80	92	100	110	116
700	80	92	100	106	110
720	80	92	100	104	107
740	80	92	100	103	105
760	80	92	100	102	105
780	80	92	96	100	103
800	80	92	95	96	100
820	80	92	95	96	100
840	80	88	95	95	100
860	80	86	94	94	98
880	76	85	94	90	95
900	74	83	95	90	95
920			93	89	92
940			93	86	92
960					92

APPENDIX G
EXPERIMENTAL DATA FOR
NON-DESTRUCTIVE TEST
IN REACTOR C

TABLE G1

EXPERIMENTAL DATA CORRESPONDING
TO FIGURE 16

Reactor C with mesh outer electrode configuration
Ambient Air
Temperature 30.5 °C

PRIM. VOLT FREQUENCY	50 SC. VOLT	70 SC. VOLT	80 SC. VOLT	90 SC. VOLT	100 SC. VOLT
300	5	7.8	9.2	11	13
320	5.2	8.6	10.2	12.2	15.3
340	5.6	9.6	11.6	17.6	17.2
360	6.2	11	13.2	16.8	17.6
380	7.2	12.8	15.4	17.2	17.6
400	8.6	15.4	17.8	17.6	17
420	10.6	17.8	18.2	17.8	16.6
440	13.6	18.2	18.3	17.8	16.2
460	15	18	18.5	17.8	16
480	16.2	17.6	18	18	15.6
500	17	17.2	17.6	18	15.4
520	17	16.6	17.6	17.9	15.2
540	16.6	16	17.2	17.8	15.2
560	16	16	16.6	17.6	14.8
580	15.8	16	18.2	17.6	14.6
600	15	15.2	17.6	17.4	14.2
620	12.2	14.4	15.4	16.6	14.2
640	10	13.8	14.8	16.6	14
660	8.2	12.8	14.8	16.4	13.8
680	6.6	10.8	12.8	14.6	13.6
700	5.6	9.4	11	12.6	13.4
720	5.2	8	9.6	10.8	12.8
740		6.8	8.2	9.6	11.4
760		6	7.2	8.6	10.2
780			6.4	7.6	9
800			5.8	6.8	8.2
820				6.2	7.6
840				5.8	7
860					6.4
880					6

TABLE G2

EXPERIMENTAL DATA CORRESPONDING
TO FIGURE 17

Reactor C with mesh outer electrode configuration
Nitrogen at flowrate of 10 setting
Temperature 30.5 °C

PRIM. VOLT FREQUENCY	50 SC. VOLT	70 SC. VOLT	80 SC. VOLT	90 SC. VOLT	100 SC. VOLT
300	5.2	7.6	9.4	11.2	14.8
320	5.2	8.4	10.3	12.4	14
340	5.6	4.6	55.6	14	13.4
360	6.2	10.8	13.2	15.9	12.8
380	7	12.6	15.4	17.6	12.6
400	8.4	15	18.1	18	12.2
420	10.3	17.6	18.8	17.8	11.9
440	13	18	18.8	17.6	55.6
460	15.6	18.6	19	16.4	11.4
480	16.9	18.6	19	13.2	11.2
500	17.5	18.8	18.3	12.6	11.2
520	17.6	18.6	18.4	12.4	11
540	17.2	19.6	17.8	12	11
560	17.5	18.3	17.4	11.8	11
580	16.8	17.6	16.6	11.6	11
600	15.9	17.6	16.6	11.6	10.8
620	13	17.3	16.2	11.4	10.8
640	10.6	15.2	15.6	11.4	11
660	8.8	13	14.4	11.6	11
680	7.2	11	12.4	11.9	10.2
700	6	9.4	10.4	11.8	11.4
720	5	8	9.4	11.4	11.6
740		7	8.2	10	11.6
760		6	7.2	8.8	10.4
780		5.4	6.4	7.8	9.4
800			5.8	7.2	8.6
820				6.4	7.8
840				6	7.2
860					6.6
880					6.2
900					5.6

TABLE G3

EXPERIMENTAL DATA CORRESPONDING
TO FIGURE 18

Reactor C with mesh outer electrode configuration
Propane at flowrate of 10 setting
Temperature 30.5 °C

PRIM. VOLT	50	70	80	90	100	110
FREQUENCY	SC. VOLT	SC. VOLT	SC. VOLT	SC. VOLT	SC. VOLT	SC. VOLT
300	4.8	7.4	9	11	12.6	13.2
320	5.2	8.2	10	11.4	12.6	12.2
340	5.6	9.2	11.2	11	12.2	11.8
360	6	10.4	10.6	10.8	11	11.4
380	7	10.4	10.2	10.6	10.8	11.2
400	8.4	10	10	10.2	10.4	11
420	10.2	9.8	9.8	10.2	10.2	11
440	13.2	9.6	9.6	10	10.2	10.8
460	10.4	9.6	9.6	9.8	10.2	10.8
480	10.3	9.4	9.4	9.7	10	10.6
500	10.1	9.4	9.3	9.7	10	10.6
520	10	9.4	9.2	9.6	10	10.4
540	10	9.4	9.2	9.6	9.8	10.4
560	10	9.6	9.2	9.6	10	10.4
580	9.8	9.2	9.2	9.6	9.8	10.6
600	9.8	9.2	9.3	9.6	10	10.6
620	9.6	9.4	9.7	9.8	10	10.6
640	9.6	9.4	9.3	9.8	10.2	10.6
660	9.4	9.4	9.2	9.8	10.2	10.6
680	7.6	9.6	9.4	9.8	10.2	10.6
700	6.2	10	9.4	9.8	10.4	11
720	5.4	8.4	10	9.6	10.2	11
740		7.2	8.8	10.4	10.2	11
760		6.4	7.6	9.2	10.6	11.8
780		5.6	6.8	8.2	9.4	10.6
800			6	7.2	8.6	9.6
820				6.6	7.8	8.8
840				6	7.2	8.2
860						7.6
880						7

TABLE G4

EXPERIMENTAL DATA CORRESPONDING
TO FIGURE 19

Reactor C with mesh outer electrode configuration
Propane at flowrate of 10 setting
Temperature 30.5 °C

PRIM. VOLT FREQUENCY	50 POWER	70 POWER	80 POWER	90 POWER	100 POWER	110 POWER
300	65	60	60	60	155	167
320	62	69	60	132	155	167
340	62	60	61	133	156	167
360	62	60	120	133	156	167
380	62	106	120	133	156	167
400	62	106	120	132	156	163
420	63	108	120	132	153	160
440	74	108	120	132	150	157
460	94	108	120	132	145	154
480	94	108	119	132	143	152
500	95	108	119	130	140	146
520	95	108	119	128	137	144
540	95	108	119	125	138	142
560	95	108	119	125	135	136
580	94	108	119	125	128	135
600	94	108	119	122	125	130
620	94	108	116	119	125	130
640	94	106	111	116	123	125
660	94	105	109	115	120	125
680	94	105	107	112	116	123
700	94	103	105	110	115	120
720	88	101	105	107	113	116
740	85	95	100	105	110	114
760		90	95	100	108	114
780		82	92	96	103	106
800			82	94	99	103
820				92	96	100
840				86	93	95
860						95
880						88

APPENDIX H

**SUPPORTING DATA FOR
SECONDARY VOLTAGE LOSS
RATE IN REACTORS
A & B**

TABLE H 1
SUPPORTING DATA FOR
LINEAR REGRESSION
ANALYSIS

Fluid:	Air		
Primary Voltage:	40 Volts		
Electrode Configuration			
	Sec. Voltage		
Frequency	wrap	mesh	
640		11	9.4
660		10.9	9.2
680		10.8	9.2
700		10.6	9
720		10.1	9
740		9.3	9
760		8.8	9
780		7.6	9
800		6.4	8.8

Fluid:	Nitrogen		
Primary Voltage:	40 Volts		
Electrode Configuration			
	Sec. Voltage		
Frequency	wrap	mesh	
660		13.4	10.3
680		13.4	10.3
700		13	10.3
720		12.6	10.2
740		11.8	10.2
760		10.1	10.2
780		9.2	10.2
800		8	10.1

Fluid:	Propane		
Primary Voltage:	40 Volts		
Electrode Configuration			
	Sec. Voltage		
Frequency	wrap	mesh	
620			8.4
640			8.1
660			8
680		13.8	7.8
700		13.6	7.7
720		13.2	7.6
740		12.6	7.4
760		11.6	7.4
780		10.2	7.4
800		8.8	7.2

TABLE H 1
(continued)

Fluid: Air		
Primary Voltage: 70 Volts		
Electrode Configuration		
	Sec. Voltage	
Frequency	wrap	mesh
500		11.4
520		11
540		10.8
560		10.6
580	14.4	10.1
600	14.2	9.9
620	13.8	9.8
640	13.8	9.4
660	13.7	9.2
680	13.2	9.2
700	13	9
720	12.7	9
740	12.2	8.8
760	11.4	8.8
780	10.3	8.6
800	9.4	8.6

Fluid: Nitrogen		
Primary Voltage: 70 Volts		
Electrode Configuration		
	Sec. Voltage	
Frequency	wrap	mesh
480		11.4
500		11.2
520		9.2
540	14.7	9.2
560	14.4	9
580	14.2	8.8
600	13.6	8.4
620	13.2	8.3
640	12.8	8.3
660	12.4	8.2
680	12	8
700	11.8	8
720	11.4	7.8
740	11.1	8
760	10.5	8
780	9.8	7.7
800	9	7.8

APPENDIX I
EXPERIMENTAL DATA FOR
LENGTH EFFECTS IN
REACTOR C

TABLE II

EXPERIMENTAL DATA CORRESPONDING
TO FIGURE 21

Outer Electrode: One Wrap of 12 Gauge Wire

Fluid: Nitrogen

Temperature: 30.5 °C

Pressure: 10 psig

PRIM. VOLT	30	40	50	60	70	80
FREQUENCY	SC. VOLT	SC. VOLT	SC. VOLT	SC. VOLT	SC. VOLT	SC. VOLT
300	2.4	3.2	3.8	4.6	5.4	6.2
320	2.4	3.2	3.8	4.6	5.4	6.2
340	2.4	3.2	3.8	4.6	5.4	6.3
360	2.5	3.2	3.9	4.8	5.4	6.4
380	2.6	3.2	4	4.8	5.6	6.6
400	2.6	3.4	4	4.9	5.8	7
420	2.6	3.4	4.2	5	5.9	7.2
440	2.7	3.4	4.2	5	6	7.4
460	2.8	3.5	4.3	5.2	6.2	7.6
480	2.8	3.6	4.4	5.4	6.6	8
500	2.8	3.7	4.5	5.6	6.8	8.6
520	2.9	3.8	4.6	5.8	7.2	8.8
540	3	4	4.8	6	7.6	9.4
560	3	4	5	6.4	8.2	10
580	3.2	4.2	5.1	6.8	8.6	10.6
600	3.2	4.5	5.3	7.2	9.4	11.4
620	3.4	4.4	5.6	7.8	10	12.4
640	3.5	4.6	6	8.6	10.8	13.7
660	3.6	4.5	6.6	9.4	11.8	14.6
680	3.8	5.2	7.4	10.4	13	16
700	4.1	5.6	8.2	11.4	14.4	17.6
720	2.4	6.4	9.2	12.8	16.2	19.4
740	2.6	7.2	10.4	14.4	17.5	19.6
760	5	8.2	12	15.4	18.4	19
780	5.6	9.6	13.6	16.1	18.6	18.4
800	6.6	11.2	13.8	16.2	17.6	17.6
820	7.8	11.5	15	15.8	17	16.2
840	9	12.5	14.6	15.3	16.2	15.6
860	9.8	12.9	14.4	15.1	15.7	14.2
880	9.8	12.9	14	14.9	13.9	13.6
900	10	13.2	14.2	15.4	13.4	13.4
920	9.8	13	15.6	16.5	13.4	13.6
940	9.4	13.2	15.6	16.2	14.2	14.2

TABLE I2

EXPERIMENTAL DATA CORRESPONDING
TO FIGURE 22

Outer Electrode: Wire Mesh 2.5"

Fluid: Nitrogen

Temperature: 30.5 °C

Pressure: 10 psig

PRIM. VOLT FREQUENCY	30 SC. VOLT	40 SC. VOLT	50 SC. VOLT	60 SC. VOLT	70 SC. VOLT	80 SC. VOLT
300	2.5	3.2	3.9	4.8	5.4	6.4
320	2.6	3.2	4	4.8	5.6	6.4
340	2.6	3.4	4	4.8	5.6	6.6
360	2.6	3.4	4.2	5	5.8	6.8
380	2.6	3.4	4.2	5	6	7
400	2.8	3.6	4.4	5.2	6.2	7.6
420	2.8	3.6	4.4	5.4	6.2	7.6
440	2.8	3.7	4.6	5.4	6.6	8
460	2.8	3.8	4.6	5.6	7	8.4
480	3	3.8	4.8	5.8	7.2	8.8
500	3	4	5	6	7.8	9.4
520	3.2	4.2	5.2	6.4	8.2	10
540	3.2	4.2	5.2	6.8	8.8	10.8
560	3.4	4.5	5.6	7.4	9.6	11.6
580	3.5	4.6	6	8	10.4	12.6
600	3.6	5	6.4	8.8	11.8	14
620	3.8	5.2	7.2	9.8	12.6	15.4
640	4	5.6	8	11	14	14.2
660	4.4	6.2	9	12.4	15.8	13.8
680	4.6	7.2	10.4	14	13.6	13
700	5	8.4	12	13.4	13	12.6
720	5.6	9.8	14	13.2	12.4	12
740	6.8	11.4	16.4	13	11.8	11.6
760	8.2	13.4	12.2	12.6	11.4	11
780	9.6	11	12.2	12	11	10.6
800	10.6	10.8	11.8	11.4	10.6	10.2
820	11	10.8	11.6	11	10.2	9.6
840	10.6	10.4	11.2	10.4	9.6	9.4
860	9.8	10.4	11	10	9.2	9
880	8.6	12	10.6	9.8	9	8.8
900	7.4	10.3	10.6	9.6	9	8.6
920	6.6	9.6	11.8	9.8	9.2	8.8
940	5.8	8.6	11	10.2	9.6	9.2

TABLE I3

EXPERIMENTAL DATA CORRESPONDING
TO FIGURE 23

Outer Electrode: Wire Mesh 6.5"

Fluid: Nitrogen

Temperature: 30.5 °C

Pressure: 10 psig

PRIM. VOLT FREQUENCY	30 SC. VOLT	40 SC. VOLT	50 SC. VOLT	60 SC. VOLT	70 SC. VOLT	80 SC. VOLT	90 SC. VOLT	100 SC. VOLT
300	2.4	3.2	4	4.8	5.4	6.6	7.8	4.6
320	2.6	3.2	4	4.8	5.6	6.8	8	4.8
340	2.6	3.4	4.2	5	5.8	7	8.4	5
360	2.6	3.4	4.2	5.2	6	7.2	8.8	7.3
380	2.8	3.6	4.4	5.2	6.2	7.6	9.2	7.8
400	2.8	3.6	4.8	5.4	6.8	8	9.8	7.2
420	2.8	3.8	4.6	5.6	6.8	8.4	10.4	7
440	3	3.8	4.8	5.8	7.2	9	11	6.7
460	3	4	5	6	7.6	9.6	13.6	6.3
480	3.2	4.2	5.2	6.6	8.2	10.4	13.2	6
500	3.2	4.4	5.4	7	9	11.2	12.6	5.7
520	3.4	4.6	5.8	7.6	9.8	13.4	12.2	5.5
540	3.6	4.8	6.2	8.4	10.4	12.8	11.8	5.3
560	3.8	5.2	7	9.4	12.2	12	11	5.1
580	4	5.6	7.8	10.6	13.6	11.6	10.6	4.9
600	4.4	6.4	9	12.2	13.8	11	10.2	4.7
620	4.8	7.4	10.6	13.6	13.6	10.8	10	4.6
640	5.2	8.8	12.2	14.2	12.6	10.4	9.6	4.4
660	6.4	10.1	12.4	14.4	12.4	10.2	9.2	4.3
680	7.8	10.5	13.2	14	11.8	10	9	4.1
700	9.4	11.2	13.2	13.8	11.4	9.6	8.6	4
720	9.6	11.4	13.2	13.4	11	9.7	8.4	3.9
740	9.8	11.2	13	13.2	10.4	9.2	8.2	3.8
760	9.6	11	12.6	12.4	10	9	8	3.7
780	9.4	10.4	12	11.8	9.8	8.8	7.8	3.5
800	9	10.4	11.6	11.4	9.4	8.4	7.4	3.5
820	8.4	9.6	11.2	11	9	8.2	7.2	3.3
840	7.8	10.8	10.4	10.2	8.8	8	7	3.2
860	6.4	9.4	11.8	10.2	8.6	7.8	7	3.2
880	5	7.6	10.2	11.6	8.2	7.6	6.8	3.1
900	4.4	6.6	8.6	10	7.8	7.4	6.6	
920			7.2	8.6	7.8	7.4	6.6	
940			6.2	7.6	7.8	7.6		

TABLE I4

EXPERIMENTAL DATA CORRESPONDING
TO FIGURE 24

Outer Electrode: Wire Mesh 12.5"
Fluid: Nitrogen
Temperature: 30.5 °C
Pressure: 10 psig

PRIM. VOLT FREQUENCY	30		40		50		60		70		80		90		100	
	SC. VOLT	SC. VOLT	SC. VOLT	SC. VOLT	SC. VOLT	SC. VOLT	SC. VOLT	SC. VOLT	SC. VOLT	SC. VOLT	SC. VOLT	SC. VOLT	SC. VOLT	SC. VOLT	SC. VOLT	SC. VOLT
300	2.5	3.4	4.2	5	5.8	7	8.4	9.8								
320	2.6	3.4	4.4	5.2	6	7.4	8.8	10.4								
340	2.6	3.6	4.4	5.2	6.4	7.8	9.2	13.6								
360	2.8	3.6	4.6	5.5	6.6	8.2	9.8	12.8								
380	2.8	3.8	4.8	5.8	7.1	8.6	10.6	12.4								
400	3	4	5.2	6	7.6	9.2	11.8	11.8								
420	3	4.2	5.2	6.4	8.2	10	11.4	11.4								
440	3.2	4.4	5.4	7	9	11	11	10.8								
460	3.4	4.6	5.8	7.6	9.8	10.8	10.6	10.2								
480	3.6	4.8	6.4	8.5	11	10.4	10.2	10								
500	4	5.2	7.2	10	10.2	10	9.8	9.8								
520	4.2	5.6	8.2	10	9.8	9.8	9.6	9.4								
540	4.4	6.6	9.6	9.6	9.6	9.4	9.4	9.2								
560	5	7.8	11.2	9.4	9.2	9.2	9.2	9								
580	5.6	9.2	13.6	9.2	9.2	9	8.8	8.6								
600	6.8	11.4	9.6	9	9	8.8	8.6	8.4								
620	8.4	9.6	9.2	8.8	8	8.6	8.4	8.2								
640	10	9.2	9.2	8.6	8.4	8.4	8.2	8								
660	11.6	9	9	8.6	8.4	8.2	8	7.8								
680	12.2	8.8	8.8	8.4	8.1	8.2	8	7.8								
700	11.8	8.8	8.6	8.4	8	7.8	7.8	7.6								
720	10.8	8.6	8.6	8	7.8	7.8	7.6	7.4								
740	9.4	8.6	8.4	8	7.8	7.6	7.6	7.4								
760	7.8	8.2	8.2	7.8	7.6	7.6	7.4	7.4								
780	6.4	8	8	7.6	7.6	7.4	7.4	7.2								
800	5.2	8	7.9	7.4	7.4	7.4	7.2	7.2								
820		6.6	7.6	7.4	7.4	7.2	7.2	7								
840		5.4	7.2	7.2	7.2	7.2	7	7								
860			6.2	7.8	7	7.2	7	7								
880				6.6	6.8	7	7	7								
900						6.8										

TABLE 15

EXPERIMENTAL DATA CORRESPONDING
TO FIGURE 25

Outer Electrode: Wire Mesh 17.375"
Fluid: Nitrogen
Temperature: 30.5 °C
Pressure: 10 psig

PRIM. VOLT FREQUENCY	50 SC. VOLT	60 SC. VOLT	70 SC. VOLT	80 SC. VOLT	90 SC. VOLT	100 SC. VOLT	110 SC. VOLT	115 SC. VOLT
140								5.5
160								5.3
180								5.5
200							10.6	5.8
220							11.6	6.6
240							13.2	7.4
260							14.8	7.6
280							14.6	7.4
300	4.4	5.2	6.2	7.4	9	10.3	14	7.1
320	4.6	5.4	6.4	8	9.4	11.2	13.4	6.8
340	4.8	5.6	6.8	8.4	10	12.6	13	6.5
360	4.8	5.9	7.4	9	10.8	12.2	12.6	6.3
380	5.2	6.4	8	9.8	11.6	11.8	12	6.1
400	5.6	7.2	9.6	11	11.2	11.4	11.6	5.9
420	6	7.6	10.4	10.6	10.8	11.2	11.4	5.7
440	6.6	8.4	10.4	10.4	10.6	10.8	11	5.6
460	7.2	9.6	10.2	10.2	10.4	10.6	10.8	5.4
480	8.6	11	10.2	10.2	10	10.4	10.6	5.3
500	9.4	10.2	10	10	9.8	10	10.4	5.2
520	9.4	9.8	9.6	9.6	9.6	9.8	10	5.1
540	9.4	9.6	9.4	9.4	9.4	9.6	10	5
560	9.2	9.4	9.2	9.2	9.2	9.4		
580	9	9.4	9	9	9.2	9.2		
600	9	9.2	8.8	8.8	9.2	9.2		
620	8.6	9	8.6	8.8	8.8			
640	8.6	8.8	8.6	8.6	8.6			
660	8.4	8.6	8.4	8.4	8.6			
680	8.4	8.6	8.4	8.4	8.4			
700	8.2	8.6	8.2	8.2	8.4			
720	8.2	8.4						
740	8	8.4						
760	8	8.3						
780	8	8.2						
800	6.6	8.8						
820		7.6						
840		6.4						

TABLE I6

EXPERIMENTAL DATA CORRESPONDING
TO FIGURE 26

Various Lengths at 30 Volts Primary Voltage

Fluid: Nitrogen

Temperature: 30.5 °C

Pressure: 10 psig

Length Freq.	1 wrap	2.5"	6.5"	12.5"
300	4.8	5	4.8	5
320	4.8	5.2	5.2	5.2
340	4.8	5.2	5.2	5.2
360	5	5.2	5.2	5.6
380	5.2	5.2	5.6	5.6
400	5.2	5.6	5.6	6
420	5.2	5.6	5.6	6
440	5.4	5.6	6	6.4
460	5.6	5.6	6	6.8
480	5.6	6	6.4	7.2
500	5.6	6	6.4	8
520	5.8	6.4	6.8	8.2
540	6	6.4	7.2	8.8
560	6	7.2	7.8	10
580	6.4	7.4	8	11.2
600	6.4	7.2	8.8	13.6
620	6.8	7.6	9.6	16.8
640	7	8	10.4	20
660	7.2	8.8	12.8	23.2
680	7.6	9.2	15.8	24.4
700	8.1	10	18.4	23.6
720	8.8	11.2	19.6	21.6
740	9.2	13.6	19.6	18.8
760	10	16.2	19.2	15.6
780	11.2	19.2	18.8	12.8
800	13.2	21.2	18	10.4
820	15.6	22	19.8	
840	18	22.8	15.6	
860	19.6	193.6	12.8	
880	19.6	17.2	10	
900	20	15.4	8.8	
920	19.6	13.2		
940	18.8	11.6		

TABLE I7

EXPERIMENTAL DATA CORRESPONDING
TO FIGURE 27

Various Lengths at 40 Volts Primary Voltage

Fluid: Nitrogen

Temperature: 30.5 °C

Pressure: 10 psig

Length Freq.	1 wrap	2.5"	6.5"	12.5"
300	6.4	6.4	6.2	6.8
320	6.4	6.4	6.2	6.8
340	6.4	6.8	6.8	7.2
360	6.4	6.8	6.8	7.2
380	6.4	6.8	7.2	7.6
400	6.8	7.2	7.2	8
420	6.8	7.2	7.6	8.4
440	6.8	7.4	7.6	8.8
460	7	7.6	8	9.2
480	7.2	7.6	8.4	9.6
500	7.4	8	8.8	10.4
520	7.6	8.4	9.2	11.2
540	8	8.4	9.6	13.2
560	8	9	10.4	15.8
580	8.4	9.2	6	18.4
600	8.6	10	12.8	18.8
620	8.8	10.4	14.8	19.2
640	9.2	11.2	17.6	18.4
660	9.8	12.4	21	18
680	10.4	14.4	21	17.6
700	11.2	16.8	22.4	17.6
720	12.8	19.6	22.4	17.2
740	14.4	23.4	22.4	17.2
760	16.4	23.6	22	16.4
780	19.2	22	20.8	16
800	22.4	21.6	20.8	16
820	23	21.6	19.2	13.2
840	24.6	20.8	19.6	10.8
860	25	20.8	18.4	
880	25.8	24	15.2	
900	25.4	21.2	13.2	
920	26	19.2		
940	26.4	19.2		

TABLE I8
 EXPERIMENTAL DATA CORRESPONDING
 TO FIGURE 28

Various Lengths at 50 Volts Primary Voltage
 Fluid: Nitrogen
 Temperature: 30.5 °C
 Pressure: 10 psig

Length Freq	1 wrap	2.5"	6.5"	12.5"	17.75"
300	3.8	3.9	4	4.2	4.4
320	3.8	4	4	4.4	4.3
340	3.8	4	4.2	4.4	4.8
360	3.9	4.2	4.2	4.6	4.8
380	4	4.2	4.4	4.8	5.2
400	4	4.4	4.8	5.2	5.6
420	4.2	4.4	4.6	5.2	6
440	4.2	4.6	4.8	5.4	6.6
460	4.3	4.6	5	5.8	7.4
480	4.4	4.8	5.2	6.4	8.6
500	4.5	5	5.4	7.2	9.4
520	4.6	5.2	5.8	8.2	9.4
540	4.8	5.2	6.2	9.6	9.4
560	5	5.6	7	11.2	9.2
580	5.1	6	7.8	11.6	9
600	5.3	6.4	9	9.6	9
620	5.6	7.2	10.6	9.2	8.6
640	6	8	12.2	9.2	8.6
660	6.6	9	12.2	9	8.4
680	7.4	10.4	13.2	8.8	8.4
700	8.2	12	13.2	8.6	8.2
720	9.2	14	13.2	8.6	8.2
740	10.4	14.2	13	8.4	8
760	12	12.2	12.6	8.2	8
780	13.6	12.2	12	8	8
800	13.8	11.8	11.6	7.9	6.6
820	15	11.6	11.2	7.6	
840	14.6	11.2	11.4	7.2	

TABLE I9

EXPERIMENTAL DATA CORRESPONDING
TO FIGURE 29

Various Lengths at 60 Volts Primary Voltage

Fluid: Nitrogen

Temperature: 30.5 °C

Pressure: 10 psig

Length Freq.	1 wrap	2.5"	6.5"	12.5"	17.75"
300	4.6	4.8	4.8	5	5.2
320	4.6	4.8	4.8	5.2	5.4
340	4.6	4.8	5	5.2	5.6
360	4.8	5	5.2	5.5	5.9
380	4.8	5	5.2	5.8	6.4
400	4.9	5.2	5.4	6	7.2
420	5	5.4	5.6	6.4	7.6
440	5	5.4	5.8	7	8.4
460	5.2	5.6	6	7.6	9.6
480	5.4	5.9	6.6	8.6	11
500	5.6	6	7	10	10.2
520	5.8	6.4	7.6	10	9.8
540	6	6.8	8.4	9.6	9.6
560	6.4	7.4	8.7	9.4	9.4
580	6.8	8	10.6	9.2	9.4
600	7.2	8.8	12.2	9	9.2
620	7.8	9.8	13.6	8.8	9
640	8.6	11	14.2	8.6	8.8
660	9.4	12.8	14.4	8.6	8.6
680	10.4	14	14	8.4	8.6
700	11.4	13.4	13.8	8.2	8.4
720	12.8	13.2	13.4	8	8.4
740	14.4	13	13.2	8	8.3
760	15.4	12.6	12.4	7.8	8.2
780	16	12	11.8	7.6	8.2
800	16.2	11.4	11.4	7.4	8.1
820	15.8	11	11	7.4	7.6
840	15.3	10.4	10.2	7.2	7.6
860	15.1	10	10.2	7.8	
880	14.9	9.8	11.6	6.6	
900	15.4	9.6	10		
920	15.5	9.8	8.6		
940	16.2	10.2	7.6		

TABLE I10

EXPERIMENTAL DATA CORRESPONDING
TO FIGURE 30

Various Lengths at 70 Volts Primary Voltage

Fluid: Nitrogen

Temperature: 30.5 °C

Pressure: 10 psig

Length Freq.	1 wrap	2.5"	6.5"	12.5"	17.75"
300	5.4	5.4	5.4	5.8	6.2
320	5.4	5.6	5.6	6	6.4
340	5.4	5.6	5.8	6.4	6.8
360	5.4	5.8	6	6.6	7.4
380	5.6	6	6.2	7.1	8
400	5.8	6.2	6.8	7.6	9.6
420	5.9	6.4	6.8	8.2	10.4
440	6	6.6	7.2	9	10.4
460	6.2	7	7.6	9.8	10.2
480	6.6	7.2	8.2	11	10.2
500	6.8	7.8	9	10.2	10
520	7.2	8.2	9.8	9.8	9.6
540	7.6	8.8	10.8	9.6	9.7
560	8.2	9.6	12.2	9.2	9.2
580	8.6	10.4	13.6	9.2	9
600	9.4	11.8	13.8	9	8.8
620	10	12.6	13.6	8.8	8.6
640	10.8	14	12.6	8.4	8.6
660	11.8	15.8	12.4	8.4	8.2
680	13	13.6	11.8	8.2	8.2
700	14.4	13	11.4	8	8.2
720	16.2	12.4	11	7.8	
740	18	11.8	10.4	7.8	
760	18.4	11.4	10	7.6	
780	18.6	11	9.8	7.6	
800	17.6	10.6	9.4	7.4	
820	17	10.2	9	7.4	
840	16.2	9.6	8.8	7.2	
860	15.4	9.2	8.6	7	
880	13.9	9	8.1	6.8	
900	13.4	9	7.8		
920	13.4	9.2	7.8		
940	14.2	9.6	7.8		

TABLE I11

EXPERIMENTAL DATA CORRESPONDING
TO FIGURE 31

Various Lengths at 80 Volts Primary Voltage

Fluid: Nitrogen

Temperature: 30.5 °C

Pressure: 10 psig

Length Freq.	1 wrap	2.5"	6.5"	12.5"	17.75"
300	6.2	6.4	6.6	7	7.4
320	6.2	6.4	6.8	7.4	8
340	6.3	6.6	7	7.8	8.4
360	6.4	6.8	7.2	8.2	9
380	6.6	7	7.6	8.6	9.8
400	7	7.6	8	9.2	11
420	7.2	7.6	8.4	10	10.6
440	7.4	8	9	11	10.4
460	7.6	8.4	9.6	10.8	10.2
480	8	8.8	10.4	10.4	10.2
500	8.6	9.4	11.2	10	10
520	8.8	10	13.4	9.8	9.6
540	9.4	10.8	12.8	9.4	9.4
560	10	11.6	12	9.2	9.2
580	10.6	12.6	11.6	9	9
600	11.4	14	11	8.8	8.8
620	12.4	15.4	10.8	8.6	83.8
640	13.4	14.2	10.4	8.4	8.6
660	14.6	13.6	10.2	8.2	8.4
680	16	13	10	8.2	8.4
700	17.6	12.6	9.6	7.9	8.2
720	19.4	12	9.4	7.9	
740	19.6	11.6	9.2	7.6	
760	19	11	9	7.6	
780	18.4	10.6	8.8	7.4	
800	17.6	10.2	8.4	7.4	
820	16.2	9.6	8.2	7.2	
840	15.2	9.4	8	7.2	
860	14.4	9	7.8	7.2	
880	13.6	8.8	8.6	7	
900	13.4	8.6	7.4	6.8	
920	13.6	8.8	7.4		
940	14.2	9.2	7.6		

TABLE I12

EXPERIMENTAL DATA CORRESPONDING
TO FIGURE 32

Various Lengths at 90 Volts Primary Voltage

Fluid: Nitrogen

Temperature: 30.5 °C

Pressure: 10 psig

Length Freq.	6.5"	12.5"	17.75"
300	7.8	8.4	9
320	8	8.8	9.4
340	8.4	9.2	10
360	8.8	9.8	10.4
380	9.2	10.6	11.6
400	9.8	11.8	11.2
420	10.4	11.4	11.8
440	11	11	11.6
460	13.6	10.6	10.2
480	13.2	10.2	10
500	12.6	9.8	9.8
520	12.2	9.6	9.6
540	11.8	9.4	9.4
560	11	9.2	9.2
580	10.6	8.8	9.2
600	10.2	8.6	9.2
620	10	8.4	8.8
640	9.6	8.4	8.6
660	9.2	8	8.6
680	9	8	8.4
700	8.6	7.8	8.4
720	8.4	7.6	
740	8.2	7.6	
760	8	7.4	
780	7.8	7.4	
800	7.4	7.2	
820	7.2	7.2	
840	7	7	
860	7	7	
880	6.8		
900	6.6		
920	6.6		

TABLE I13

EXPERIMENTAL DATA CORRESPONDING
TO FIGURE 33

Various Lengths at 100 Volts Primary Voltage
Fluid: Nitrogen
Temperature: 30.5 °C
Pressure: 10 psig

Length	6.5"	12.5"	17.75"
Freq.			
300	9.2	9.8	10.6
320	9.6	10.4	11.2
340	10	13.6	12.6
360	14.6	12.8	12.1
380	15.6	12.4	11.8
400	14.4	11.8	11.4
420	14	11.4	11.2
440	13.4	10.8	10.8
460	12.6	10.4	10.6
480	12	10	10.4
500	11.4	9.8	10
520	11	9.4	9.8
540	10.6	9.2	9.6
560	10.2	9	9.4
580	9.8	8.6	9.2
600	9.4	8.4	9.2
620	9.2	8.2	
640	8.8	8.2	
660	8.6	8	
680	8.2	7.8	
700	8	7.6	
720	7.8	7.4	
740	7.6	7.4	
760	7.2	7.4	
780	7	7.2	
800	7	7.2	
820	6.6	7	
840	6.4	7	
860	6.4		
880	6.2		

APPENDIX J
STATISTICAL DATA FROM
TABLECURVE ANALYSIS

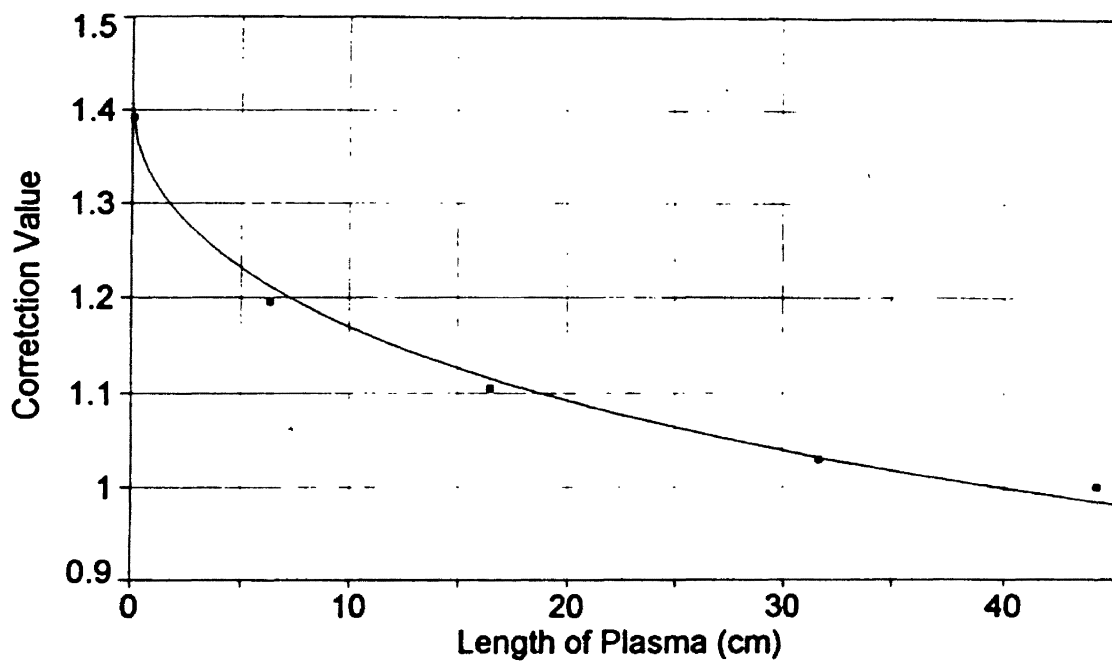


Figure J1. Graphical Representation of Correction Values

TABLE JI

STATISTICAL DATA FROM
TABLECURVE ANALYSIS

Numeric Summary

Rank 1387 Eqn 54 $1/y=a+bx^{0.5}$

r ² Coef Det	DF Adj r ²	Fit Std Err	F-value
0.9925242061	0.9850484122	0.0157594678	398.29517114

Parm	Value	Std Error	t-value	95% Confidence Limits	
a	0.709079220	0.007932651	89.38742563	0.684021262	0.734137178
b	0.046329084	0.002242994	20.65501938	0.039243829	0.053414338

Area Xmin-XmaxArea Precision

48.454303440	1.168094e-09		
Function min	X-Value	Function max	X-Value
0.9834270716	44.132000000	1.3817311933	0.1000001133
1st Deriv min	X-Value	1st Deriv max	X-Value
-0.139852620	0.1000001133	-0.003372339	44.132000000
2nd Deriv min	X-Value	2nd Deriv max	X-Value
6.133608e-05	44.132000000	0.7275729696	0.1000001133

Soln Vector

Direct	Covar Matrix
r ² Coef Det	LUDecomp
0.9925242061	DF Adj r ²
	Fit Std Err
	0.0157594678

Source	Sum of Squares	DF	Mean Square	F
Regr	0.098920918	1	0.098920918	398.295
Error	0.00074508248	3	0.00024836083	
Total	0.099666	4		

X Variable:

Xmin:	0.1000000000	Xmax:	44.132000000	Xrange:	44.032000000
Xmean:	19.768400000	Xstd:	18.129122505	Xmedian:	16.510000000
X@Ymin:	44.132000000	X@Ymax:	0.1000000000	X@Yrange:	44.032000000

Y Variable:

Ymin:	1.0000000000	Ymax:	1.3920000000	Yrange:	0.3920000000
Ymean:	1.1440000000	Ystd:	0.1578496120	Ymedian:	1.1040000000
Y@Xmin:	1.3920000000	Y@Xmax:	1.0000000000	Y@Xrange:	0.3920000000

APPENDIX K
OPERATION PARAMETERS AND ANALYSIS
OF PRELIMINARY RUNS

TABLE K1

OPERATION PARAMETERS

Run #	S.V. (kV)	Flow Rate (ml/min)	Frequency (Hz)	Reactor	Length (cm)
HR-004	6.00	69.8	620	A	27.5
HR-005	8.00	69.8	480	A	27.5
HR-006	15.8	69.8	380	A	27.5
HR-015	18.5 ¹	69.8	540	D	45.09
HR-016	19.4 ¹	69.8	540	D	45.09

1. Average of total run variations.

TABLE K2

ANALYSIS OF PRELIMINARY SAMPLES
04, 05, AND 06

Run #	Component	%
04	Methane, H ₂ , Air	0.000
	Ethane, Ethylene	0.266
	Propane	99.658
	Isobutane	0.076
05	Methane, H ₂ , Air	0.000
	Ethane, Ethylene	2.139
	Carbon Dioxide	0.124
	Propane	94.272
	Propylene	1.166
	Isobutane	0.730
	N-Butane	0.689
	Isopentane	0.579
	N-Pentane	0.302
06	Methane, H ₂ , Air	0.000
	Ethane, Ethylene	3.871
	Carbon Dioxide	0.000
	Propane	88.670
	Propylene	1.712
	Isobutane	1.255
	N-Butane	1.177
	1-Butene	0.237
	Isopentane	0.959
	N-Pentane	0.492
	1-Pentene	0.070
	C ₆ and Heavier	1.556

TABLE K3

ANALYSIS OF PRELIMINARY SAMPLES
015 AND 016

Run #	Group1 %	Group 2 %	Group 3 %
015	98.068	0.1091	0.843
016	72.691	27.198	0.111

APPENDIX L
OPERATION PARAMETERS AND ANALYSIS
OF DESTRUCTIVE TEST

TABLE L1

OPERATION PARAMETERS OF
DESTRUCTIVE TEST

Run #	S.V. (kV)	Frequency (Hz)	Flowrate (ml/min)	Temp. (°F)
01	19.2	310	68.9	68
02	20.0	310	68.9	62
03	18.0	310	68.9	58
04	17.0	310	68.9	48
05	21.6	310	68.9	50
06	19.2	260	68.9	60
07	19.2	210	68.9	58
08	19.2	327	68.9	56
09	19.2	280	68.9	56
10	19.2	280	34.45	56
11	19.2	280	129.6	52
12	19.2	280	111.3	52

TABLE L2

ANALYSIS SUMMARY OF
DESTRUCTION TEST

Run #	Group 1 %	Group 2 %	Group3 %	Amt. (g)
01	51.994	44.801	3.205	0.59
02	47.088	47.464	5.454	0.35
03	59.477	37.347	3.190	0.25
04	40.153	52.260	7.592	0.19
05	25.071	54.191	16.680	0.18
06	97.997	2.003	0.000	0.33
07	0.000	0.000	0.000	0.00
08	38.631	50.182	11.189	0.29
09	73.360	18.173	8.472	0.46
10	38.178	41.953	17.518	0.20
11	0.000	0.000	0.000	0.00
12	30.109	38.812	31.021	0.27

APPENDIX M
ANALYTICAL CHROMATOGRAMS

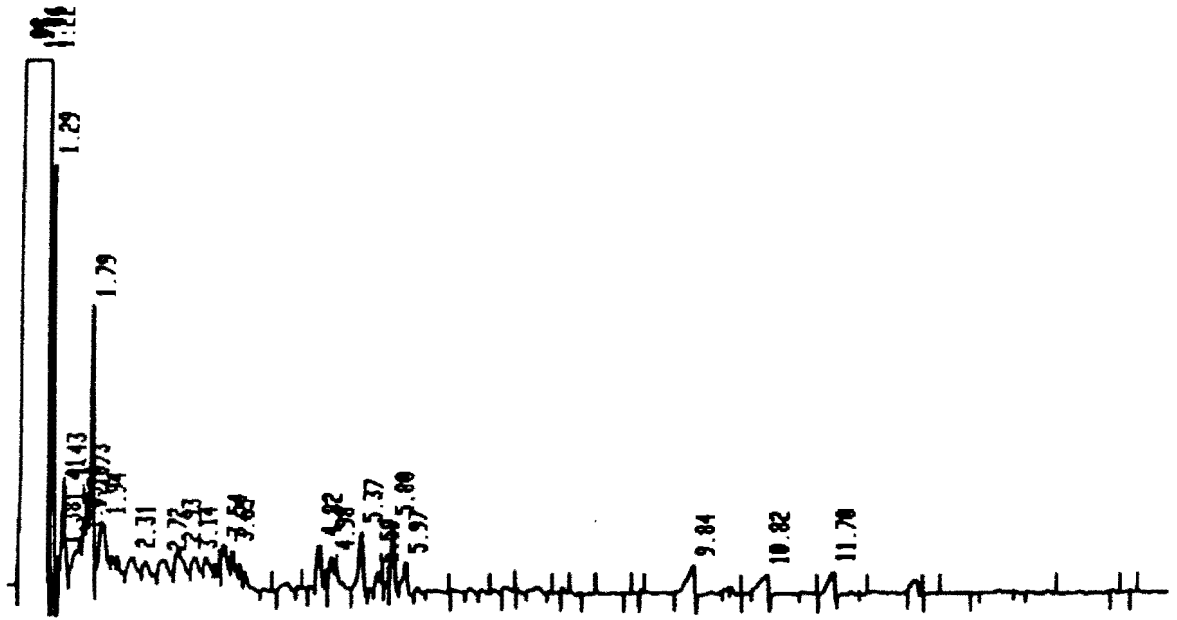


Figure M1. Run # HR-015

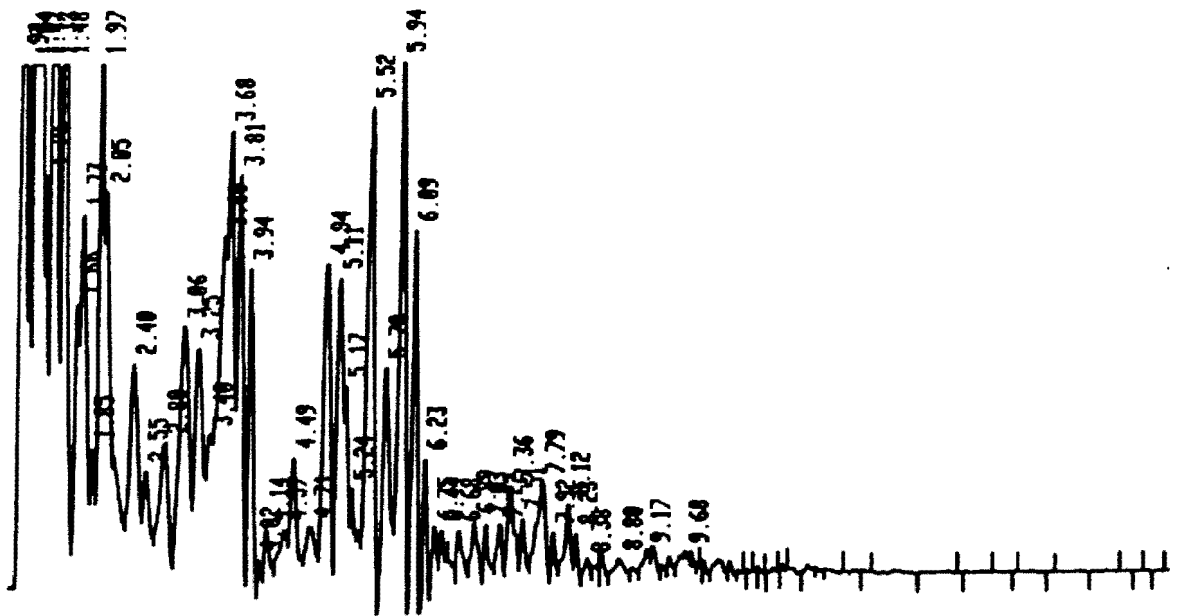


Figure M2. Run # HR-016

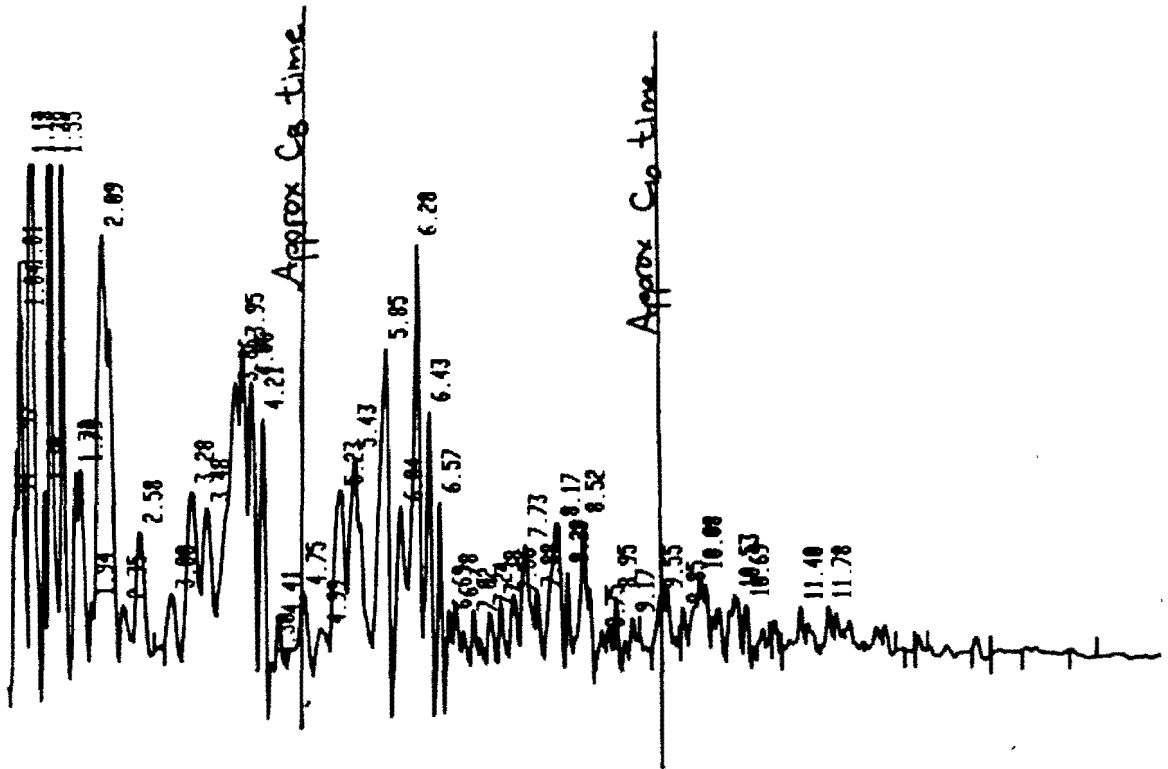


Figure M3. Run # D-1

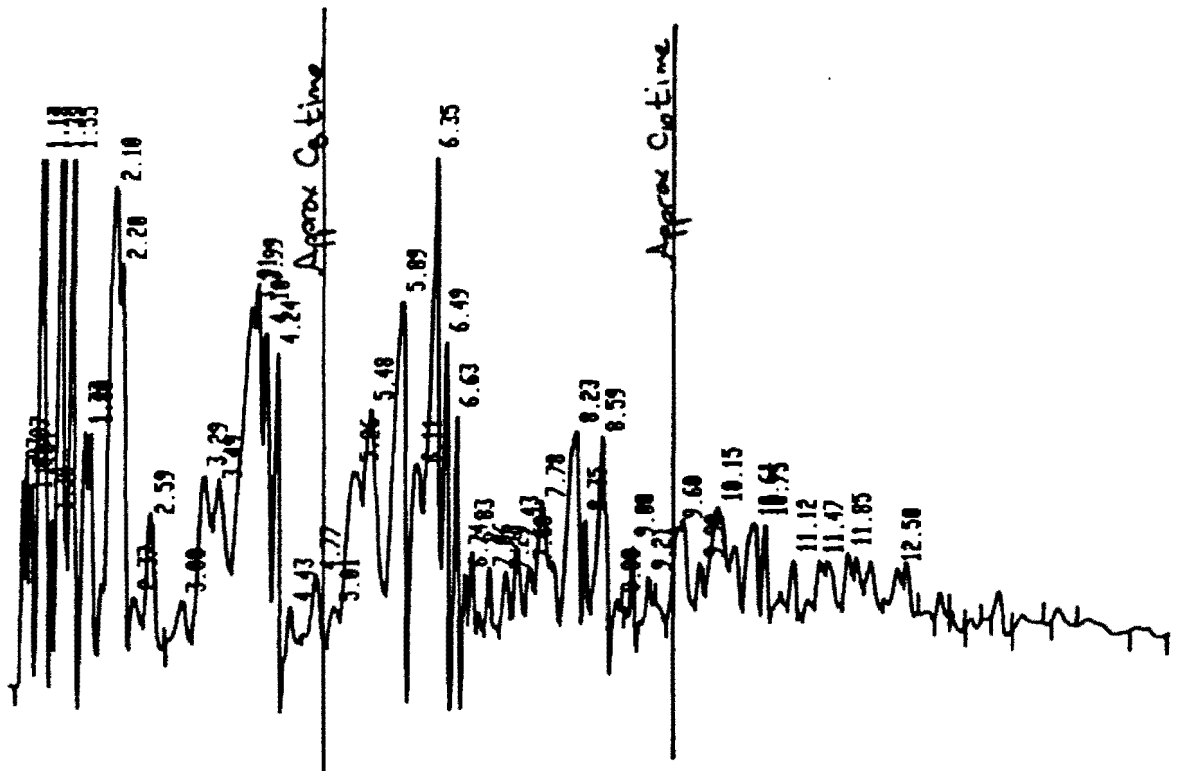


Figure M4. Run # D-2

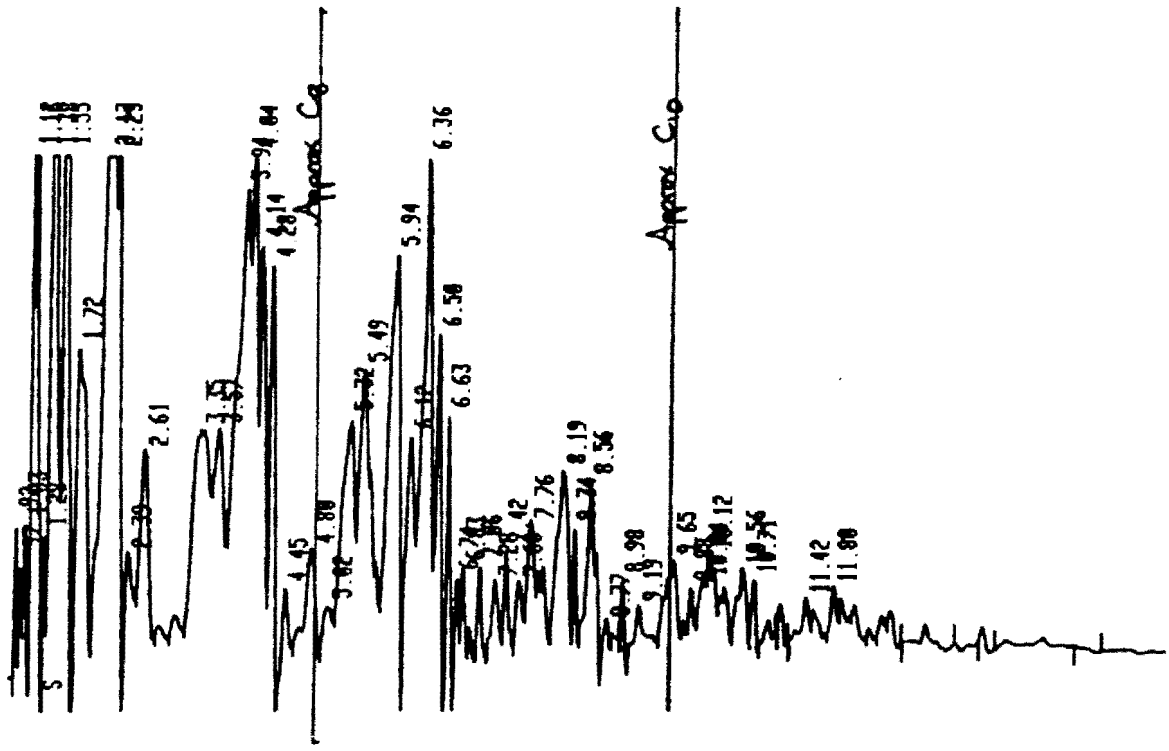


Figure M5. Run # D3

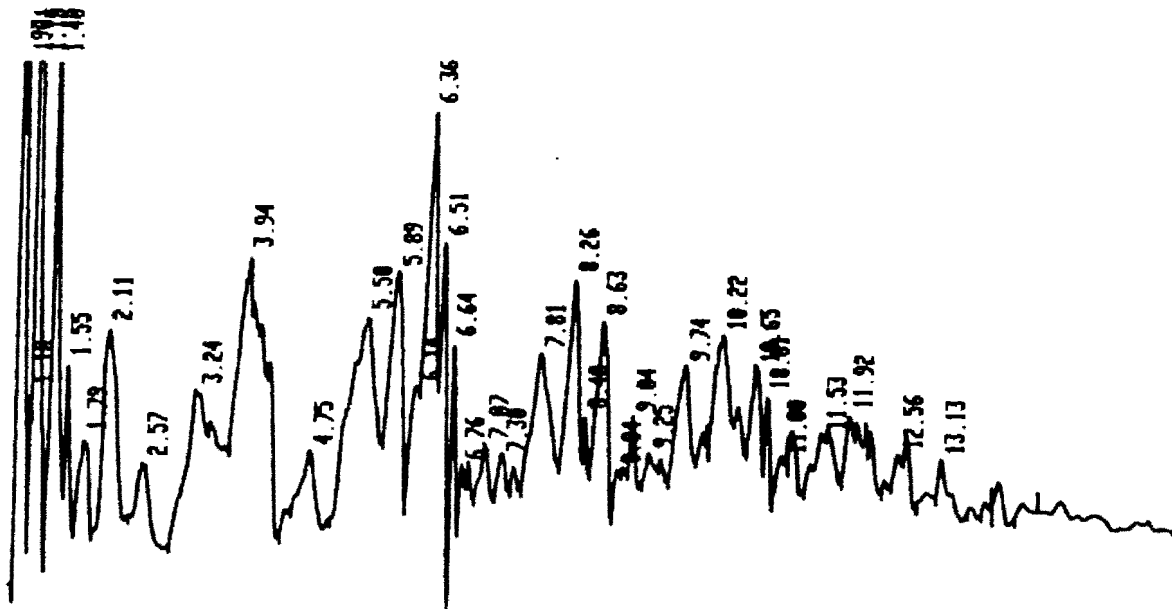


Figure M6. Run # D-4

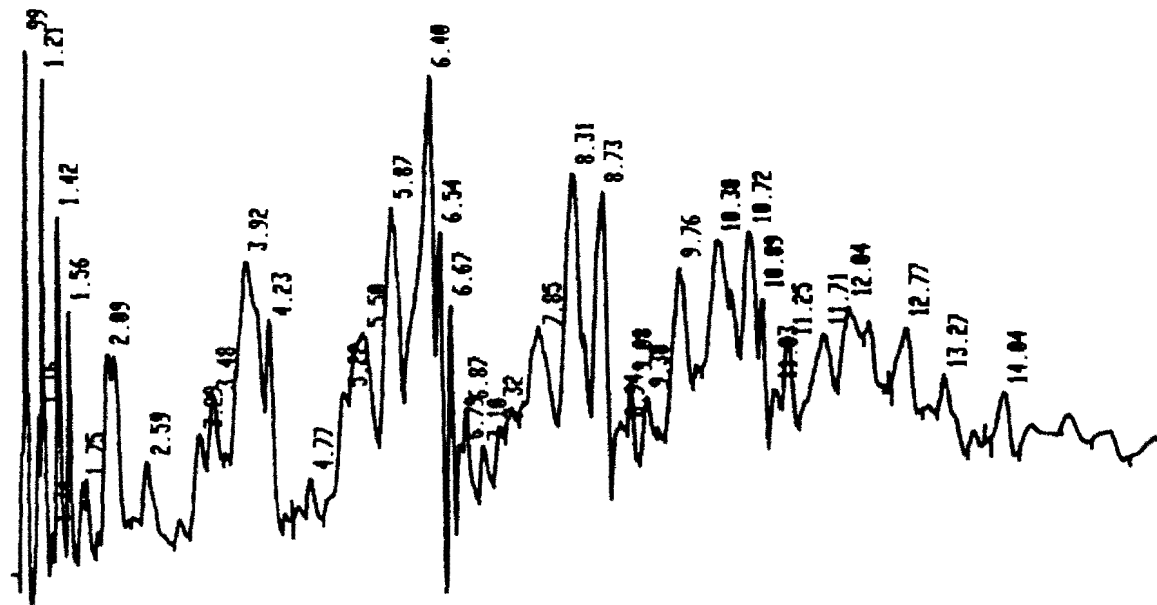


Figure M7. Run # D-5

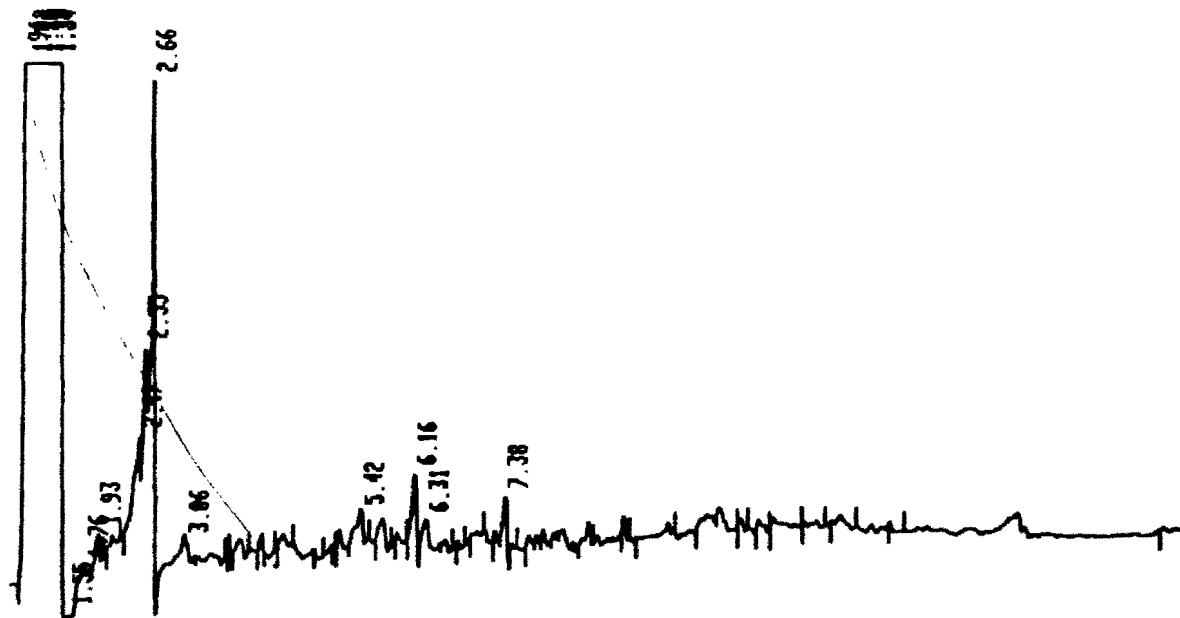


Figure M8. Run D-6

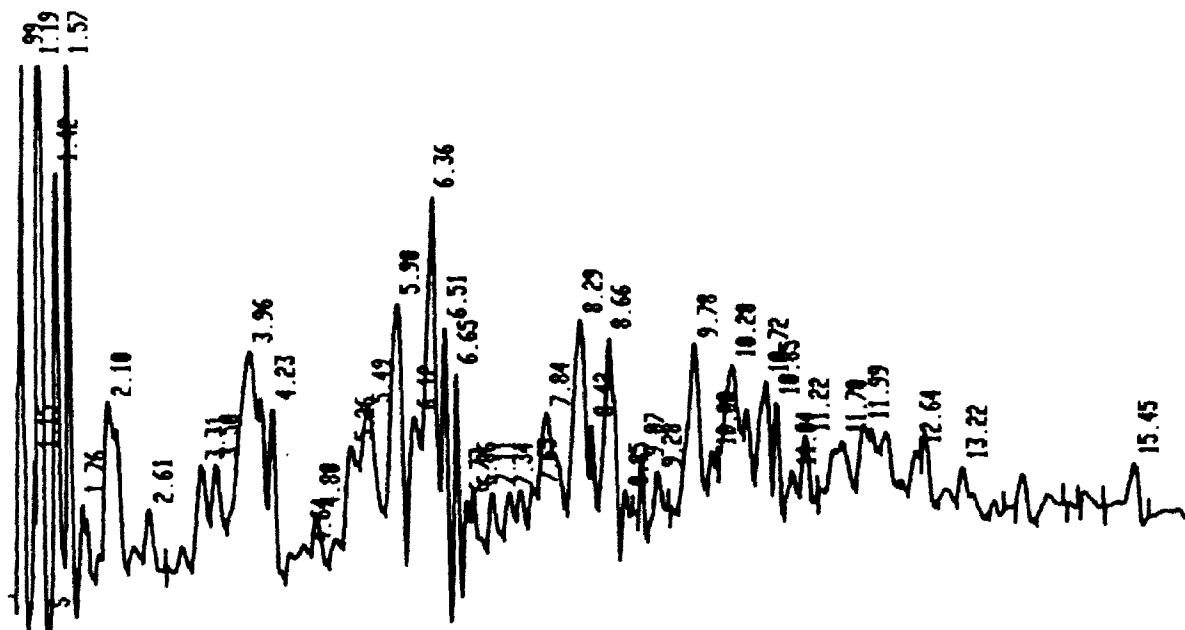


Figure M9. Run D-8

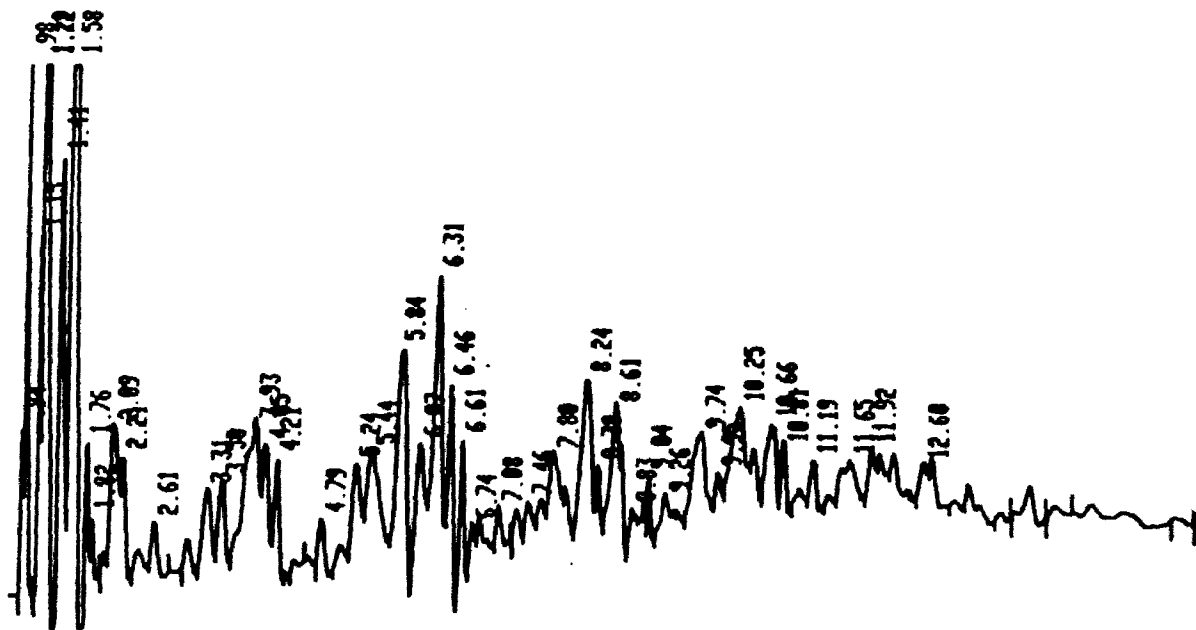


Figure M10. Run # D-9

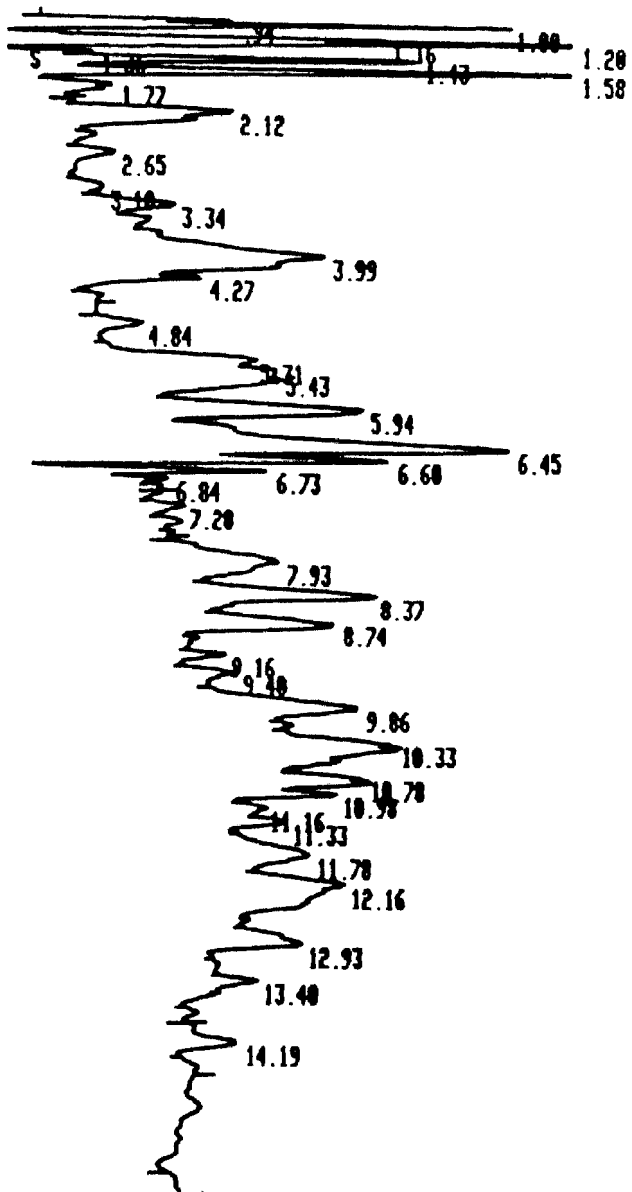


Figure M12. Run # D-12

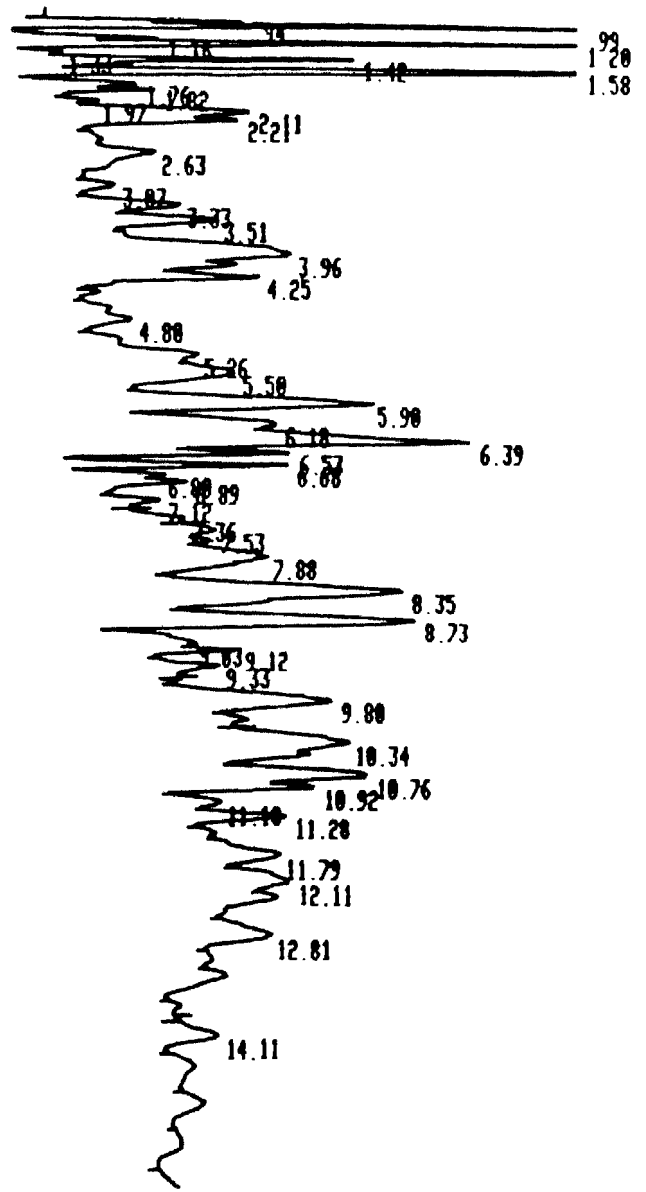


Figure M11. Run # D-10

VITA

Dennis Keith Manning

Candidate for the Degree of

Master of Science

Thesis: HYDROCARBON REARRANGEMENT AND SYNTHESIS USING AN
ALTERNATING CURRENT SILENT GLOW DISCHARGE REACTOR

Major Field: Chemical Engineering

Biography:

Personal Data: Born in Miami, Oklahoma, April 22, 1960.

Education: Graduated from Fairland High School, Fairland, Oklahoma in May 1978; received Associates of Science Degree in Chemistry from NEO A&M College, Miami, Oklahoma, May, 1990; received Bachelor of Science Degree in Chemistry with Minor in Math from Pittsburg State University, Pittsburg Kansas, July, 1991; completed requirements for the Master of Science Degree at Oklahoma State University, Stillwater, Oklahoma, December, 1993

Professional Experience: Research Engineer, NATCO R&D, Tulsa, Oklahoma, Teaching Assistant Oklahoma State University, Consultant Engineer, Chemical Engineering Consultants Inc., Stillwater, Oklahoma; Inorganic Analysts, Eagle-Picher Environmental Laboratory, Miami, Oklahoma, Ceramic Technician Ozark Technical Ceramics, Webb City, Missouri